

UNIVERSITÀ DEGLI STUDI DI VERONA

DEPARTMENT OF MEDICINE

GRADUATE SCHOOL OF BIOMOLECULAR MEDICINE

DOCTORAL PROGRAM IN PROTEOMICS AND GENOMICS

WITH THE FINANCIAL CONTRIBUTION OF ATENEO - UNIVERSITY OF VERONA

Cycle XXXVI, year 2020-2021

The role of Mesenchymal Stem Cells (MSCs) in physiological and pathological conditions

S.S.D. BIO/11

Coordinator: Prof.ssa Lucia De Franceschi

Firma:

Tutor: Prof. Luca Giuseppe Dalle Carbonare

Firma:

Co-tutor: Prof.ssa Maria Teresa Valenti

Firma:

PhD student: Arianna Minoia

This work is licensed under a Creative Commons Attribution-NonCommercial-NoDerivs 3.0 Unported License, Italy. To read a copy of the license, visit the web page:

<http://creativecommons.org/licenses/by-nc-nd/3.0/it/>



Attribution -You must give appropriate credit, provide a link to the license, and indicate if changes were made. You may do so in any reasonable manner, but not in any way that suggests the licensor endorses you or your use.

Noncommercial- You may not use the material for commercial purposes.

No Derivatives- If you remix, transform, or build upon the material, you may not distribute the modified material.

The role of Mesenchymal Stem Cells (MSCs) in physiological and pathological conditions

Arianna Minoia

Verona, February 2024.

*A mia madre,
che illumina il mio cammino con amore e saggezza.
Il suo amore e la sua mancanza sono il
motore che mi spinge a raggiungere i miei traguardi.*

*A mio padre e mio fratello,
per il coraggio e sostegno instancabile
in ogni fase della mia vita.*

*Ad Andrea,
mio compagno di vita.*

CONTENTS

ABSTRACT	9
ABSTRACT (ITALIANO)	10
ABBREVIATIONS	11
1 INTRODUCTION	13
1.1 Mesenchymal stem cells (MSCs)	13
1.1.1 Osteogenic differentiation	14
1.1.1.1 Runx2	14
1.1.1.2 The Role of FBXW11	18
1.1.2 Adipogenic differentiation	20
1.1.3 Myogenic differentiation	21
1.1.4 Induced Pluripotent Stem Cells	22
1.2 Bone cells and tissue	24
1.2.1 Pathological conditions: Cleidocranial dysplasia (CCD)	25
1.3 Impact of physical activity in modulating MSCs	26
1.4 Crosstalk between bone and neuronal system	28
2 AIM OF THE STUDY	31
2.1 Clarifications	33
3 MATERIALS AND METHODS	34
3.1 Cell cultures	34
3.1.1 Mesenchymal stem cells	34
3.1.2 Osteogenic differentiation	34
3.1.3 Adipogenic differentiation	34
3.1.4 Osteosarcoma cells	34
3.1.5 In Vitro Myogenic Differentiation	35
3.1.6 iPSC derived MSCs	35

3.1.7	Circulating progenitor cells (CPCs)	35
3.1.8	Peripheral Blood Mononuclear Cells (PBMCs) and Sera Collection	36
3.1.9	Fibroblasts	36
3.1.10	iPSCs transduction from PBMC	37
3.2	Transfection analysis	37
3.3	Patients	38
3.3.1	CCD patients	38
3.3.2	iPSC derived MSC Patients	39
3.3.3	Half-marathon participants	39
3.3.4	4400km race participants	39
3.4	Alkaline phosphatase staining	40
3.5	Alizarin Red Staining	40
3.6	Immunofluorescence	40
3.7	DNA Extraction	40
3.8	RNA extraction and reverse transcription	41
3.9	Gene expression	42
3.9.1	Taqman Real-time PCR	42
3.9.2	Sybr Green Real-Time PCR	44
3.9.3	TaqMan Gene Expression Assay	46
3.9.4	PCR array	47
3.9.5	Digital droplet PCR	47
3.10	Western blotting analysis	48
3.11	Sanger Sequencing	50
3.12	Generation of mid-brain organoids	51
3.12.1	Sectioning, staining, and mounting organoids	52
3.12.2	Confocal imaging	53
3.13	Flow cytometry analysis	53

3.13.1	iPSC-derived MSCs	53
3.13.2	Mid-brain Organoids	54
3.14	Statistical analysis	55
4	RESULTS	55
4.1	Identification of new molecular mechanisms associated with osteogenic differentiation.	55
4.1.1	FBXW11 expression during osteogenesis	55
4.1.2	FBXW11 regulates the expression of RUNX2, and genes associated with osteogenic maturation	56
4.1.3	FBXW11 and RUNX2 undergo disparate modulations in CCD cell	59
4.1.4	The role of FBXW11 in osteosarcoma cells	60
4.2	Focus on examining mutations in RUNX2 gene in patients diagnosed with CCD	61
4.2.1	RUNX2 mutations	61
4.2.2	Osteogenically-Stimulated CCD Fibroblasts Express Increased Levels of Runx2 Protein	63
4.2.3	The Expression of P53 and PTEN Are Lowered in osteogenically-stimulated fibroblasts derived from individuals with CCD	63
4.3	iPSC-derived mesenchymal stem cells obtained from a patient with RUNX2-mutation	66
4.3.1	Gene arrays for expression analysis in Control and RUNX2 mutation-patient	66
4.3.2	Characterization of iPSCs-derived MSCs and evaluation of iPSCs-derived MSCs through cytofluorimetric analysis	66
4.3.3	Modulation of TGF β 1, TGF β R1 and miR9 in circulating progenitors' cells and iPSCs-derived MSCs	67
4.3.4	Autophagy in circulating progenitors' cells and iPSCs-derived MSCs.	69
4.3.5	Transfection in MSCs cell line with MiR9 mimic and MiR9 silencer	69
4.4	Impact of physical activity in MSCs	70

4.4.1	Gender-Associated microRNAs Profiles in Peripheral Blood	70
4.4.2	Regardless of Gender, Half Marathon Distinctly Alters the Expression of Other PBMCs miRNAs	72
4.4.3	Modulation of Circulating miRNAs After Half Marathon	73
4.4.4	Half Marathon Performance Enhances MYOD Expression in Myoblasts	73
4.5	NorthCape4000 (NC4000) race	75
4.5.1	Impact of training and NC4000 on the commitment of mesenchymal stem cells	76
4.5.2	In SK muscle cells, training raises the amounts of sestrins and sirtuin.	77
4.5.3	Training and ultra-cycling mitigate the aging process of adipogenesis and enhance brown adipogenesis.	78
4.6	3D mid-brain organoid models	79
4.6.1	Comparison between wild-type/gene correct mid-brain organoids vs mutated mid-brain organoids	80
4.6.2	Comparison between BIL wild-type mid-brain organoids vs T413 mutated organoids	81
4.6.3	Immunofluorescence analysis of organoids at 40 days of differentiation	82
5	DISCUSSION	83
6	CONCLUSIONS	94
7	REFERENCES	96
	RINGRAZIAMENTI	116

ABSTRACT

This study addresses several aspects of mesenchymal stem cells and their differentiation, with a focus on the impact of FBXW11 in osteogenesis. The research reveals an upregulation of FBXW11 during the middle phase of osteogenesis, influencing the expression of key genes such as RUNX2 and β -catenin. Silencing FBXW11 in osteogenic cells resulted in elevated levels of both RUNX2 and β -catenin. However, FBXW11 silenced cells exhibited reduced expression of osteogenic maturation-associated genes in the late phase of differentiation, emphasizing FBXW11's crucial role in osteogenic maturation.

The study also explores the relationship between FBXW11, RUNX2, and β -catenin in pathological conditions such as cleidocranial dysplasia (CCD) and osteosarcoma. In CCD, FBXW11 levels may counteract dysregulated β -catenin, while osteosarcoma cells show lower FBXW11 levels and higher β -catenin, indicating a potential role in disease development.

Furthermore, the research identifies novel C-terminus RUNX2 mutations in CCD patients and highlights their impact on osteogenic commitment. Mutations lead to an accumulation of autophagic genes, hindering osteogenesis.

The study also delves into the gender-specific modulation of microRNAs following physical activity, emphasizing their role in myogenesis.

The investigation extends to the effects of ultra-endurance cycling on progenitor cells, demonstrating changes in body composition, adipogenesis, and myogenesis. The study introduces the evaluation of potential driver genes and transcription factors involved in these mechanisms, shedding light on the impact of physical training and ultra-cycling on cellular metabolism.

Finally, the research concludes by emphasizing the need for further exploration of the crosstalk between the brain and bone and suggests testing the molecules used in mid-brain organoids on mesenchymal cells in osteogenic differentiation.

ABSTRACT (ITALIANO)

Questo studio affronta diversi aspetti delle cellule staminali mesenchimali e della loro differenziazione, con particolare attenzione all'impatto di FBXW11 nell'osteogenesi. La ricerca rivela una sovraregolazione di FBXW11 durante la fase intermedia dell'osteogenesi, influenzando l'espressione di geni chiave come RUNX2 e β -catenina. Il silenziamento di FBXW11 nelle cellule osteogeniche ha portato a livelli elevati sia di RUNX2 che di β -catenina. Tuttavia, le cellule silenziate da FBXW11 hanno mostrato una ridotta espressione dei geni associati alla maturazione osteogenica nella fase tardiva della differenziazione, sottolineando il ruolo cruciale di FBXW11 nella maturazione osteogenica.

Lo studio esplora anche la relazione tra FBXW11, RUNX2 e β -catenina in condizioni patologiche come la displasia cleidocranica (CCD) e l'osteosarcoma. Nella CCD, i livelli di FBXW11 possono contrastare la β -catenina disregolata, mentre le cellule dell'osteosarcoma mostrano livelli di FBXW11 inferiori e β -catenina più elevati, indicando un potenziale ruolo nello sviluppo della malattia.

Inoltre, la ricerca identifica nuove mutazioni RUNX2 del segmento C-terminale nei pazienti con CCD e ne evidenzia l'impatto sull'impegno osteogenico. Le mutazioni portano ad un accumulo di geni autofagici, ostacolando l'osteogenesi.

Lo studio approfondisce anche la modulazione genere-specifica dei microRNA in seguito all'attività fisica, sottolineando il loro ruolo nella miogenesi.

L'indagine si estende agli effetti del ciclismo di ultra-resistenza sulle cellule progenitrici, dimostrando cambiamenti nella composizione corporea, nell'adipogenesi e nella miogenesi. Lo studio introduce la valutazione di potenziali geni driver e fattori di trascrizione coinvolti in questi meccanismi, facendo luce sull'impatto dell'allenamento fisico e dell'ultra ciclismo sul metabolismo cellulare.

Infine, la ricerca si conclude sottolineando la necessità di approfondire il crosstalk tra cervello e ossa e suggerisce di testare le molecole utilizzate negli organoidi del mesencefalo sulle cellule mesenchimali in differenziamento osteogenico.

ABBREVIATIONS

- **3'UTR**: 3' untranslated region
- **AbI**: primary antibody
- **AbII**: secondary antibody
- **AD**: Alzheimer's disease
- **AD3**: a transactivation domain
- **ALPL**: alkaline phosphatase
- **AN**: after NC4000
- **ARS**: alizarin red staining
- **ATG**: autophagy-related gene
- **BAT**: brown adipose tissue
- **BBB**: blood-brain barrier
- **Bglap**: bone carboxyglutamate protein
- **BIA**: Bioelectrical Impedance Analysis
- **BM**: bone marrow
- **BMI**: Bone Mineral Index
- **BMPs**: Bone Morphogenetic Proteins
- **BMSCs**: Bone Marrow Stem Cells
- **BN**: a week before NC4000
- **BPP**: before the preparation period
- **C/EBP**: CCAAT/enhancer-binding protein
- **CCD**: Cleidocranial dysplasia
- **CCR**: C-C chemokine receptor
- **CD**: cluster of differentiation
- **cDNA**: complementary DNA
- **cMSCs**: Circulating mesenchymal stem cells
- **CNS**: central nervous system
- **CPCs**: Circulating progenitor cells
- **DA**: dopaminergic
- **ddPCR**: digital droplet PCR
- **DEXA**: Dual-Energy X-ray Absorptiometry
- **Dlx5**: distal-less homeobox 5
- **ECM**: Extracellular Matrix
- **EGR1**: early growth response 1
- **Erk1/2**: extracellular signal-regulated kinase 1 and 2
- **ESC**: embryonic stem cell
- **ESR1**: Estrogen receptor 1
- **FAM**: carboxyfluorescein
- **FFM**: fat-free mass
- **FM**: fat mass
- **GC**: gene correct
- **GFAP**: Glial Fibrillary Acidic Protein
- **hHNR**: Human Hormone Nuclear Receptor
- **HOB**: human osteoblasts
- **IGF**: Insulin-like Growth Factor
- **iPSCs**: Induced pluripotent stem cells
- **iPSCs-MSCs**: Induced Pluripotent Stem Cells-derived Mesenchymal Stem Cells
- **MAP2**: Microtubule-associated protein 2

- **MHY2**: myosin heavy chain 2
- **miR**: microRNA
- **MM**: muscle mass
- **MRFs**: myogenic regulatory factors
- **mRNA**: messenger RNA
- **MSCs**: Mesenchymal Stem Cells
- **NAD+**: nicotinamide adenine dinucleotide
- **NC4000**: NorthCape4000
- **NESCs**: Neuronal epithelial stem cells
- **NLS**: nuclear localization signal
- **NMTS**: nuclear matrix targeting signal
- **Os**: osteogenically
- **PBMCs**: Peripheral Blood Mononuclear Cells
- **PBS**: phosphate-buffered saline
- **PD**: Parkinson's disease
- **PFA**: paraformaldehyde
- **PGC-1 α** : peroxisome proliferator-activated receptor- γ co-activator-1 α
- **pHM**: post-half marathon
- **PKA**: protein kinase A
- **PNS**: peripheral nervous system
- **PPAR γ** : Peroxisome Proliferator-Activated Receptor Gamma
- **PSA**: Penicillin Streptomycin Amphotericin B
- **PTEN**: phosphatase and tensin homolog
- **PTH**: parathyroid hormone
- **PTS**: proline/serine/threonine-rich domain
- **QA**: glutamine/alanine-rich domain
- **RD**: repression domain
- **RHD**: Runt homology domain
- **RT**: room temperature
- **RUNX2**: Runt-related transcription factor 2
- **SCF**: Skp1-cullin-F-box
- **SESN1**: sestrin 1
- **SESN2**: sestrin 2
- **SeV**: Sendai virus
- **SIRT1**: Sirtuin 1
- **SKMC**: Human Skeletal muscle cells
- **TFs**: Transcription Factors
- **TGF- β** : Transforming Growth Factor-beta
- **TH**: Tyrosine Hydroxylase
- **UCP1**: uncoupling protein 1
- **UPS**: ubiquitin-proteasome system
- **VAT**: visceral adipose tissue
- **WAT**: white adipose tissue
- **WT**: molecular weight

1 INTRODUCTION

1.1 Mesenchymal stem cells (MSCs)

Adult multipotent progenitor stromal cells with a mesodermal origin are known as *mesenchymal stem cells*. Friedenstein et al. ¹⁻³ successfully identified and characterized the first mesenchymal stem cells (MSCs).

MSCs are non-hematopoietic cells that exhibit substantial tissue heterogeneity, long-term *ex vivo* proliferation, self-renewal potential, and multilineage differentiation ^{4 5}. MSCs are defined by their ability to differentiate into distinct mesenchymal lineages, such as bone, fat, and cartilage. Recent research revealed the existence of pluripotent cells that can differentiate into hepatocytes, and endothelia as well as cells of the mesoderm and endoderm lineages ^{5 6}. Although MSCs lack specific surface markers, they can be identified for the presence of some, such as CD44, CD73, CD90, and CD105, and the absence of others, such as CD45, CD34, CD19, and CD31 ⁷. MSCs have been extensively studied for their multi-lineage differentiation potential both *in vitro* and *in vivo*. The differentiation of mesenchymal stem cells (MSCs) into specific mature cell types is a highly regulated and complex process that involves a multitude of stimuli, inhibitors, and signaling pathways ⁸. Some of the key factors and regulators involved in this process are cytokines and growth factors that are crucial for driving the differentiation of MSCs into specific lineages⁹. These signaling molecules include Bone Morphogenetic Proteins (BMPs) promote osteogenic differentiation¹⁰, Transforming Growth Factor-beta (TGF- β) plays a role in chondrogenic differentiation ¹¹, Insulin-like Growth Factor (IGF) promote both osteogenic and chondrogenic differentiation ¹², Extracellular Matrix (ECM) Molecule with a role in the composition and mechanical properties of the ECM in the cellular microenvironment can influence MSC differentiation ¹³ (Figure 1), Transcription Factors (TFs) are proteins that regulate gene expression and are central to the differentiation process associated with specific transcription factors such as RUNX2 is essential for osteogenic differentiation ¹⁴; *Sox9* is important for chondrogenic differentiation¹⁵; MyoD is required for myogenic differentiation¹⁶ and PPAR γ regulates adipogenic differentiation¹⁷. In addition, Microenvironmental Factors like oxygen tension, pH, and mechanical forces can influence MSC differentiation, and Epigenetic Regulation such as DNA methylation and histone

modifications, are essential for determining cell fate during differentiation. These modifications can either activate or suppress genes involved in lineage commitment.

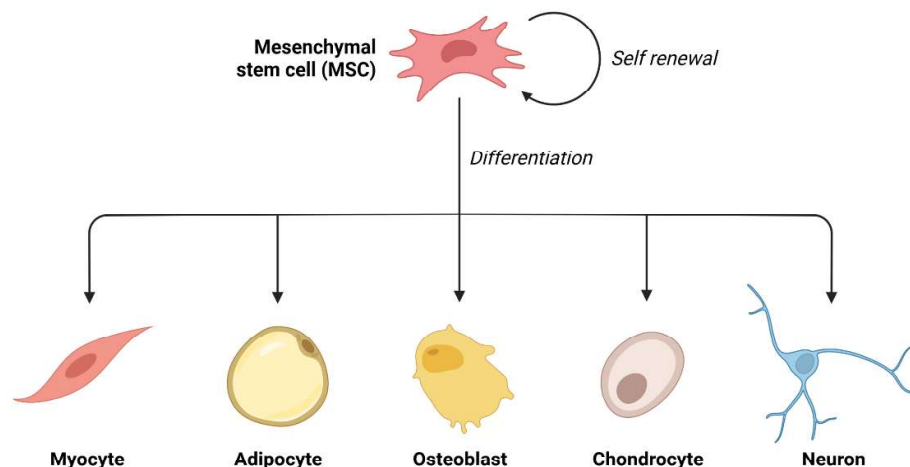


Figure 1 MSCs differentiation. (created by biorender.com)

1.1.1 Osteogenic differentiation

The expression of the osteogenic master gene RUNX2 is essential for Mesenchymal Stem Cells (MSCs) commitment to osteogenic differentiation¹⁸. A crucial role is carried out by WNT signaling pathways and Bone morphogenetic proteins (BMP) for osteogenesis. BMP signaling activates Smad proteins, leading to the expression of the master regulator RUNX2, which commits mesenchymal stem cells to the osteogenic lineage. The WNT pathway, specifically the canonical WNT/ β -catenin signaling, also influences RUNX2 expression and osteoblast formation^{19 20}.

Systemic hormones like parathyroid hormone (PTH), glucocorticoids, and estrogens, as well as local growth factors like TGF- β , IGF, FGF-2, and VEGF, regulate osteogenic commitment and differentiation¹⁸.

1.1.1.1 Runx2

RUNX2 is part of a family of small transcription factors characterized by a Runt-domain²¹. Eight exons and many introns compose up the 227,766-nucleotide-long mRNA sequence for RUNX2 (Figure 2).

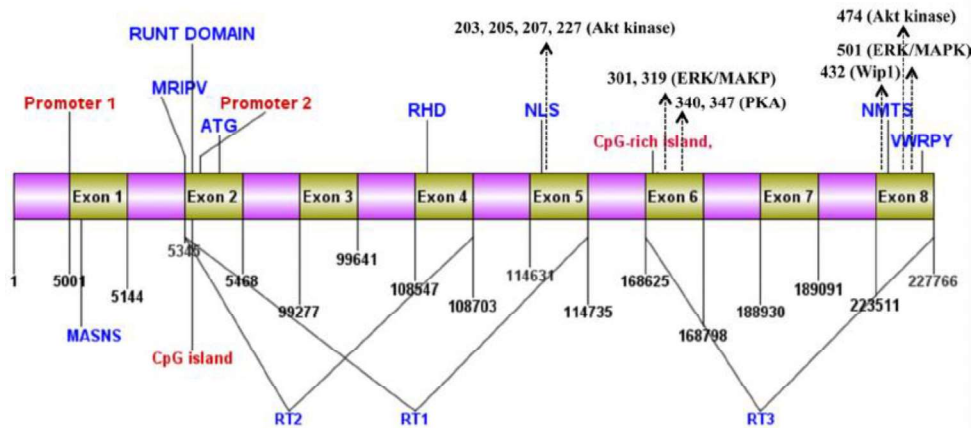


Figure 2. The mRNA sequence of *RUNX2* includes its respective exons and introns, as well as specific functional domains. (*Runx2: Structure, function, and phosphorylation in osteoblast differentiation. Int J Biol Macromol.* 2015)

It also has two alternative promoters (P1 and P2) that control the transcription of the gene in all vertebrates, resulting in the production of two major gene products: P1 promotes the transcription of the isoform MASNS, which includes all eight exons and results in a total of 521 amino acids, while P2 promotes the transcription of the isoform MRIPV, which includes exons 2 to 8 and results in a total of 507 amino acids^{21 22}. Most enhancers that control *RUNX2* expression have yet to be discovered²² such as early growth response 1 (EGR1)²³. *RUNX2* gene is known to be characterized by heterogeneous active domains, such as the nuclear localization signal (NLS), Runt homology domain (RHD), VWRPY region, glutamine/alanine-rich domain (QA), proline/serine/threonine-rich domain (PST), and nuclear matrix targeting signal (NMTS), which all play important roles in the functionality of the Runx2 protein. Additionally, the majority of its functional characteristics, including DNA binding, are derived from a 128 amino acid sequence that is remarkably conserved²¹. In exons 2 and 6, the CpG-rich islands may be seen. Exon 5 encodes the nuclear localization signal (NLS), and exons 2-4 contain the runt homology domain (RHD). Exon 6 contains the PST domain, while exon 8 has the VWRPY and nuclear matrix targeting signal (NMTS) domains. RT1, RT2, and RT3 are the names of the *RUNX2* truncated exons that are expressed during viral infections and cancers: Exons 2–5 are used to code for RT1, exons 2–4 are used for RT2, and exons 6–8 are used for RT3^{21 22}.

During osteoblast formation, *RUNX2* is only minimally expressed in uncommitted mesenchymal cells, but its protein level rises in pre-osteoblasts, reaches a peak in immature osteoblasts, and then declines once more in mature osteoblasts²⁴.

Essential for the expression of RUNX2 and osteoblast commitment lineage from mesenchymal stem cells (Figure 3) is the expression of *Ihh* in the prehyperitrophic chondrocytes²⁵. The Hedgehog signaling pathway (*Ihh*, *Gli1*, and *Ptch1*), Fgf signaling pathway (*Fgfr2* and *Fgfr3*), Wnt signaling pathway (*Tcf7*, *Wnt10b*, and *Wnt1*), *Pthlh* (*PthrP*), and *Dlx5* (distal-less homeobox 5) signaling pathway proteins have been identified to directly and reciprocally upregulate *Runx2*. This leads to an increase in the expression and protein activity of *Runx2*^{26 27 28}.

In mice, it has been demonstrated that an essential role in osteoblast commitment is also played by *SP7* and *CTNNB1* which in turn activate the Wnt signaling pathway¹⁹. In the absence of these two transcription factors, there is no presence of osteoblasts²⁹. Although mice with *Runx2* deletion are also completely devoid of osteoblasts; *RUNX2* is expressed in the mesenchymal cells of mice lacking *SP7* and *CTNNB1*, indicating that *RUNX2* acts upstream of *SP7* and Wnt signaling in osteoblast differentiation^{28 30}.

RUNX2 boosts the synthesis of PI3K subunits (p85 and p110) and AKT, improving its DNA binding activity, in immature MSCs, pre-chondrocytes, and osteoblastic cells. Another indication of *RUNX2*'s function in bone growth is its binding site in the promoter region of *RANKL*³¹. Pre-osteoblasts are then developed into immature osteoblasts through the canonical Wnt signaling pathway^{32 33}. *RUNX2* promotes *Sp7* expression during the pre-osteoblast stage. Additionally, *SP7* and WNT signaling activate the osteoblast-specific *RUNX2* enhancer, whereas *RUNX2* promotes the Wnt signaling pathway by upregulating the expression of *TCF7* and *WNT10b*^{34 26}. Furthermore, Gaur et al.³⁴ provide evidence of the direct regulation of *RUNX2* through canonical WNT signaling and suggest that *RUNX2* is a target of β -catenin/*TCF1* for the stimulation of bone formation. It is hypothesized that WNT/*TCF1* signaling, akin to BMP/TGF- β signaling, activates the gene expression of *RUNX2* in mesenchymal cells to control osteoblast differentiation and skeletal development.

In developing osteoblasts, *RUNX2* promotes the expression of the bone matrix protein genes *Colla1*, *Colla2*, *Ibsp*, *Spp1*, and bone carboxyglutamate protein (*Bglap*)/*Bglap2*^{28 35}. The osteoblasts grow as a result, and they produce a lot of bone matrix proteins. Osteocalcin (*Bglap*/*Bglap2*) is in charge of keeping the distinctive collagen fibers and apatite crystals parallel during this osteoblast maturation³⁶. Furthermore, the co-transcriptional factor *CBFB*, which stabilizes the

Runx2 protein by inhibiting its ubiquitination, enhances RUNX2's DNA binding. Runx2/Cbfb thus regulates the proliferation and development of osteoblast-lineage cells and chondrocytes by activating several signaling pathways and by the reciprocal regulation of those signaling pathways^{37 26}.

Moreover, Deiana et al.³⁸ have also shown the involvement of RUNX2 in the development of melanoma and identified RUNX2 as a stemness marker for cancer. In breast cancer, pancreatic cancer, prostate cancer, lung cancer, ovarian epithelial cancer, and melanoma, heightened levels of RUNX2 expression have been observed.

In melanoma, RUNX2 has been considered a molecular regulator of epithelial-to-mesenchymal transition and proliferation^{36 37}. In general, increased expression of the RUNX2 gene has been found in patients with bone metastases, suggesting that this transcription factor may be considered a mesenchymal stem marker for cancer⁴¹. The role of RUNX2 in the different stages of malignancies has been widely demonstrated to induce gene expression of molecular targets associated with tumor progression, invasion, metastasis as well as migration. In addition, was reported that RUNX2 promotes migration and melanoma proliferation and restricts the apoptosis through its Runt domain⁴²; the upregulation of angiogenesis, consequent to RUNX2 overexpression, may represent a critical step for tumor metastasis.⁴¹

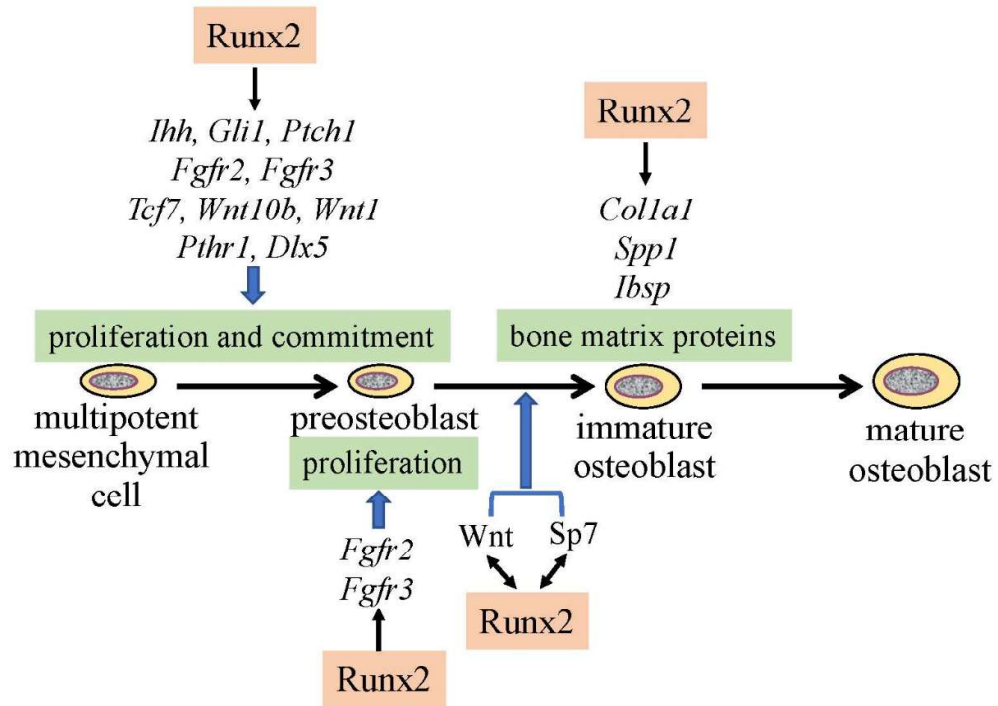


Figure 3 RUNX2 regulates the proliferation and differentiation of osteoblast-lineage cells by influencing multiple signaling pathways. (Differentiation and Functions of Osteoblasts by Runx2. *Int. J. Mol. Sci.* 2019)

1.1.1.2 The Role of FBXW11

The presence of damaged materials or non-functional proteins can result in significant harm and alterations to cellular homeostasis⁴³. Crucially, microRNAs play a post-transcriptional regulatory role in modulating the ubiquitin-proteasome system. It has been shown that miR-221, by targeting E3 ubiquitin-protein ligase homolog (MDM2), can influence the activity of p53 (TP53) in hepatocellular carcinoma⁴⁴. The recognition of proteins targeted for degradation is facilitated by members of the F-box protein family, which are implicated in various biological processes, including hematopoietic regulation and neoplastic transformation⁴⁵. Furthermore, the FBXW11 gene, responsible for encoding an F-box protein that is a constituent of the Skp1-cullin-F-box (SCF) ubiquitin ligase complex, plays a pivotal role in various signaling pathways. This includes essential contributions to cell cycle regulation, differentiation, development, and metabolism. Specifically, FBXW11 is capable of recognizing and binding phosphorylated β -catenin, exerting a negative regulatory influence on the Wnt/ β -catenin pathway⁴⁶. The FBXW subfamily consists of 10 members, including FBXW1, 2, 4, 5, and 7–12. Notably, FBXW1 is alternatively designated as b-TrCP1, while FBXW11 is also recognized as b-TrCP2. These two members, b-TrCP1 and b-TrCP2, have been extensively

studied and are implicated in various cellular processes. They play significant roles in cell cycle progression, migration, and the regulation of signal transduction pathways⁴⁷. b-TrCP1 is encoded by the BTRC gene on chromosome 10, while b-TrCP2 (also known as FBXW11, FBXW1B, and HOS) is encoded by the FBXW11 gene on chromosome 5⁴⁷. There is a suggestion that b-TrCP1 and b-TrCP2 are functionally redundant proteins with similar characteristics. However, reports indicate that silencing b-TrCP2 leads to a reduction in cell growth while silencing b-TrCP1 has the opposite effect and promotes cell growth. Furthermore, silencing b-TrCP2 has been shown to decrease cell migration and induce autophagy, whereas silencing b-TrCP1 does not elicit these effects. These findings suggest distinct and non-overlapping roles for b-TrCP1 and b-TrCP2 in cellular processes, despite their structural similarities⁴⁸. These results imply that b-TrCP2 is primarily involved in the regulation of cellular activities and that b-TrCP1 and b-TrCP2 do not have any redundant roles. FBXW11 has the ability to modify transcription factors and regulators linked to the cell cycle. Given that FBXW11 can either stimulate or inhibit cellular growth, a role that is depending on the type of cell has been proposed for it.⁴⁶ The contrasting outcomes arise from substrates that function as either activators or suppressors of the cell cycle, and both types are susceptible targets for FBXW11.

Lower expression of FBXW11 has been observed by Wang et al.⁴⁹ in long-term hematopoietic stem cells, while its expression is higher in short-term hematopoietic stem cells and various hematopoietic progenitor cells. This pattern suggests that FBXW11 is predominantly expressed in mature progenitor cells. Interestingly, overexpression of FBXW11 has been noted in acute lymphocytic leukemia, indicating its potential involvement in this type of leukemia. Additionally, FBXW11 has been found to play a crucial role in hematopoietic stem cell repopulation. These findings underscore the diverse roles of FBXW11 in different stages of hematopoiesis and its potential implications in hematological disorders⁵⁰⁵¹. Moreover, FBXW11 is subject to post-transcriptional regulation by microRNAs. In studies conducted on tumor cells, it has been established that FBXW11 is a target of miR-221. Specifically, in the context of osteosarcoma, it has been reported that miR-221 promotes resistance to cisplatin. This suggests a potential role for the miR-221/FBXW11 axis in influencing the sensitivity of osteosarcoma cells to cisplatin-based treatments⁵². While FBXW11 has been extensively studied in the

context of hematopoietic stem cells and various tumor types, there is a notable gap in research regarding its role in the osteogenic lineage. It is established that the Wnt/ β -catenin pathway is involved in inducing RUNX2 expression during osteogenic commitment. However, the specific interplay between FBXW11 and the osteogenic lineage remains unexplored. Further investigations into the potential involvement of FBXW11 in osteogenesis could provide valuable insights into the regulatory mechanisms governing this process and expand our understanding of its broader functional roles³⁴. Indeed, the regulation of RUNX2 extends beyond transcriptional control, involving post-transcriptional mechanisms. Notably, recent findings indicate that miR-204 silencing in MSCs leads to an increase in RUNX2 protein levels, particularly observed during the intermediate phase of osteogenic differentiation. This suggests that miR-204 plays a role in modulating RUNX2 expression levels during the osteogenic differentiation process, shedding light on the intricate post-transcriptional regulatory network involved in osteogenesis⁵³.

1.1.2 Adipogenic differentiation

Adipogenic differentiation typically begins with the induction of MSCs or precursor cells toward the adipocyte lineage. Adipogenic differentiation is a tightly regulated process influenced by various factors, including hormones like insulin, glucocorticoids, and specific growth factors. The balance of these factors and the activation of the transcriptional machinery ultimately determine whether precursor cells differentiate into adipocytes^{54 55}. The two main transcription factors that drive adipogenesis are PPAR γ (Peroxisome Proliferator-Activated Receptor Gamma) which is often referred to as the master regulator of adipogenesis and activates genes involved in lipid metabolism and adipocyte maturation and C/EBP (CCAAT/enhancer-binding protein) family where these transcription factors, including C/EBP α , C/EBP β , and C/EBP λ , work together with PPAR γ to promote adipocyte differentiation⁵⁶. The activation of PPAR γ and C/EBP transcription factors leads to the upregulation of genes associated with adipocyte formation and function. These genes include those involved in lipid synthesis (such as FABP4 and adiponectin) and lipid storage (lipoprotein lipase)⁵⁵. As adipogenic differentiation progresses, cells change morphology, become more spherical, and acquire the characteristic appearance of mature adipocytes. Fully differentiated adipocytes are

capable of actively taking up and storing lipids. They also secrete adipokines, which are signaling molecules that regulate various physiological processes, including metabolism⁵⁷ (Figure 4).

1.1.3 Myogenic differentiation

Myogenic differentiation is tightly regulated and influenced by various factors, including growth factors like insulin-like growth factor (IGF), cytokines, and environmental cues⁵⁸.

Myogenic differentiation is initiated by exposing precursor cells, such as MSCs or satellite cells (found in muscle tissue), to specific signals that promote muscle lineage commitment. One of the key inducers of myogenic differentiation is the family of transcription factors known as myogenic regulatory factors (MRFs).

MRFs are a group of transcription factors that are central to myogenic differentiation. The key MRFs include MYOD which is often referred to as the master regulator of myogenesis. It plays a crucial role in activating genes associated with muscle differentiation; Myogenin is another MRF that promotes the differentiation of myoblasts into mature muscle cells. MYF5 and MRF4 are additional MRFs that are involved in muscle development and differentiation⁵⁸. The activation of MRFs leads to the upregulation of genes associated with muscle development and function. These genes include those encoding structural proteins like myosin, actin, and troponin (Figure 4).

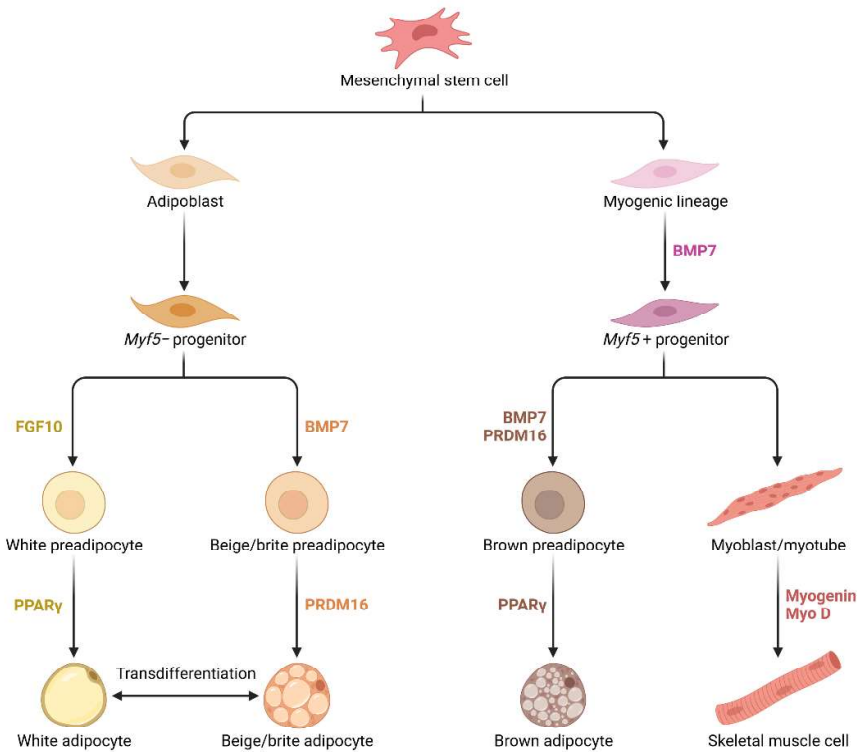


Figure 4 Adipogenic and myogenic commitment (created by biorender.com)

1.1.4 Induced Pluripotent Stem Cells

Induced pluripotent stem cells (iPSCs) represent a distinct cell population capable of dedifferentiating from adult cells through gene reprogramming technology. This transformation is achieved by introducing a cocktail of pluripotency transcription factors, namely Oct4, Sox2, Klf4, and c-Myc, which are subsequently expressed artificially^{59 60}. When this process involves the integration of these genes into the cell's genome using viral vectors or integrating plasmids, it has the potential to lead to persistent or reactivated transgene expression during iPSC differentiation, as well as tumorigenic insertional mutations and epigenetic changes. Various techniques, including plasmid vectors, minicircle DNA vectors, mRNA, adenovirus, Sendai virus, proteins, small molecules, and episomal methods, have been explored to generate transgene-free iPSCs to address these concerns⁶¹. In this context, the Sendai virus serves as a non-integrating system that can infect cells, delivering its genome into the cytoplasm without the risk of genomic insertion and modification, thereby enabling iPSCs to be free of the virus after nearly ten culture passages⁵⁹.

iPSCs were initially discovered in 2006 during the retroviral transduction of mouse fibroblasts. They exhibited an embryonic stem cell (ESC) morphology, the potential for in vitro differentiation, and the ability to induce teratomas due to the influence of oncogenes in the stemness vectors⁵⁹. It was noted that reprogramming efficiency was low, with fewer than 1% of iPSC colonies undergoing successful transduction. The advancement of iPSC technology from somatic cells has eliminated the need to terminate embryos to create pluripotent cells. This not only addresses ethical concerns but also eliminates the risk of immune rejection, enabling autologous transplantation, enhanced accessibility, and personalized treatment. iPSCs have proven to be a valuable resource for regenerative medicine due to their ability to self-renew and differentiate into a wide range of specialized cells, derived from any human source⁵⁹. Furthermore, iPSCs have been instrumental in understanding the causes and pathology of certain diseases through the development of disease models. They have been employed to replicate rare genetically driven disorders, such as Marfan syndrome, meta tropic dysplasia, craniometaphyseal dysplasia, and fibrodysplasia ossificans progressive⁶⁰.

In specific cases of over-confluency in cell culture, iPSC colonies can be induced toward differentiation, which is valuable for clinical applications related to various diseases. For instance, iPSC-derived mesenchymal stem cells (MSCs) exhibit greater stability than primary MSCs obtained from other tissues in terms of molecular signature, proliferation capacity, tissue healing, and differentiation capabilities. Moreover, iPSC-derived MSCs closely resemble their primary counterparts in terms of immunophenotype, three-lineage differentiation capacity, and structure. In animal disease models, iPSC derived MSCs exhibit a higher regenerative potential. Additionally, they are suitable for large-scale production in cell culture bioreactors, given that iPSCs represent a homogeneous, stable, and virtually limitless source⁶² (Figure 5).

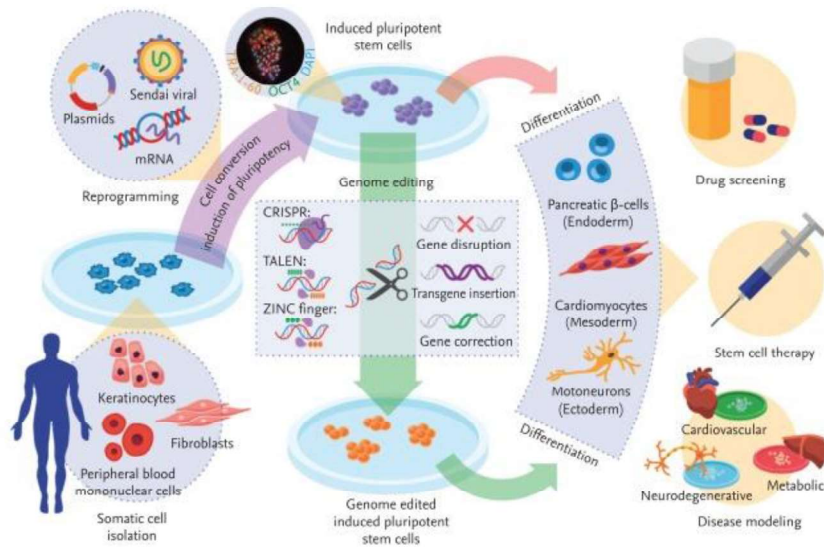


Figure 5 Generation of iPSCs tailored to individual patients and their clinical applications (Diecke S. et al Recent technological updates and clinical applications of induced pluripotent stem cells. Korean J Intern Med. 2014 Sep.)

1.2 Bone cells and tissue

Bone is a connective tissue with strong mineralization and metabolic activity. It carries out essential biological processes like mechanical support, mineral storage, blood cell production, and protection of internal organs like the heart, lungs, brain, and spinal cord. It also includes the bone marrow, the principal repository of mesenchymal stem cells⁶³.

Bone can replace worn-out or injured tissue by remodeling, which is a fundamental and complex process necessary to adjust the constant mechanical changes required for skeletal activities in a variety of environmental settings¹⁸.

The main players in the bone remodeling process are osteoblasts and osteoclasts, with a special involvement in bone creation and bone resorption, respectively. Osteocytes derived from mature osteoblasts, regulated osteoblasts and osteoclast activity to maintain bone homeostasis and structure. The balance between bone synthesis and resorption is influenced by several regional and systemic factors including hormones, cytokines, chemokines, and biomechanical stimulation^{64 18}.

1.2.1 Pathological conditions: Cleidocranial dysplasia (CCD)

Skeletal dysplasia represents a diverse and significant group of hereditary skeletal conditions, often posing challenges for accurate diagnosis. This difficulty arises from the rarity of individual cases, with the most common skeletal dysplasia, such as achondroplasia and osteogenesis imperfecta, affecting only a small fraction of the population (approximately 1 in 20,000 to 30,000 individuals). However, it's important to note that these conditions collectively impact a relatively higher number of people, with an estimated occurrence in the range of 1 in 3,000 to 5,000 individuals ⁶⁵.

Cleidocranial dysplasia (CCD), also known as cleidocranial dysostosis, mutational dysostosis, or Scheuthauer Marie-Sainton syndrome, is a rare hereditary skeletal disorder. CCD primarily affects bones formed through intramembranous ossification, including the clavicles, cranium, facial bones, as well as the appendicular skeleton and spine ⁶⁵.

The disease can manifest with a wide range of phenotypic variations, even within the same family. These variations can encompass mild dental changes to severe osseous disorders and osteoporosis. It's important to note that CCD, while impacting quality of life, is not life-threatening, and individuals with the condition typically have a normal life expectancy ^{65 66 67}.

CCD does not exhibit ethnic or gender preferences, and it can affect several consecutive generations within a family ⁶⁸. Mutations in the RUNX2 gene (Runt-related transcription factor 2) have been confirmed as the causative factor behind Cleidocranial Dysplasia (CCD) ⁶⁹. In RUNX2 knockout mice, bone development is impaired, even though cartilage development remains unaffected. Moreover, heterozygous RUNX2 mutant mice exhibit CCD characteristics, including open fontanelles ⁷⁰. Two RUNX2 c-terminus nonsense mutations that had never been previously reported on affected osteogenic differentiation, according to Dalle Carbonare et al. ⁶⁷.

The decreased expression of RUNX2 downstream genes contributes to poor osteogenic differentiation. Nonetheless, they brought attention to the p53 dysregulation's role in CCD illness for the first time. It has been proposed that RUNX2 mutations impact osteogenesis via inhibiting p53, which prevents osteogenic maturation, as well as by reducing the expression of genes that code for skeletal matrix proteins. Thus, the knowledge that RUNX2 mutations may disrupt

signaling pathways provides fresh opportunities for therapeutic targets and could have significant effects on the way CCD is treated clinically.

1.3 Impact of physical activity in modulating MSCs

The recognition that bone functions as an endocrine organ, responsible for regulating energy metabolism, has affirmed the understanding that hormones produced by bones play a pivotal role in the regulation of muscle functions and the facilitation of adaptation to exercise ⁷¹. Numerous tissues, including bone, have been shown to secrete proteins in response to exercise. These proteins may contribute to the advantages of exercise and have prospects for therapeutic approaches to maximize its advantages ^{10 72}. Physical exercise is widely recognized to be beneficial for enhancing mental health and well-being as well as for preventing and treating degenerative disorders ⁷³. Exercise can increase the quantity and caliber of stem cells that develop into bone or muscle. A higher quality of life for both young and old is made possible in large part by stem cells ⁷⁴. Several studies support exercise as a possible treatment strategy to improve bone and muscle health in patients with illnesses, to reduce the negative impacts of these disorders ^{75 76 77 78}.

Non-coding RNAs and cytokines have been shown to play a role in promoting bone metabolism, both in the absence of bone pathologies and in physiological conditions, also known as the body's normal state of health, as well as in response to lifestyle factors like a physical activity that demands energy expenditure. Conversely, leading a sedentary lifestyle increases the risk of metabolic changes, which in turn increases the risk of diseases like cardiovascular disorders or conditions associated with skeletal degenerative processes ^{79 80}.

Primarily, recognizing the significance of physical activity in preventing non-communicable diseases like obesity, hypertension, or elevated cholesterol levels, it is evident that promoting physical activity represents a successful strategy for alleviating the strain on healthcare systems and enhancing overall well-being.

In recent years, there has been a growing interest in running, particularly among recreational runners participating in 10 km and half-marathon races, where the physical demands are less intense compared to longer distances like marathons. Despite the lower physical strain, these races still offer appreciable health benefits associated with endurance exercise ⁸¹.

During a half marathon, recreational runners typically maintain an exercise intensity ranging from 75% to 85% of their maximal aerobic capacity (VO₂max) for approximately 80 to 120 minutes⁸². This level of exertion elicits various acute cellular responses, including an upsurge in mitochondrial oxidative phosphorylation. Consequently, this metabolic activity results in the generation of reactive oxygen species (ROS)⁸³. Furthermore, during glycolysis, there is an increased anaerobic regeneration of nicotinamide adenine dinucleotide (NAD⁺) in its oxidized state, which results in the production of lactates and H⁺.⁸⁴

These mechanisms contribute to both muscle fatigue and exercise-induced muscle injury^{85 86}, form the basis for chronic training adaptations and the beneficial outcomes of endurance exercise. These favorable effects encompass cardio myogenesis, optimization of peripheral tissue microcirculation, augmentation of muscular satellite cells, and modulation of mesenchymal cell differentiation⁸⁷.

In this context, the expression of microRNAs (miRNAs) is enhanced under conditions of injury or excessive stress⁸⁵. MiRNAs are considered modulators of inflammation and mitochondrial metabolism, playing a role in muscle recovery and hypertrophy⁸⁸. Myogenesis and muscle activity are intricately regulated by various signaling pathways, with their modulation governed by a diverse array of microRNAs (miRNAs). This includes the participation of both ubiquitous and tissue-specific miRNAs in the processes of muscle differentiation and activity⁸⁹.

Therefore, the modulation of miRNA expression plays a crucial role during physical exercise, and fluctuations in miRNA levels can be viewed as valuable biomarkers for assessing physical performance, stress, and muscle recovery. Overall, understanding the molecular mechanisms involving miRNAs provides insights into the intricate relationship between exercise, gene expression, and physiological adaptations in the context of endurance running.

Moreover, ultra-cycling events result in significant energy deficits, particularly in master athletes. In such cases, it becomes physiologically challenging to maintain a positive energy balance through caloric replenishment⁹⁰. The primary mechanism underlying the loss of fat mass (FM) is a prolonged energy deficit⁹¹. In recent years, there has been a notable trend toward increased participation and improved performance times in ultra-endurance cycling, despite the rising average age of participants^{92 93}.

Discrepancies in the literature exist regarding weight loss and potential alterations in lean mass during ultra-endurance cycling. A study analyzing FM and fat-free mass (FFM) before the Swiss Cycling Marathon aimed to characterize competitive ultra-cyclers⁹⁴. Other races, such as XX Alps 2004, showed a decrease in both FM and FFM using skin-fold measurements⁹⁵. Comparable findings were noted when employing Dual-Energy X-ray Absorptiometry (DEXA) following an 8,835 km mountain bike race⁹⁶. Conversely, an increase in lean mass was reported after an 883 km 6-day cycling stage race⁹⁷. Bioelectrical Impedance Analysis (BIA) demonstrated a reduction in FM and an increase in body mass and FFM after a 1000 km laboratory-based nonstop cycling, possibly due to liquid retention⁹⁸. Another study documented an augmentation in total body water after a 600 km ultra-cycling race. This led to a decrease in fat mass (FM), although there was no observed reduction in skeletal muscle mass (MM) when measured using skin-fold methods⁹⁸.

Despite the increasing popularity of amateur sports, there is a scarcity of studies investigating the impacts of ultra-endurance exercise on health. Specifically, the changes in fat mass (FM) and lean mass, and their potential associations with markers of muscle and adipose cell metabolism following ultra-endurance races, are not well-understood. A comprehensive analysis of training parameters and aerobic capacity may provide clarity on these modifications.

1.4 Crosstalk between bone and neuronal system

Innate immunity processes are managed by microglia, a different subpopulation of BM-derived cells that are responsible for the brain's immunological defense^{99 100}. It has been shown that hematopoietic cells generated from bone marrow (BM) can reach the brain and develop into microglia, which are brain-specific macrophages. In certain neurodegenerative illnesses, in particular, this permits them to colonize the central nervous system (CNS) while the blood-brain barrier (BBB) is still intact¹⁰¹.

CCR2 (C-C chemokine receptor type 2) and CCR5 (C-C chemokine receptor type 5) play essential roles as chemokine receptors involved in the migration of microglial cells. These receptors have been demonstrated to direct microglia derived from bone marrow through the blood-brain barrier (BBB), resulting in their accumulation within the brain parenchyma⁹⁹. When CCR2 expression is reduced,

the quantity of BM-derived microglial cells in the brain falls and amyloid-peptide levels increase ⁹⁹. Disturbances in the delicate balance of bone metabolism elevate the susceptibility to fractures and contribute to an increased prevalence of osteoporosis, particularly associated with aging or certain pathological conditions. One of the principal and vital pathways connecting bone metabolism and the brain is the Wnt/ β -catenin pathway. This pathway plays a critical role in the development of various aspects of midbrain dopaminergic (DA) neuron development. Parkinson's disease (PD) is characterized by the degeneration of neurons in the midbrain nigrostriatal dopaminergic (DA) system, influencing not only neuronal functions but also impacting bone metabolism ¹⁰². Parkinson's disease (PD) stands as the second most prevalent age-related neurodegenerative disorder impacting the nervous system, following Alzheimer's disease (AD). Clinically, PD manifests as a movement disorder. Individuals afflicted by this condition frequently exhibit an increased susceptibility to fractures, joint complications, and bone issues compared to age-matched controls. This heightened vulnerability can be attributed to diminished mobility, postural instability, and neurological impairment associated with PD ¹⁰³. The Wnt pathway is regulated through the activation and inactivation of non-canonical and canonical signals during brain development ¹⁰⁴. Recent findings shed light on the interaction between Parkin and β -catenin. In mice lacking the parkin protein, there were observed heightened levels of modified through conjugation and active (dephosphorylated) β -catenin. This suggests a potential regulatory role of Parkin in influencing the phosphorylation status of β -catenin, highlighting a novel aspect of their molecular interplay ¹⁰⁵. Its increase in Wnt/ β -catenin signalling leads to increased proliferation and death of dopaminergic (DA) neurons, suggesting that reduced β -catenin degradation may result in DA neurons being lost as they attempt to re-enter the cell cycle. This latter finding contrasts with the active role of Wnt/ β -catenin signaling during the development of midbrain DA neurons and stem cells, suggesting that pathological adult DA neurons may require less Wnt/ β -catenin signaling, while DA precursors may benefit from enhanced Wnt activation/ β -catenin signaling ^{106 107}.

The homeostasis of bone tissue is primarily governed by the Wnt/ β -catenin pathway. Upon secretion of Wnt, it binds to Frizzled and LRP5/6 receptors, leading to the accumulation of β -catenin in the cytoplasm. Subsequently, β -catenin translocates into the nucleus, where it regulates gene expression ¹⁰⁸. Moreover, it

has been established that Parkin can regulate the differentiation of Bone Marrow Stem Cells (BMSCs) into osteogenic lineages by modulating both β -catenin signaling and the autophagy process. The overexpression of parkin, serving as an E3 ubiquitin ligase, plays a role in these regulatory processes¹⁰⁹, could induce β -catenin expression and the process of autophagy, through the expression of specific osteomarkers¹¹⁰. Moreover, parkin overexpression accelerates bone healing in tibial fracture model markers¹¹⁰. Furthermore, parkin, identified as mutated in patients with recessive Parkinson's disease (PD), leads to impaired mitophagy characterized by the accumulation of damaged mitochondria. This mitochondrial dysfunction contributes to the loss of dopaminergic (DA) neurons at age¹⁰². Additionally, NR2F1, also referred to as nuclear receptor 2 families 1, is a member of the Human Hormone Nuclear Receptor (hHNR) family. It has been observed to be upregulated during osteogenesis and plays a crucial role in neurogenesis¹¹¹. Specifically, recent reports indicate a significant downregulation of NR2F1 transcript in dopaminergic neurons and midbrain organoids derived from Parkinson's disease (PD) patients with the LRRK2-G2019S mutation, in comparison to healthy controls¹¹² (Figure 6).

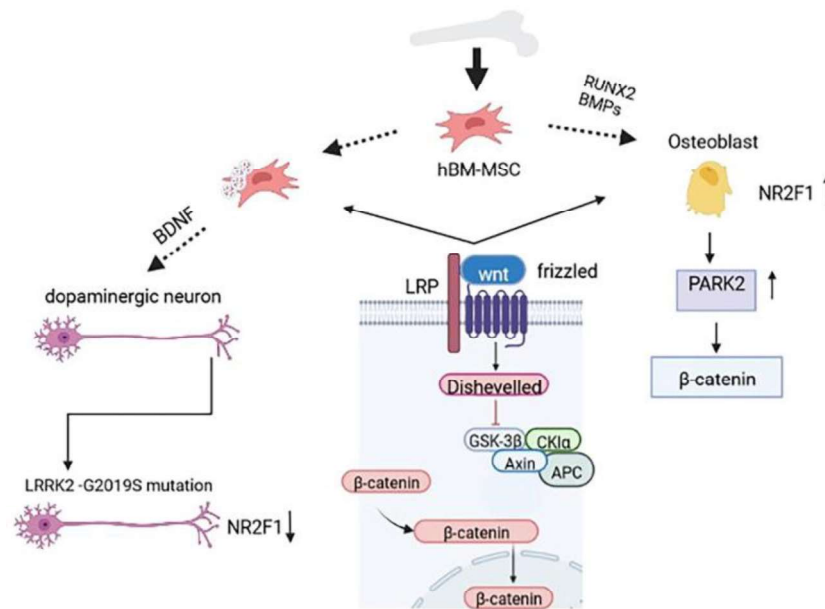


Figure 6 Bone morphogenetic proteins (BMPs) and the master regulator gene of osteoblastic commitment, *RUNX2*, are crucial contributors to the process of osteogenic differentiation (Minoia A, Dalle Carbonare L, Schwamborn JC, Bolognin S, Valenti MT. *Bone Tissue and the Nervous System: What Do They Have in Common?* *Cells*. 2022 Dec 22;12(1):51. doi: 10.3390/cells12010051. PMID: 36611845; PMCID: PMC9818711).

2 AIM OF THE STUDY

Mesenchymal stem cells are a source of pluripotent stem cells with the ability to differentiate into cells derived from connective tissue, including bone, fat, cartilage, muscle and non-mesodermal cells^{113 114 115}. Through a series of specific intrinsic signals, MSCs can undergo specific osteoblastic differentiation. Specifically, osteogenesis during skeletal development is driven by a succession of well-coordinated events involving epithelial-mesenchymal interaction, aggregation, and differentiation. A crucial role is carried out by WNT signaling pathways and Bone morphogenetic proteins (BMP). The classic WNT pathway is represented by WNT / β -catenin signaling which acts by inhibiting or inducing the formation of osteoblasts. In addition, the expression of the osteogenic master genes RUNX2 is essential for Mesenchymal Stem Cells (MSCs) commitment to osteogenic differentiation¹¹⁶.

The role of RUNX2 in the different stages of malignancies has been widely demonstrated to induce gene expression of molecular targets associated with tumor progression, invasion, metastasis as well as migration. In addition, our interest is understanding the function of the FBXW11 gene, which encodes an F-box protein, part of the Skp1-cullin-F-box (SCF) ubiquitin ligase complex, that plays an irreplaceable role in multiple signaling pathways, including the cell cycle, differentiation, development, and metabolism. FBXW11 can recognize and bind phosphorylated β -catenin and negatively regulate the Wnt/ β -catenin pathway⁴⁶.

As the Wnt/ β -catenin pathway plays a central role in stem cell differentiation, we aimed to analyze the modulation of FBXW11 during osteogenic commitment and differentiation. Additionally, we conducted string analyses to find proteins interacting with RUNX2 and examined p53 expression levels to gain a better understanding of how RUNX2 mutations affect osteogenic differentiation.

In addition, we deeply analyzed the CDD dysplasia, and we investigated the osteogenic capacity of two CCD patients' cells as well as the expression of the RUNX2 gene to analyze the impact of RUNX2 mutations in CCD patients.

We also aimed to investigate the effect of RUNX2 mutation on the expression levels of several genes involved in osteogenesis as well as on the autophagic process by analyzing Circulating progenitor cells (CPCs) and Induced Pluripotent Stem Cells-derived Mesenchymal Stem Cells (iPSCs-MSCs) obtained by using a

non-integrating and non-transmissible Sendai viral vector system from the blood of RUNX2-mutation patient characterized by a heterozygous variant NM_001024630.3: c.505C>T in exon 4 of the gene RUNX2.

Furthermore, modulation of mesenchymal stem cells and their differentiation can also be induced by different stimuli such as physical activity. Ultra-cycling events and half-marathons lead to important energy deficits, especially in master athletes, with the physiological impossibility of maintaining a positive balance with caloric replenishment ⁹⁰. A persistent energy deficit is the primary mechanism contributing to the loss of fat mass (FM) ⁹¹. The modulation of microRNA (miRNA) expression plays a significant role during physical exercise, and fluctuations in miRNA levels can serve as valuable biomarkers for assessing physical performance, stress, and muscle recovery. Sirtuin 1 (SIRT1) is a NAD⁺-dependent lysine deacetylase expression, that is downregulated in chronic inflammatory conditions and the aging process, both of which involve oxidative stress ¹¹⁷. Furthermore, miR146b is involved in the regulation of sirt1. Moreover, the peroxisome proliferator-activated receptor (PPAR) family of transcription factors, also plays a role in transcriptional regulation of SIRT1, in particular, PPAR γ is a negative regulator of SIRT1 expression ¹¹⁸. Here, we aim to deeply understand the effects of physical activity by evaluating transcription factor expression in circulating progenitor cells as well as adipogenic and myogenic target genes in progenitor cells. The final part of our study aims, ultimately, to understand the connections between bone metabolism and neuronal metabolism and to what extent patients with Parkinson's disease are more prone than age-matched controls to fractures, and joint and bone problems due to reduced mobility, postural instability, and neurological impairment ¹⁰³. Understanding that the Wnt/ β -catenin pathway is a key link between bone metabolism and the brain, crucial for the development of various aspects of midbrain dopaminergic (DA) neuron development, we aim to investigate the effects of chronic treatment with certain molecules on 3D mid-brain organoids. These organoids are derived from two distinct cell lines of NESCs (Neuronal Embryonic Stem Cells) over a period of 40 days. Our focus will be on studying the genes associated with the Wnt/ β -catenin pathway and neuronal degeneration.

2.1 Clarifications

Most of the data presented in this study have already been reviewed and published in scientific journals. Below are the references:

1. Dalle Carbonare L, Antoniazzi F, Gandini A, Orsi S, Bertacco J, Li Vigni V, **Minoia A**, Griggio F, Per-duca M, Mottes M, Valenti MT. Two Novel C-Terminus RUNX2 Mutations in Two Cleidocranial Dysplasia (CCD) Patients Impairing p53 Expression. *Int J Mol Sci.* 2021 Sep 25;22(19):10336. doi: 10.3390/ijms221910336. PMID: 34638677; PMCID: PMC8508986.
2. Dalle Carbonare L, Dorelli G, Li Vigni V, **Minoia A**, Bertacco J, Cheri S, Deiana M, Innamorati G, Comi-nacini M, Tarperi C, Schena F, Mottes M, Valenti MT. Physical Activity Modulates miRNAs Levels and Enhances MYOD Expression in Myoblasts. *Stem Cell Rev Rep.* 2022 Jun;18(5):1865-1874. doi: 10.1007/s12015-022-10361-9. Epub 2022 Mar 22. PMID: 35316486; PMCID: PMC9209351.
3. Valenti MT, Braggio M, **Minoia A**, Dorelli G, Bertacco J, Bertoldo F, Cominacini M, De Simone T, Romanelli MG, Bhandary L, Mottes M, Dalle Carbonare L. Effects of a 4400 km ultra-cycling non-competitive race and related training on body composition and circulating progenitors differentiation. *J Transl Med.* 2022 Sep 4;20(1):397. doi: 10.1186/s12967-022-03591-5. PMID: 36058924; PMCID: PMC9441096.
4. **Minoia A**, Dalle Carbonare L, Schwamborn JC, Bolognin S, Valenti MT. Bone Tissue and the Nervous System: What Do They Have in Common? *Cells.* 2022 Dec 22;12(1):51. doi: 10.3390/cells12010051. PMID: 36611845; PMCID: PMC9818711.
5. Dalle Carbonare L, Gomez Lira M, **Minoia A**, Bertacco J, Orsi S, Lauriola A, Li Vigni V, Gandini A, Anto-niazzi F, Zipeto D, Mottes M, Bhandary L, Guardavaccaro D, Valenti MT. Expression of FBXW11 in normal and disease-associated osteogenic cells. *J Cell Mol Med.* 2023 Jun;27(11):1580-1591. doi: 10.1111/jcmm.17767. Epub 2023 May 17. PMID: 37199076; PMCID: PMC10243156.
6. Dalle Carbonare L, **Minoia A**, Zouari S, Piritore FC, Vareschi A, Romanelli MG, Valenti MT. Crosstalk between Bone and Muscles during Physical Activity. *Cells.* 2023 Aug 18;12(16):2088. doi: 10.3390/cells12162088. PMID: 37626898; PMCID: PMC10453939.

3 MATERIALS AND METHODS

3.1 Cell cultures

3.1.1 Mesenchymal stem cells

Human mesenchymal stem cells (hMSCs) sourced from human bone marrow were acquired from PromoCell (C-12974; PromoCell). PromoCell affirmed that these hMSCs underwent testing for cellular morphology, proliferation ability, and viability. They were characterized using flow cytometric analysis of a comprehensive panel of markers, specifically CD73, CD90, CD105 for identification and CD14, CD19, CD34, CD45, HLA-DR as suggested by the International Society for Cellular Therapy (ISCT) (<https://promocell.com/wp-content/uploads/product-information/manual/C-12974.pdf>). For the experiments of this study, we used hMSCs in three passages. hMSCs were plated at a density of 5×10^4 cells in the presence of cultured in the MesenPro Basal Medium (Gibco), supplemented with 2% of MesenPRO Growth Supplement (Gibco), 1% of PSA antibiotics (Penicillin Streptomycin Amphotericin B solution, Biological Industries), 1% of L-Glutamine and 0,1% of Plasmocin prophylactic (InvivoGen).

3.1.2 Osteogenic differentiation

MSC cells were cultured under a humidified atmosphere of 5% CO₂ and passage in a specific growth StemPro® Medium (Thermo Fisher Scientific, Gibco™) with osteogenesis supplement and antibiotics (1% penicillin/streptomycin-Lonza). After 3-, 7-, 14- and 21 days cells were harvested using accutase, washed, and pellet for RNA and protein extraction.

3.1.3 Adipogenic differentiation

MSC cells were cultured under a humidified atmosphere of 5% CO₂ and passage in a specific growth StemPro® Medium (Thermo Fisher Scientific, Gibco™) with adipogenic supplement and antibiotics (1% penicillin/streptomycin-Lonza). Cells were harvested using accutase, washed, and pellet for RNA and protein extraction.

3.1.4 Osteosarcoma cells

Human osteosarcoma cell lines, including MG63 (CRL-1427, aliquots used at five passages) and U2OS (HTB-96, aliquots used at four passages), were procured from ATCC. These cell lines were cultured using high-glucose DMEM (ECB7501L; EuroClone), as documented ¹¹⁹. Primary human osteoblasts (HOB, aliquots used at

four passages) were purchased by Promocell (C-12720) and cultured in the presence of osteoblast growth medium (C-27001; PromoCell).

3.1.5 In Vitro Myogenic Differentiation

Human skeletal muscle cells (SKMC) were sourced from PromoCell (C-12580; PromoCell, GMBH Heidelberg, Germany). These SKMCs were cultured using Skeletal Muscle Cell Growth medium (Low serum) (C-23060; PromoCell, GMBH Heidelberg, Germany) and induced to differentiate with Skeletal Muscle Differentiation Medium Supplements (C-23061; PromoCell, GMBH Heidelberg, Germany). The differentiating SKMCs were cultivated with or without pooled sera from participants, with a final concentration of 5%. The medium was refreshed every 3 days after the initial plating.

3.1.6 iPSC derived MSCs

The iPSC-derived Mesenchymal Stem Cells (MSCs) are multipotent stem cells that originally differentiate from iPSC collected by venipuncture from a control patient and a RUNX2-mutation patient and that can further differentiate toward the osteoblastic lineage. They were cultured in the MesenPro RS™ Basal Medium (Gibco), supplemented with 2% of MesenPro RS™ Growth Supplement (Gibco), 1% of PSA antibiotics (Penicillin Streptomycin Amphotericin B solution, Biological Industries), 1% of L-Glutamine. They were incubated at 37 °C, with a 5% CO₂-humified atmosphere.

3.1.7 Circulating progenitor cells (CPCs)

Blood samples of each subject were collected by venipuncture under a biological hood, and PBS (phosphate-buffered saline, Lonza) was added to the blood in a volume-to-volume ratio. Next, the mixture was poured gently over a certain quantity of the Ficoll-Paque™ PLUS solution (GE Healthcare) in a ratio of 2:1, which is a hydrophilic polysaccharide able to achieve the stratification of cells.

A density gradient centrifugation was then performed at 800 rcf for 30 minutes at 20°C. The PBMC ring (composed of monocytes and lymphocytes along with MSCs) was collected with a Pasteur and washed together with PBS during another centrifugation performed at 400 rcf for 10 minutes. After the supernatant removal, 200 µL of RosetteSep™ (Human Mesenchymal Stem Cells enrichment cocktail) was added to a 5 mL blood amount set aside at first to be incubated for 20 minutes. cocktail (RosetteSep Mesenchymal Enrichment Cocktail; code #15128, StemCells,

Vancouver, BC, Canada); this RosetteSep Mesenchymal Enrichment Cocktail contains bi-specific antibody against red blood cells (glycophorin A) and CD3-, CD14-, CD19-, CD38- and CD66b-positive cells (Stem Cell Technologies, Inc., Vancouver, BC, Canada). These antibodies crosslinked the unwanted cells with red blood cells, causing them to pellet together when centrifuged over the second Ficoll. Then, in this mixture Fetal Bovine Serum 2% and EDTA were included, to be later used to perform another Ficoll-Plaque-based centrifugation in a ratio 2:1 (10 mL of mixture + ~5 mL of Ficoll-Plaque) for 30 minutes at 800 rcf at 20°C.

The purified PBMC ring was again absorbed, and a washing step with PBS was carried out with centrifugation at 400 rcf for 10 minutes. The pellet was obtained, and a 2 mL PBS-washing step with centrifugation for 15 minutes at 21000 rcf was done. The supernatant was discharged, and the collected pellet was stored at -80°C until subsequent experiments.

3.1.8 Peripheral Blood Mononuclear Cells (PBMCs) and Sera Collection

Peripheral blood was collected through venipuncture before and after a stimulus, following informed consent. Mononuclear cells (PBMCs) and sera were obtained using standard procedures involving centrifugation. Subsequently, PBMCs and sera were preserved at -80°C until they were ready for use.

3.1.9 Fibroblasts

Fibroblast cells were isolated from a skin biopsy obtained from both patients and a healthy donor. The biopsy specimens were immediately rinsed with 1× PBS containing 1% antibiotics (Penicillin-Streptomycin-Amphotericin), cut into small pieces, and plated in culture flasks containing 1× DMEM (Dulbecco's Modified Eagle's Medium) complete medium (20% FBS (fetal bovine serum) + 1% Glutamax + 1% antibiotic) under sterile conditions. After a period of 2 weeks, fibroblasts that had grown out from the tissues were collected and then plated in new culture flasks containing 1× DMEM complete medium with 10% FBS. The cells were allowed to grow until they reached 80% confluency, and fresh medium was added every other day. Subsequently, the cells were treated with 10 mM of β -glycerophosphate and 50 μ g/mL of ascorbic acid (Sigma St. Louis, MO, USA) for a duration of 7 days. Following this treatment, the cells were collected, and the cell pellet was stored until further use.

3.1.10 iPSCs transduction from PBMC

After PBMCs extraction with the protocol described before, these cells were subjected to a transduction procedure of vectors operated by a modified and non-transmissible form of Sendai virus (SeV).

These reprogramming factor genes were necessary to induce the cells to an artificial pluripotent stem cell-like state, which is like an embryonic stem cell-like state.

The kit utilized for this procedure was the Cytotune™ – iPS 2.0 Sendai Reprogramming Kit by Invitrogen (Thermo Fisher Scientific, Catalog Numbers: A16517, A16518), pursuing the section “Reprogram PBMCs (Feeder-free)”.

The experiment was conducted by visualizing the cells with the instrument EVOS XL Core Imaging System (Invitrogen, Thermo Fisher Scientific) and the cells were incubated at 37 °C, with a 5% CO₂ humidified atmosphere.

In [Figure 7](#) there are summarized all the steps describing the transduction procedure.

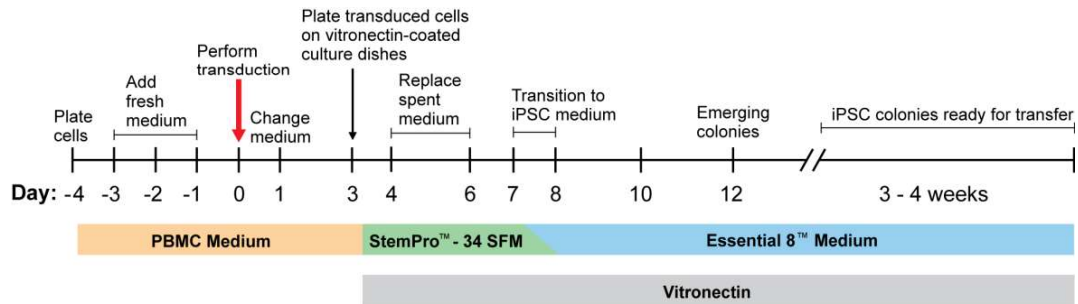


Figure 7 PBMC-to-iPSCs transduction scheme as it is illustrated on the Cytotune™ – iPS 2.0 Sendai Reprogramming Kit protocol, describing the different stages and mediums employed.

3.2 Transfection analysis

MSCs were seeded into T25 flasks and induced to differentiate towards the osteogenic lineage. When cell confluence reached 60%-70%, transfection was carried out using Lipofectamine 3000 Reagent (L3000-008; Invitrogen by Thermo Fisher Scientific Baltics UAB). To downregulate gene expression, cells were transfected with Silencer Select Pre-designed siRNA against miR-204-5p (Cat#: AM17000, ID: AM11116; Ambion by Thermo Fisher Scientific), Silencer Select Pre-designed siRNA against FBXW11 (Cat#4392420, ID: s23487; Ambion by Thermo Fisher Scientific), miR-9-5p mimic, and miR-9-5p inhibitor (Ambion by Life Technologies), along with a scramble-negative control (Cat#: AM17010;

Ambion by Thermo Fisher Scientific). The concentrations used were 591 pmol per T75 flask, as per the manufacturer's instructions. The efficacy of silencing was assessed through gene expression and Western blot analyses. Cells were collected after 24/48 h of transfection.

3.3 Patients

3.3.1 CCD patients

Skin biopsies and peripheral blood were obtained from two pediatric patients with cleidocranial dysplasia (CCD) ([P1: mutation: c.897 T > G -> p (Tyr299*); 8-year-old male] and [P2: c.1019del-> p (Ser340*); 10-year-old female]) and from age-matched healthy donors. Informed consent was provided by the parents of each patient and donor. The analyses conducted on patient and donor samples were ethically approved by the Azienda Ospedaliera Universitaria Integrata of Verona, Italy ethical committee (number 1538; 3 December 2012; local ethical committee of Azienda Ospedaliera Integrata di Verona). Human dermal fibroblast cultures were established from explanted skin biopsies, with cells used at five [P1], four [P2], and five [P2] passages. The cells were cultured using high-glucose DMEM (ECB7501L; EuroClone) supplemented with 10% FBS (10270–106, Gibco; Life Technologies Limited), 2 mM l-glutamine (5-10 K00-H; BioConcept AG), and 100 U/mL penicillin and 100 µg/mL streptomycin (penicillin–streptomycin; ECB3001D; EuroClone). Circulating mesenchymal stem cells (MSCs) were obtained from peripheral blood using a two-step Ficoll procedure. A cocktail of antibodies (RosetteSep Mesenchymal Enrichment Cocktail; code #15128; StemCells) was applied to concentrated mononuclear cells mixed with additional peripheral blood. The antibodies targeted glycophorin A, CD3, CD14, CD19, CD38, and CD66b (Stem Cell Technologies, Inc.) and cross-linked the unwanted cells. The cMSCs phenotype was analyzed, assessing the expression of CD3, CD14, CD19, CD45, and CD34 hematopoietic markers, as well as MSC-positive markers CD73 and CD105 at the RNA levels. This method was employed for phenotypic analyses of cells obtained through stringent stem cell purification techniques.

3.3.2 iPSC derived MSC Patients

One female individual and one age-matched female control were taken into consideration. The first female is known to possess a missense mutation in the RUNX2 gene, with the presence of a single nucleotide variant on the shorter arm of exon 4: a base substitution of position 169 of the nucleotide C towards the nucleotide T, leading to the replacement of an arginine with tryptophan (NM_001024630.4(RUNX2): c.505C>T (p.Arg169Trp)).

3.3.3 Half-marathon participants

A total of 38 age-matched runners (18 women and 20 men) participated in a 21.1 km half marathon as part of the "Run for Science" event held in Verona, Italy, in April 2019. The participants, with a median age of women 41.4 ± 7.2 and men 41.7 ± 8.3 , were all physically fit recreational runners. The median values for Bone Mineral Index (BMI) and CTX were as follows: median BMI (women 21.6 ± 1.3 ; men 23.1 ± 1.8) and median CTX (women 0.34 ± 0.08 mg/ml; men 0.36 ± 0.03 mg/ml). All runners underwent a clinical evaluation and a medical history interview to exclude comorbidities or drug intake. Written informed consent was obtained from all participants, and the study received approval from the ethical committee of Azienda Ospedaliera Universitaria Integrata of Verona, Italy (number 1538; Dec. 3, 2012; local ethical committee of Azienda Ospedaliera Integrata di Verona). The study design and methods adhered to the Declaration of Helsinki.

3.3.4 4400km race participants

Eight healthy male amateur Caucasian cyclists (47.5 ± 13.5 years) who participated in the NC4000 4th edition were recruited through social media. They underwent a clinical evaluation and venipuncture for blood sample collection at three different time points: before the preparation period (BPP) from December 21, 2020, to March 2, 2021, the week before NC4000 (BN), and up to 10 days after NC4000 (AN). The study received approval from the ethical committee of Azienda Ospedaliera Universitaria Integrata of Verona, Italy (number 1538; Dec. 3, 2012; local ethical committee of Azienda Ospedaliera Integrata di Verona). The study design and methods adhered to the principles of the Declaration of Helsinki. Prior to the procedures, cyclists provided voluntary written consent.

3.4 Alkaline phosphatase staining

Alkaline phosphatase staining was performed in MSCs after 3, 7, and 14 days of differentiation in 96 well-plate and fixed with 4% paraformaldehyde (PFA) (P6148; Sigma-Aldrich) by using the Alkaline Phosphatase staining kit (SCR004; Merck Millipore). The stained area has been calculated using Image J.

3.5 Alizarin Red Staining

We performed Alizarin red staining as described ¹²⁰. In summary, following a 14-day culture period under osteogenic stimulation, fibroblasts were fixed with 70% ethanol. After washing, the cells were stained with 40 mM of Alizarin red S for 5 minutes at pH 4.1 and then rinsed for 15 minutes with 1x phosphate-buffered saline. The stained area was analyzed by using ImageJ software (NIH, Bethesda, MD, USA).

3.6 Immunofluorescence

Immunofluorescence analyses were performed according to the manufacturer's protocols. After the cells were fixed with 4% PFA (P6148; Sigma-Aldrich) and processed, the Primary antibody MYOD (cat. #MA1-41017; ThermoFisher) was diluted (as reported in the datasheet) in antibody dilution buffer and incubated overnight at 4°C. Slides were then incubated with secondary antibodies goat mouse fluorescein-conjugated (cat. Ap124f, Millipore, Burlington, Massachusetts, USA). Nuclear staining was performed by ProLong™ Gold Antifade Mountant with DAPI. Images were recorded using a Leica (Wetzlar, Germany) inverted microscope at 10x. To express data in a semi-quantitative way, four different fields were measured for each sample, in three independent experiments with about 80–100 total cells.

3.7 DNA Extraction

We performed DNA extraction from dermal fibroblasts and MSC dry pellets using the QIAampDNA Blood Mini Kit (Qiagen, Milan, Italy) following the manufacturer's protocol.

DNA quantification was done using Qubit 4 Fluorometer (Invitrogen, Thermo Fisher Scientific, Waltham, MA, USA) with QubitdsDNA HS Assay Kit (Invitrogen, Thermo Fisher Scientific, Waltham, MA, USA).

3.8 RNA extraction and reverse transcription

The collected pellets were stored at -80°C until further use. Subsequently, total RNA was extracted using the ‘RNeasy® protect mini kit’ (Qiagen) following the manufacturer's protocol. For microRNA extraction, the miRNeasy Qiagen mini kits (Qiagen) were employed. The quantity and quality of RNA samples were assessed using the ‘Qubit™ RNA HS assay kit’ (Invitrogen) and a Qubit 3 Fluorometer (Invitrogen by Thermo Fisher Scientific; REF Q3321).

For total RNA, reverse transcription was performed with the first-strand cDNA synthesis kit (GE Healthcare) (Table 1). MicroRNAs were transcribed using the TaqMan MicroRNA Reverse Transcription Kit (Thermo Fisher Corporation; 4366596) (Table 2). The thermocycler steps are outlined in Tables 3 and 4. The resulting cDNA samples were then stored at -80°C until further use.

Reagent	Quantity (for each sample)
10x RT Buffer	2 μL
10x RT Random Primers	2 μL
dNTP mix (100 mM)	0,8 μL
Multiscribe™ Reverse Transcriptase	1 μL
H₂O RNase free	4,2 μL

Table 1 . List of reagents and their respective quantities used in Reverse Transcription reaction from RNA

Reagent	Quantity (for each sample)
10x RT Buffer	1,5 μL
RNase Inhibitor	0,19 μL
dNTP mix (100 mM)	0,15 μL
Multiscribe™ Reverse Transcriptase	1 μL
H₂O RNase free	4,16 μL

Table 2 List of reagents and their respective quantities used in Reverse Transcription reaction from miRNA.

Step	Temperature	Time
Step 1	25 $^{\circ}\text{C}$	10 minutes
Step 2	37 $^{\circ}\text{C}$	2 hours
Step 3	85 $^{\circ}\text{C}$	5 minutes

Table 3 Steps of Reverse Transcription reaction from RNA in the GeneExplorer™ Thermal Cycler, with their respective temperature and duration. The second and third steps are carried out for 45 cycles to allow better amplification.

Step	Temperature	Time
Step 1	16 °C	30 minutes
Step 2	42 °C	30 minutes
Step 3	85 °C	5 minutes

Table 4 Steps of Reverse Transcription reaction from miRNA in the GeneExplorer™ Thermal Cycler, with their respective temperature and duration. The second and third steps are carried out for 45 cycles to allow better amplification.

3.9 Gene expression

3.9.1 Taqman Real-time PCR

Gene expression was analyzed by performing real-time PCR. The kit used for this procedure was TaqMan™ Universal PCR Master Mix (Thermo Fisher Scientific), and the housekeeping probe varied based on the gene analyzed. In both singleplex and multiplex reactions, the mix that was first prepared for each sample contained a total of 18 µL. Each component for these reactions, both in singleplex and multiplex, is listed in the following tables (Table 5,6).

Reagent	Quantity (for each sample)
TaqMan® Universal PCR Master Mix (applied biosystems; Thermo Fisher Scientific, Ref: 4304437)	10 µL
TaqMan Target Gene/ Housekeeping Gene	1 µL
H₂O RNase free	7 µL

Table 5 List of reagents and their respective quantities used in TaqMan Real-Time PCR in singleplex

Reagent	Quantity (for each sample)
TaqMan® Universal PCR Master Mix (applied biosystems, Thermo Fisher Scientific. Ref: 4304437)	10 µL
Taqman Target Gene	1 µL
Housekeeping Gene	1 µL
H₂O RNase free	6 µL

Table 6 List of reagents and their respective quantities used in TaqMan Real-Time PCR in multiplex.

Next, the MicroAmp Optical 96-Well Reaction Plate (applied biosystems, life technologies) was used to load the 18 μ L of PCR mix into the wells that were designed. Next, to get a final volume of 20 μ L, 2 μ L of cDNA was added. Three copies of each sample were loaded. Following a brief centrifugation, the plate was covered and sealed using the proper membrane (OPTI-SEAL, AB ANALITICA). For this procedure, the LineGene 9620 Real-Time PCR System (Aurogene, Hangzhou Bioer Technology) was used since it could do the amplification that is detailed in Table 7.

Step	Temperature	Time
Step 1	95 °C	10 minutes
Step 2	95 °C	15 seconds
Step 3	60 °C	1 minute

Table 7 Steps of TaqMan Real-Time PCR reaction in the LineGene 9620 Real-Time PCR System, with their respective temperature and duration. The second and third steps are carried out for 45 cycles to allow better detection of the less expressed genes.

Probe sets for each gene analyzed through this method are reported in the next table (Table 8).

Gene	Origin	Code
ALPL	Applied Biosystems	Hs01029144_m1;
BGLAP	Applied Biosystems	Hs01587814_g1
RUNX2	Applied Biosystems	Hs1047973_m1
FBXW11	Applied Biosystems	Hs00606870_m1
β_2-microglobulin	Applied Biosystems	H200187842_m1
β-actin	Applied Biosystems	Hs99999903_m1
GAPDH	Applied Biosystems	0802021
SP7	Applied Biosystems	Hs00541729_m-1
SPP1	Applied Biosystems	hs00167093_m1
SPARC	Applied Biosystems	Hs00234160_m1
CD3	Applied Biosystems	Hs00174158_m1
CD14	Applied Biosystems	Hs02621496-s1
CD19	Applied Biosystems	Hs00174333_m1
CD45	Applied Biosystems	Hs00174541_m1
CD34	Applied Biosystems	HS00156373_m1
CD73	Applied Biosystems	Hs00159686_m1

CD105	Applied Biosystems	Hs00923996_m1
TP53	Applied Biosystems	Hs01034249_m1
PTEN	Applied Biosystems	hs02621230m1
TGFβR1	Applied Biosystems	Hs00610320_m1
has-miR-9	Applied Biosystems	000583
U6 snRNA	Applied Biosystems	001973
miR-221-3p	Applied Biosystems	000524
sestrin1	Applied Biosystems	hs00902782_m1
miR-146b-5	Applied Biosystems	PN4440886
miR-34a	Applied Biosystems	PN4427975
MYOD	Applied Biosystems	Hs00159528_m1
PPARG2	Applied Biosystems	hs01115513_m1
miR 22-3p	Applied Biosystems	000398
miR 152-3p	Applied Biosystems	000475
miR 100 5p	Applied Biosystems	000437
miR 143-3p	Applied Biosystems	002249
miR 216-5p	Applied Biosystems	002220
miR 27a-3p	Applied Biosystems	000408
miR 30b-5p	Applied Biosystems	000602
miR 200b-3p	Applied Biosystems	002251
MYH2	Applied Biosystems	Hs00430042_m1
LRP5	Applied Biosystems	Hs01124561_m1
CTNNB1	Applied Biosystems	Hs00355045_m1
NR2F1	Applied Biosystems	Hs00818842_m1
PARK2	Applied Biosystems	Hs01038322_m1

Table 8 List of genes analyzed through TaqMan Real-Time PCR reaction in this study.

β-actin, U6, GAPDH and β₂-microglobulin were used as housekeeping genes. All genes were conjugated to carboxyfluorescein (FAM), except for β₂-microglobulin and GAPDH that was conjugated to the fluorophore VIC.

3.9.2 Sybr Green Real-Time PCR

For the SYBR Green Real-Time PCR, two different PCR mixes were required: one for the target gene and another for the housekeeping gene. The mixture contained

both forward and reverse primers for every gene. Before inclusion, each primer was diluted in H₂O RNase free at a ratio of 1:10 after being resuspended in Tris-EDTA buffer solution (Fluca Analytical, Sigma-Aldrich) according to its unique nmoles. The amounts needed to create each combination are shown in the following table (Table 9).

Reagent	Quantity (for each sample)
SYBR™ Green PCR Master Mix (applied biosystems, Thermo Fisher Scientific. Ref: 4309155)	10 µL
Primer Forward	0,6 µL
Primer Reverse	0,6 µL
H₂O RNase free	6,8 µL

Table 9 List of reagents and their respective quantities used in SYBR Green Real-Time PCR.

The next table (Table 10) describes the different steps and lengths of the real-time PCR using the same apparatus as Taqman Real-Time PCR.

Step	Temperature	Time
Step 1	95 °C	3 minutes
Step 2	95 °C	10 seconds
Step 3	53-61 °C (based on primers' Melting Temperature)	10 seconds
Step 4	72 °C	30 seconds
Step 5	95 °C	10 seconds
Step 6	50 °C	5 seconds
Step 7	95 °C	15 seconds

Table 10 Steps of SYBR Green Real-Time PCR reaction in the LineGene 9620 Real-Time PCR System, with their respective temperature and duration. The second and third steps are carried out for 45 cycles to allow better detection of the less expressed genes.

The same 96-well plate used for the Real-Time PCR was loaded with both the housekeeping gene and the gene under investigation. Triplicates were achieved to verify the observed results. After loading, the plate was put on the instrument, covered, and centrifuged. The genes that were analyzed are included in the following table (Table 11).

Gene	Origin	Code
ATG3 forward	Invitrogen – Thermo Fisher Scientific	Z3215B10 (B10)

ATG3 reverse	Invitrogen – Thermo Fisher Scientific	Z3215B11 (B11)
ATG5 forward	Invitrogen – Thermo Fisher Scientific	C5871 (E05)
ATG5 reverse	Invitrogen – Thermo Fisher Scientific	C5871 (E06)
ATG7 forward	Invitrogen – Thermo Fisher Scientific	Z3215B12 (B12)
ATG7 reverse	Invitrogen – Thermo Fisher Scientific	Z3215C01 (C01)
β-actin forward	Invitrogen – Thermo Fisher Scientific	Z3215C04 (C04)
β-actin reverse	Invitrogen – Thermo Fisher Scientific	Z3215B09 (B09)
TGFβ1forward	Invitrogen – Thermo Fisher Scientific	N12206G12 (G12)
TGFβ1 reverse	Invitrogen – Thermo Fisher Scientific	N1223F06 (F06)

Table 11 List of genes analyzed through SYBR Green Real-Time PCR reaction in this study.

3.9.3 TaqMan Gene Expression Assay

The Gene Expression Assay Analysis described was conducted using cDNA derived from previous Reverse Transcriptions. The chosen kit for this assay was the TaqMan™ Human Osteogenesis Array 96-Well Plate from applied biosystems, Thermo Fisher Scientific (Ref: 4414227). This kit comprised a 96-well plate with 4 tests for potential endogenous control genes and 92 tests for genes associated with osteogenesis. This molecular biology technique is essential for simultaneously examining the differential expression of numerous mRNA species in two distinct samples, such as those from a patient with a mutation and a control patient.

The analysis involved the synthesis of tagged complementary DNA (cDNA) from two or more sources and its hybridization to identical gene arrays. Initially, a PCR mix was prepared, and the components are detailed in the following table (Table 12).

Reagent	Quantity (for the entire 96-well plate)
Master Mix (2x)	1 mL
cDNA sample	200 μ L
H₂O RNase free	800 μ L

Table 12 List of reagents and their respective quantities used in TaqMan Gene Expression Assay.

Following a brief centrifugation of the plate, the PCR mix was evenly distributed to achieve a final volume of 20 μ L per well. The distribution was carried out to attain a final cDNA concentration of 100 ng per well. Subsequently, the plate was sealed, subjected to another brief centrifugation, and then subjected to the thermal protocol

outlined in Table 13. This thermal protocol was executed using the LineGene 9620 Real-Time PCR System.

Step	Temperature	Time
Step 1	50 °C	2 minutes
Step 2	95 °C	10 minutes
Step 3	95 °C	15 seconds
Step 4	60 °C	1 minute

Table 13 Steps of TaqMan Gene Expression Assay reaction in the LineGene 9620 Real-Time PCR System, with their respective temperature and duration. The second and third steps are carried out for 45 cycles to allow better detection of the less expressed genes.

3.9.4 PCR array

MiRNA expression profiling was performed using TaqMan Advanced miRNA Human A Card (A34714; ThermoFisher Scientific) according to the manufacturer's instructions. The assay was carried out by using ViiA™7 Real-Time PCR System (Applied Biosystems). Four TaqMan Advanced miRNA Assay endogenous controls included in the card were used for data normalization and the $\Delta\Delta C_t$ method was used to evaluate the fold change as previously reported ¹²¹.

3.9.5 Digital droplet PCR

To analyze the expression of different genes in cMSCs, we used a digital droplet PCR (ddPCR) test. Five microliters of cDNA at a concentration of 0.2 ng/ μ L were added to ddPCR supermix for no UTP probes (10 μ L), with 1 μ L of RUNX2 or FBXW11 or SPARC (FAM-MGB) and B2M (VIC-NGB) control TaqMan probe (Applied Biosystems). The mix was added to the QX200 droplet generator (BioRad) containing 70 μ L of oil. The droplets were carried out to a 96-well plate and then heat-sealed with a tinfoil sheet.

The thermocycling conditions are reported in Table 14.

Step	Temperature	Time
Step 1	95 °C	10 minutes
Step 2	95 °C	30 seconds
Step 3	60 °C	1 minute
Step 4	98 °C	10 minute

Table 14 Steps of digital droplet PCR reaction, with their respective temperature and duration. The second and third steps are carried out for 40 cycles to allow better detection of the less expressed genes.

Plates with droplets were placed in a reader for QX200 droplets. The droplets were analyzed individually, through a two-color detection system (FAM and VIC). QuantaSoft (1.7.4.0917 © 2021; Bio-Rad) was used to process the results according to the manufacturer's instructions.

3.10 Western blotting analysis

Protein concentration was calculated through the BCA protein Assay Kit (Quantum Protein, Bicinchonic Protein Assay, Euroclone) and determined using the VICTOR Microplate Reader

Following protein quantification, each protein sample was collected, and the volumes of different samples were normalized by adding Pierce™ RIPA buffer 1X with protease inhibitors and the appropriate volume of Loading Buffer under the chemical hood. The resulting samples were then boiled at 99 °C for 7 minutes.

Subsequently, the samples were loaded onto precast Mini-PROTEAN® TGX gel (Bio-Rad) for sodium dodecyl sulfate-polyacrylamide gel electrophoresis (SDS-PAGE). Two gels were utilized for each Western Blot: one for Coomassie Brilliant Blue staining and the other for the electroblotting procedure.

Initially, the gels were immersed in Running Buffer solution 1X during the electrophoresis run, set at 125 mV for the first 15 minutes, and then changed to 145 mV for a total duration of 1 hour. The proteins were separated based on their molecular weight.

Upon completion of SDS-PAGE, the proteins were transferred by electroblotting to a PVDF Transfer Membrane with a pore size of 0.45 µm (Immobilon-P, Thermo Scientific. Ref: 88518). The PVDF membrane was activated through a series of steps: 2 minutes in pure ethyl alcohol followed by 5 minutes in MilliQ water. Subsequently, the blotting paper, polyacrylamide gel, and activated membrane were all immersed in a Transfer Buffer solution 1x for at least 15 minutes.

The transfer was carried out using a "sandwich" method on a transfer apparatus (Mini-PROTEAN® Tetra Cell, 4-Gel System, Bio-Rad) at an electric current of 100 mV, allowing proteins to pass from the gel to the membrane. The apparatus was submerged in ice to maintain a temperature of 4 °C for the entire 1 hour and 40 minutes transfer duration, based on the molecular masses of the transferred proteins.

Following the transfer, the membrane was stained with Red Ponceau S for 10-15 minutes to visualize the bands and verify the successful transfer. After staining, multiple washes with MilliQ water were performed to enhance visibility.

Subsequently, the membrane was blocked with fat-dry milk diluted at 5% in TBS-Tween at room temperature for 1 hour to prevent non-specific antibody binding. The membrane was then incubated with the specific primary antibody solution overnight at 4°C.

Meanwhile, the other gel was used for the Coomassie Blue staining procedure, involving two 10-minute washes in MilliQ water, followed by the addition of Coomassie Blue Solution overnight at room temperature. The following day, the stained bands were observed after a 10-minute destaining step in MilliQ water.

β -actin was employed as a housekeeping protein, and the antibodies used for obtaining results in this thesis are listed in Table 15.

AbI	Dilution	WM	Origin	AbII
RUNX2	1:1000	55-62KDa	Cell Signaling-8486	Anti-rabbit
FBXW11	1:500	61KDa	Invitrogen-PA5-109715	Anti-rabbit
βcatenin	1:1000	85KDa	Invitrogen-PA5-19469	Anti-rabbit
P53	1:1000	53KDa	Cell Signaling-2524	Anti-mouse
PTEN	1:1000	47KDa	Finetest-FNab10258	Anti-rabbit
SESN1	1:1000	65KDa	Invitrogen - PA5-98,142	Anti-rabbit
SESN2	1:700	62KDa	Abcam- ab-178518	Anti-rabbit
Sirtuin1	1:1000	110KDa	Invitrogen-PA5-23063	Anti-rabbit
UCP1	1:1000	33KDa	Abcam- ab-10983	Anti-rabbit
P21	1:700	21KDa	Dako -	Anti-

			M7202	mouse
Anti-MyoD	1:500	34KDa	Invitrogen- MA1-41017	Anti- mouse
LC3B	1:1000	14-16 kDa	Invitrogen	Anti- rabbit
p62/SQSM1	1:1000	38-47 kDa	Rockland	Anti- rabbit
β-actin	1:10000	48-55 kDa	Invitrogen	Anti- mouse

Table 15 List of Western Blot primary antibodies used in this study and their dilutions.

Following an overnight incubation, the membrane was subjected to three washes, each lasting 10 minutes. Subsequently, the membrane was incubated for an additional hour at room temperature with the suitable secondary antibody solution, as outlined in Table 16. Following this, the membrane underwent another three 10-minute washes in TBS-Tween.

AbII	Dilution	Origin
Anti-rabbit	1:1000	Cell Signaling Technology
Anti-mouse IgG	1:1000	Cell Signaling Technology

Table 16 List of Western Blot secondary antibodies used in this study and their dilutions.

The subsequent step was to utilize the ECL Select™ Western Blotting Detection Reagent Kit (Amersham™, Cytiva) to find the protein signal at the UVITEC imager (Alliance).

3.11 Sanger Sequencing

The presence of the two C-terminus RUNX2 mutations, initially identified in the cleidocranial dysplasia (CCD) patients by "Casa del sollievo e della sofferenza" U.O.C. Genetica Medica—S. Giovanni Rotondo (FG)-Italy, was confirmed through targeted Sanger sequencing. A 470 base-pair (bp) PCR product corresponding to exon 7 and adjacent intron regions of the RUNX2 gene (NM_001024630.3) was amplified using specific primers. The primers were designed with Primer3 and BLAST tools (NCBI, <https://www.ncbi.nlm.nih.gov/tools/primer-blast/>, accessed on February 3, 2019) and had the following sequences: Forward 5'-TAAGGCCTGAAAGGATGGGGT-3' and Reverse 5'-

ATGTGGGCAAGGGAATGACAA-3'. The PCR was carried out using the Mastercycler® ep Gradient S® (Eppendorf, Milan, Italy) and GoTaq® Hot Start Polymerase kit (Promega, Madison, WI, USA) with the following program: 2 min at 96 °C, 35 cycles of 96 °C for 30 s, 60 °C for 30 s, and 72 °C for 30 s, followed by a final step of 72 °C for 5 min. The purity and identity (based on length in bp) of the PCR product were verified by 1.5% agarose gel electrophoresis.

Following purification with the FastGene™ kit (Nippon Genetics, Mariaweyerstraße, Düren, Germany), 1.5 µL of the PCR product was used for Dye Terminator Cycle Sequencing (DTCS) with the Beckman Coulter Quick Start Kit (Sciex, Milan, Italy) following the manufacturer's instructions.

3.12 Generation of mid-brain organoids

Media: N2B27 base medium: DMEM HAM's F12 medium (Invitrogen, ThermoFisher) - 48 mL + Neurobasal medium (Invitrogen) - 48 mL + GlutaMAX (ThermoFisher, 2mM)- 1 mL + Pen/Strep (Invitrogen, ThermoFisher) - 1 mL + N2 (ThermoFisher) -500uL + B27 (Invitrogen, ThermoFisher) - 1 mL .

N2B27 maintenance medium: N2B27 base medium -10 mL + Ascorbic acid (Sigma, 20 mM) -75 µL + CHIR (Axon MedChem, 6 mM in DMSO) - 5uL.

N2B27 patterning medium: N2B27 base medium - 10 mL + hBDNF (Pepotech,10 mg/mL) - 10 µL + hGDNF (Pepotech,10 mg/mL) -10 µL + Ascorbic acid (Sigma, 20 mM) - 100 µL + TGFβ3 (Pepotech10 ng/uL) 1 ng/mL- 1 µL + db cAMP (Pepotech100 mM in milliQ H2O) - 50 µL + PMA (stock 10mM) 1ul.

N2B27 differentiation medium: N2B27 base medium - 10 mL + hBDNF (Pepotech,10 mg/mL) - 10 µL + hGDNF (Pepotech,10 mg/mL) -10 µL + Ascorbic acid (Sigma, 20 mM) - 100 µL + TGFβ3 (Pepotech10 ng/µL) 1 ng/mL- 1 µL + db cAMP (Pepotech100 mM in milliQ H2O) - 50 µL.

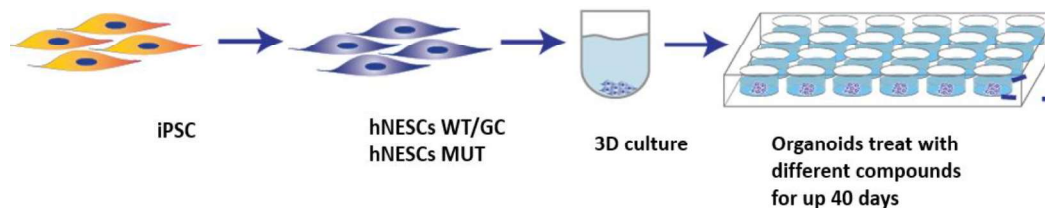
Neuronal epithelial stem cells (NESCs) derived from human induced pluripotent stem cells (iPSCs), are the starting cell population for midbrain organoid generation. NESCs were cultured in Geltrex-coated 6-well plates, routinely passaged at 80%–90% confluence, using accutase. At 80%–90% confluence, detached NESCs using accutase and counted viable cells via standard Trypan Blue protocol using an automated Cell counter. Diluted 9×10^5 cells in 15 ml of N2B27 maintenance medium and transferred 150 mL of cell suspension in each well of the 96-well ULA plate (change media every 2nd day). On day 2, N2B27 maintenance

media was replaced with N2B27 patterning media (change media every 2nd day). On day 8, for 16 organoids N2B27 patterning media was replaced with N2B27 differentiation media and started the treatment with molecules of interest:

- JH-II-127 (Merck) at the concentrations of 300nM
- Lipoic acid (lot.2009021,30-60, MESH) at the concentration of 50 μ M

For long-term culture, full media change using 500 mL of N2B27 differentiation was done every 3–4 days. We cultured organoids for 40 days, after that we collected non-embedded organoids in Eppendorf and freezing them for RNA extraction.

At day 8, 8 3D colonies were transferred to an untreated 24-well tissue culture plate (TCP), distributed 500 μ L of pre-warmed (37 °C) N2B27 maintenance medium to each well of the TCP. Embedded the NESC colonies in a Geltrex droplet adding 30 μ L of Geltrex around the 3D colony and keeping the colony in the center of the Geltrex droplet, after 25 min in an incubator to allow the Geltrex to polymerize. N2B27 maintenance media was replaced with N2B27 differentiation media and the treatment with molecules of interest. We cultured organoids for 40 days, after that we used embedded organoids for sectioning and staining. Non-embedded organoids were used to extract total RNA using the mRNA Quigen-Kit as previously described (Scheme 1).



Scheme 1 A schematic representation about mid-brain organoids generation.

3.12.1 Sectioning, staining, and mounting organoids

Embedded organoids were fixed with 4% of PFA (P6148; Sigma-Aldrich), included in 3% of agarose, and then cut using Vibratome (Leica) at 70 μ m and collected in 24 well-plates with PBS.

Organoid sections were collected in a 24 plate and then permeabilization was performed with 0.5% Triton X-100 in PBS for 30 minutes at RT on a shaker, washed twice in 0.01% Triton X-100 in PBS for 5 min at RT on a shaker and block the samples in blocking buffer for 2h at RT on a shaker. Incubation with primary antibodies was performed for 48h. After that Wash 3x in 0.01% Triton X-100 in PBS for 10 min at RT on a shaker and incubate in secondary antibody diluted in

blocking buffer for 2h at RT on a shaker; wash 3x in 0.01% Triton X-100 in PBS for 10 min at RT on a shaker and then wash once with H₂O.

3.12.2 Confocal imaging

Sections were collected with a brush and placed on an object slide with a grid (let the section dry a bit before mounting, otherwise it will float away and be covered with cover glass). We used the confocal microscopy (Leica) to see the three different neuronal markers (Figure 8):

AbI	Dilution	Origin	AbII
TH	1:1000	Cell Signaling	Anti-rabbit
GFAP	1:1000	Cell Signaling	Anti-chicken
MAP2	1:500	Cell Signaling	Anti-mouse

Figure 8 Neuronal markers for confocal imaging.

3.13 Flow cytometry analysis

3.13.1 iPSC-derived MSCs

A cytofluorimetric analysis was required to assess that the type of cell population considered from iPSC differentiation resembled a mesenchymal stem cell-like one. It was achieved through an examination performed with the BD LSRFortessa™ X-20 Cell Analyzer, which was able to distinguish for each cell distinct cellular surface molecules, allowing for the immunophenotyping of cells, in a procedure called cluster of differentiation (CD).

At first, after the observed expansion of cells in flasks, the harvesting happened using Accutase. After the centrifugations to obtain the pellet, which was resuspended in PBS, 10 µL of the sample were collected to be mixed with Trypan Blue stain 0,4% (Invitrogen, ThermoFisher Scientific) to carry out the cell counting, for which it was used the cell analyzer Countess II (Invitrogen, ThermoFisher Scientific). For each CD to be analyzed per sample, an average of 200.000 cells were considered.

Once the number of live cells was determined, a Buffer Solution was added to the sample of cells to reach a total volume of 100 µL. Then, 5 µL of the specific antibody that recognizes the desired CD was included in each tube.

Subsequently, an incubation at 4°C for 40 minutes was executed, and after that, a centrifugation of 21100 rcf for 5 minutes was performed. The pellet was then resuspended in 200 µL of Buffer Solution and taken to the instrument for analysis.

Specifically, in this inspection, there was the selection of both positive and negative surface molecules, characteristic of MSCs-like population. In particular, the molecules that should reveal a positive signal as they are usually present on the MSCs' surface are:

- CD73 conjugated with the fluorophore Bv421;
- CD90 conjugated with the fluorophore APC;
- CD105 conjugated with the fluorophore PE.

During this investigation, the cell's viability was observed through the staining with propidium conjugated with PE, which is a fluorescent intercalating chemical. Also, an unstained sample was employed to test the autofluorescence that cells automatically emit, acting as a negative control to be subtracted from the other cluster differentiation signals.

The final data were extrapolated using the software FlowJo, which is usually used to assess data from cytofluorimetric imaging.

3.13.2 Mid-brain Organoids

Flow cytometry analysis was performed to quantify the different efficiency of treatment. To do so, we analyzed three independent mid-brain organoids after 40 days of differentiation. To generate a single-cell suspension, differentiated cultures were washed once with PBS and subsequently dissociated at 37 °C using Accutase. Cells were further dissociated by pipetting gently up and down as well as by filtering them carefully through a 0.75 µm cell strainer. After centrifugation at 200 × *g* for 5 min, the cell pellet was resuspended in 2 ml PBS, and the same volume of 8% PFA in PBS was added dropwise to fix the cells for 10 min at RT. Subsequently, the same volume of 0.1% BSA in PBS was added to the suspension. To remove the PFA, the cell suspension was centrifuged and washed once with 0.1% BSA in PBS. The pellet was resuspended in 0.1% BSA in PBS and the suspension was transferred into a 1.5 ml tube. After centrifugation, the cell pellet was resuspended in permeabilization/blocking solution and incubated for 20 min at RT. Permeabilization/blocking solution was withdrawn by centrifugation and the resulting cell pellet was resuspended in primary antibody solution. The incubation with the primary antibody was performed under shaking conditions for 2 hours at RT. On the following day, cultures were washed once with 0.1% BSA in PBS, and incubated with the secondary antibody for 1 h at RT. All secondary antibodies were

obtained from Invitrogen and were conjugated to Alexa Fluor fluorochromes. Finally, cells were washed twice with 0.1% BSA in PBS-T (0.005% Tween-20). After centrifugation, the pellet was resuspended in FACS buffer (0.1% BSA in PBS). To set the gates appropriately, we stained each marker individually. Flow cytometry was performed using BD LSR-Fortessa Cell Analyzer.

3.14 Statistical analysis

The results were presented as mean \pm SD. Statistical analysis was conducted using the Mann–Whitney test for comparisons between two groups or one-way ANOVA and t-test for comparisons involving more than two groups. The analyses were based on experiments conducted six times, and outliers were included in the analyses. SPSS for Windows, version 22.0 (SPSS Inc.), was utilized for data analysis.

4 RESULTS

4.1 Identification of new molecular mechanisms associated with osteogenic differentiation.

It is established that the osteogenic lineage originates from mesenchymal stem cells (MSCs) ¹¹⁶, and their commitment is triggered by the transcription factor RUNX2 ²⁷. RUNX2 is the master gene of osteogenesis, and its expression is controlled by various cellular signals. To further comprehend the role of FBXW11 in osteogenic cells, we aim to assess its modulation both during osteogenic commitment and in aberrant osteoblastic cells characterized by RUNX2 mutations or those arising from tumor transformation.

4.1.1 FBXW11 expression during osteogenesis

After 3, 7, and 14 days of differentiation, we employed ALP staining to evaluate osteogenic differentiation. The ALP staining area exhibited an increase from the 3rd to the 14th day of osteogenic stimulation, as depicted in Figure 9A. Specifically, in comparison to the 3 or 7 days of osteogenic differentiation, a higher ALP staining was observed at the 14th day of differentiation. Furthermore, the cells displayed continuous growth throughout the observation period (Figure 9B) in response to the

osteogenic stimulus. We quantified the protein levels of Fbxw11, Runx2 and β -catenin, key players in osteogenic commitment, after 3, 7, and 14 days of osteogenic differentiation to understand the modulation of FBXW11 during osteogenic differentiation. In the mid-phase of differentiation (7 days into the process), elevated protein levels of both Runx2 and Fbxw11 were noted during osteogenic differentiation (Figure 9C). Protein levels of Fbxw11 began to decline after 14 days of differentiation (Figure 9C). However, following three days of differentiation, Runx2 levels sharply decreased below those observed (Figure 9C). Additionally, we observed that during the early osteogenic phase, β -catenin levels rose, subsequently decreasing throughout osteogenic differentiation (Figure 9C).

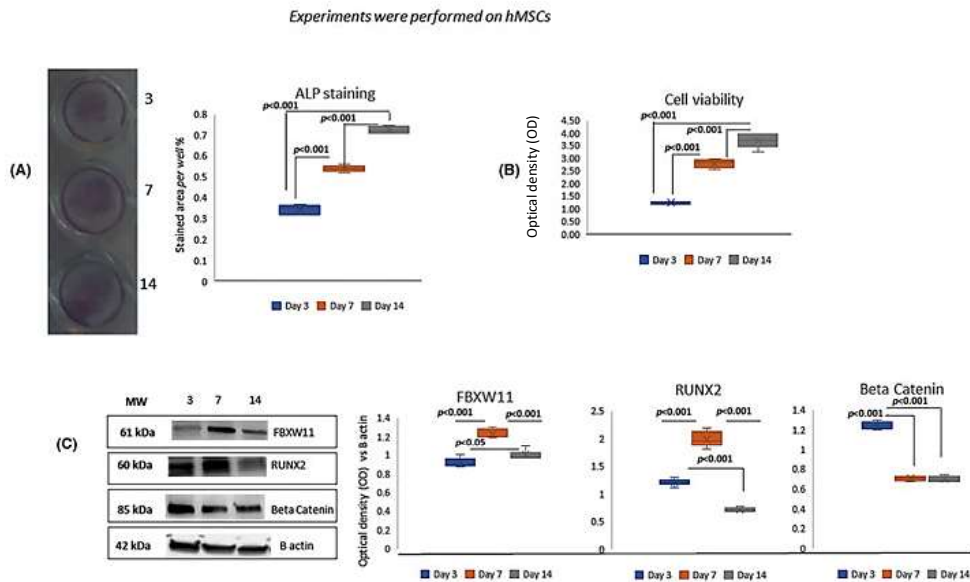


Figure 9 Evaluation of ALP expression during hMSC osteogenic differentiation (A). viability of hMSC cells cultured for 3, 7, and 14 days following osteogenic stimulation (B). Protein levels (on the left) and blot optical density (on the right) were measured using WB (C). Using one-way ANOVA, p-values were computed. Six independent analyses have been carried out for cell viability and ALPL area staining. Three separate experiments are represented by the WB photos, and six densitometric analyses are shown in the graphs.

4.1.2 FBXW11 regulates the expression of RUNX2, and genes associated with osteogenic maturation

We suppressed the expression of FBXW11 in MSCs cultured under osteogenic stimulation to investigate the interaction between FBXW11 and RUNX2 under normal conditions. Additionally, we evaluated the expression of SP7, a downstream transcription factor of RUNX2 crucial for osteoblastogenesis, in FBXW11-silenced cells. FBXW11-silenced cells exhibited higher levels of expression for both RUNX2 and SP7 (Figures 10A, B). Moreover, RUNX2 and its regulator β -catenin displayed elevated protein levels in FBXW11-silenced cells (Figure 10C). These

FBXW11-silenced cells were then used to examine the expression of BGLAP (bone gamma-carboxyglutamate protein, commonly known as osteocalcin), SPP1 (osteopontin), and ALPL (alkaline phosphatase) to assess the role of FBXW11 in osteogenic maturation. Specifically, ALPL serves as a marker for osteogenic differentiation, BGLAP is a protein released by osteoblasts, and both osteoblasts and osteoclasts in bone express SPP1¹²².

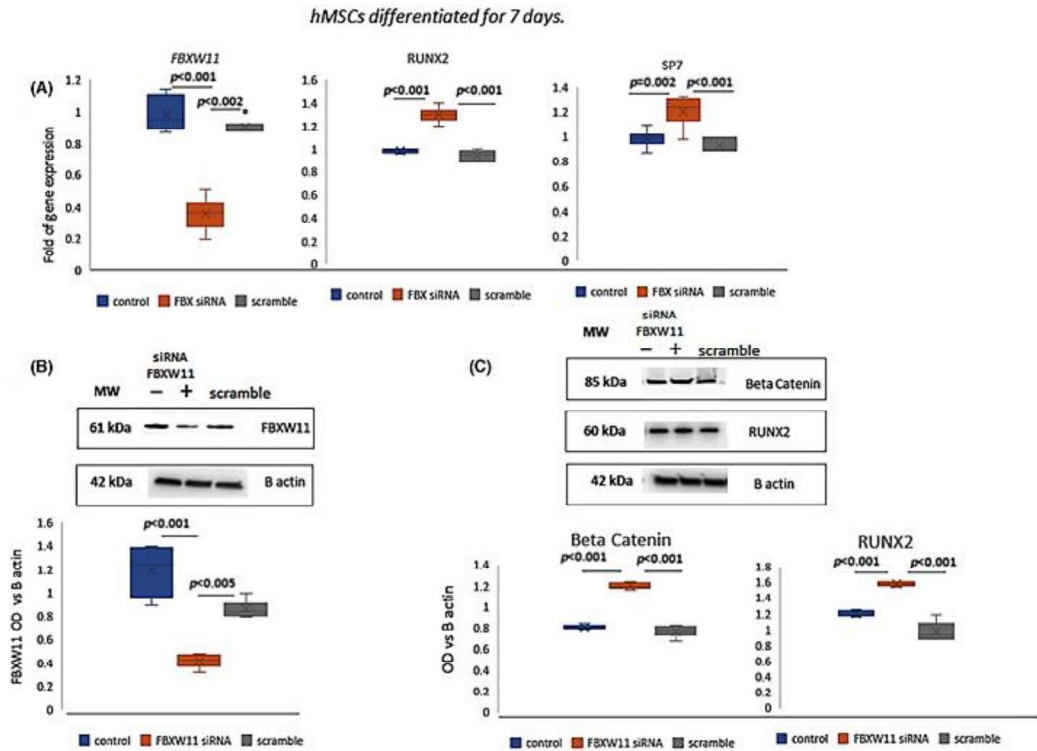


Figure 10. After seven days of osteogenic differentiation, the following protein levels were measured in silenced hMSCs and controls: FBXW11 (B), RUNX2, SP7 gene expression (A), and β -catenin and RUNX2 (C). Using one-way ANOVA, p-values were determined. Six different experiments have been conducted to assess gene expressions. Three distinct experiments' worth of WB images are represented in the graphs, which display the results of six densitometric studies.

Genes linked to osteogenic differentiation were expressed similarly in controls and FBXW11-silencing cells 3 (Figure 11A) and 7 (Figure 11B) days after differentiation. After 14 days of differentiation, however, we saw reduced expression of BGLAP, SPP1, and ALPL in FBXW11 silenced cells in comparison to controls (Figure 11C).

It has been previously shown that throughout the middle and late stages of osteogenic differentiation, miR-204 increases the expression of RUNX2⁵³. Therefore, after three days of osteogenic differentiation, we did not find any modulation of FBXW11 and RUNX2 in cells transfected with anti-miR 204 (Figure 11D). Conversely, after 7 and 14 days of osteogenic differentiation, the induced

expression of RUNX2 through transfection of MSCs with anti-miR204 resulted in an augmented expression of FBXW11 after 7 days (Figure 11E). However, this trend was not observed after 14 days of osteogenic differentiation (Figure 11F).

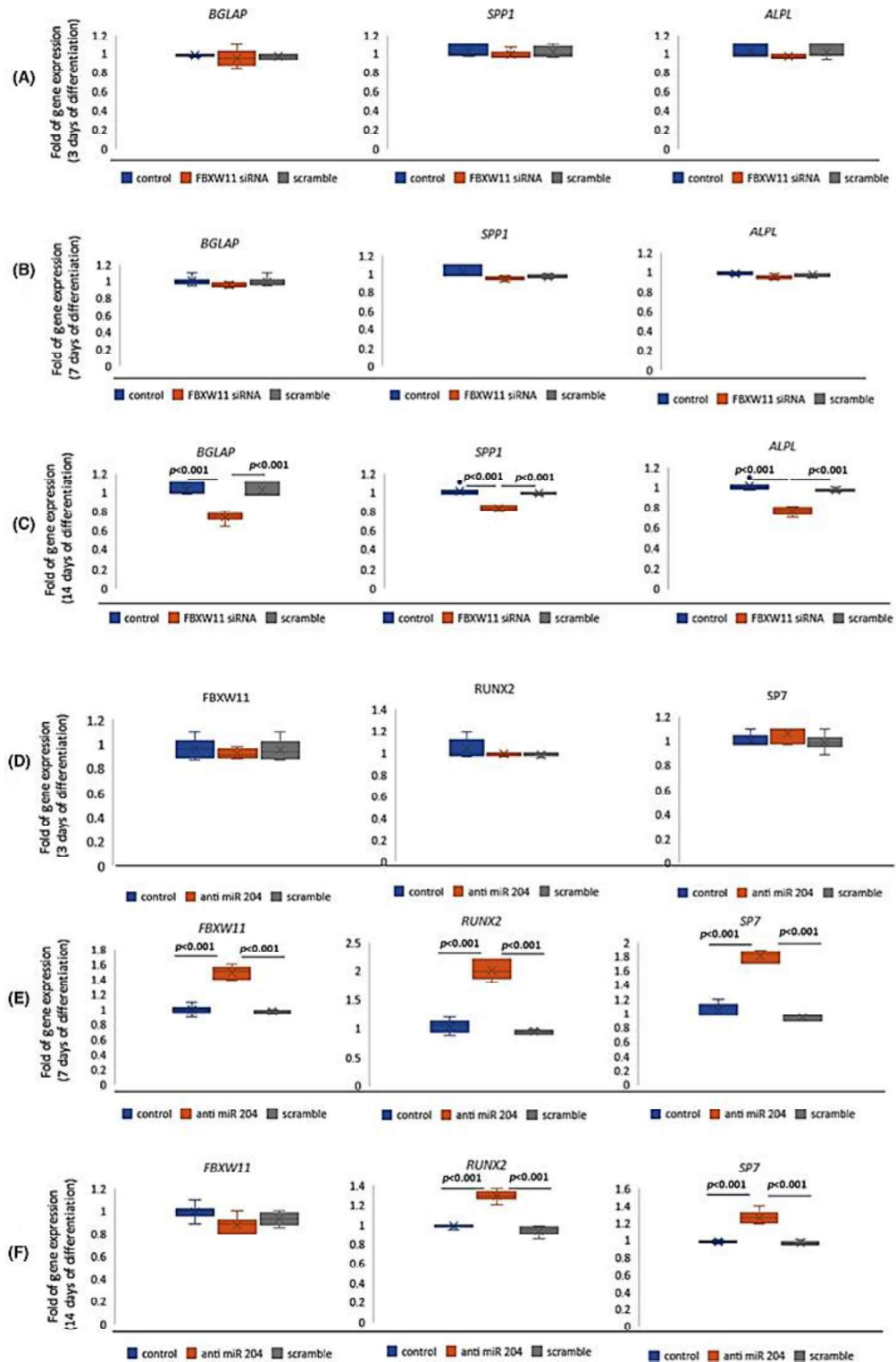


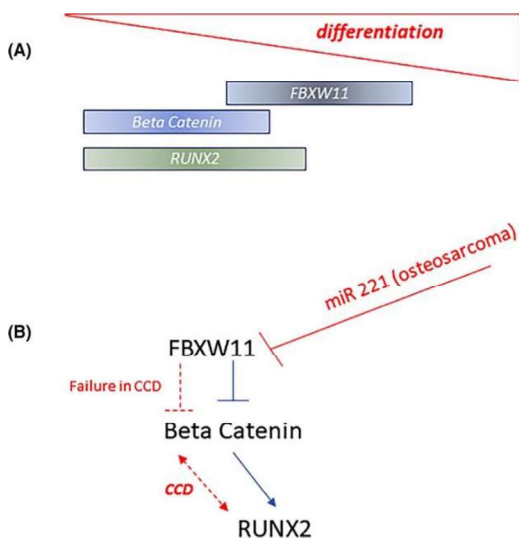
Figure 11 BGLAP, SPP1, and ALPL expression in control cells and FBXW11-silencing cells after 3 (A), 7 (B), and 14 days of differentiation (C). After 3 (D), 7 (E), and 14 (F) days of osteogenic differentiation in controls

and RUNX2 forced expression-hMSCs, the expression of FBXW11, RUNX2, and SP7 was measured. Six separate experiments have assessed gene expressions. One-way ANOVA was used to compute the p-values.

4.1.3 FBXW11 and RUNX2 undergo disparate modulations in CCD cell

We assessed FBXW11 expression in an MSCs cell line in the presence or absence of an osteogenic media in order to look into the expression of FBXW11 during the osteogenic commitment. The results revealed that RUNX2 and FBXW11 exert opposing effects on MSCs, influencing RUNX2's commitment to the osteogenic lineage. As depicted in Figure 12A, during the commitment to the osteogenic lineage (three days of differentiation), FBXW11 expression was lower compared to the expression of RUNX2 and the RUNX2-downstream transcription factor SP7.

We initially examined the expression of FBXW11 in circulating mesenchymal stem cells (cMSCs) obtained from pediatric Cleidocranial Dysplasia (CCD) patients. These cells were cultured in the presence or absence of osteogenic media to understand how FBXW11 is regulated in the context of cells with RUNX2 mutations. As shown in Figure 12B, during the osteogenic commitment phase (after 3 days of differentiation), FBXW11 levels increased in coordination with the levels of RUNX2 and SP7. To investigate whether mutations at specific locations in the RUNX2 gene could lead to differential effects on FBXW11 and β -catenin levels, we analyzed patient fibroblasts with the c.897 T > G (Pt1) transition and patient fibroblasts with the c.1019del of a C nucleotide (Pt2). Figure 12C demonstrated that both osteogenically stimulated fibroblasts from CCD patients exhibited higher levels of Fbxw11 and β -catenin compared to osteogenically stimulated fibroblasts from a normal donor (Scheme 2)



Scheme 2 In the middle phase of osteogenesis (A), FBXW11 levels rise, while β -catenin and RUNX2 levels rise in the early phase. By interacting with the β -catenin target, FBXW11 lowers RUNX2 levels (blue lines B). RUNX2 mutation may be involved in the rise in β -catenin levels in the CCD model. In this illness model, dysregulated β -catenin levels (red lines B) are attempted to be countered by enhanced FBXW11 (B). In osteosarcoma, overexpression of miR 221 results in decreased FBXW11 protein levels, which raises β -catenin.

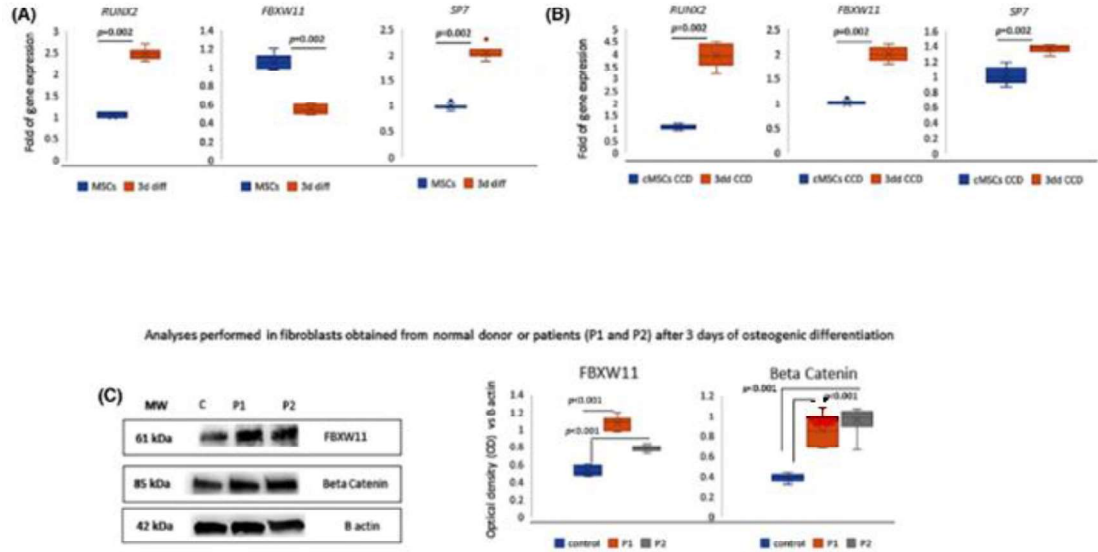


Figure 12 In undifferentiated MSCs line and after three days of osteogenic differentiation (A), as well as in CCD undifferentiated circulating MSCs and after three days of differentiation (B), RUNX2, FBXW11, and SP7 gene expression were observed. Western blot in fibroblasts induced by osteogenes derived from either healthy donors or individuals with CCD (C). P1, patient 1; P2, patient 2; C, normal donors p-Values were computed using either the one-way ANOVA (C) or the Mann-Whitney test (A and B). Six separate experiments have assessed gene expression. The graphs display information from six densitometric analyses, and the WB photos are indicative of three separate trials.

4.1.4 The role of FBXW11 in osteosarcoma cells

We examined the FBXW11 expression levels in osteoblasts that are normally expressed and in osteosarcoma cells that express greater levels of RUNX2 (Figure 13A, B). In comparison to normal osteoblasts (HOB), we found that MG63 and U2OS osteosarcoma cells have reduced amounts of the protein FBXW11, as illustrated in Figure 13C. Furthermore, MG63 and U2OS osteosarcoma cells have larger amounts of β -catenin than normal osteoblasts (HOB) (Figure 13C). Nevertheless, we found greater levels of FBXW11 gene expression in the U2OS and MG63 osteosarcoma cell lines than in healthy osteoblasts¹²³ (Figure 13D). miR 221 targets FBXW11, and its expression was examined to comprehend the opposing trends of mRNA and protein levels of FBXW11 in osteosarcoma cells. Compared to normal osteoblasts, we found increased miR221 levels in the osteosarcoma cell lines U2OS and MG63 (Figure 13E).

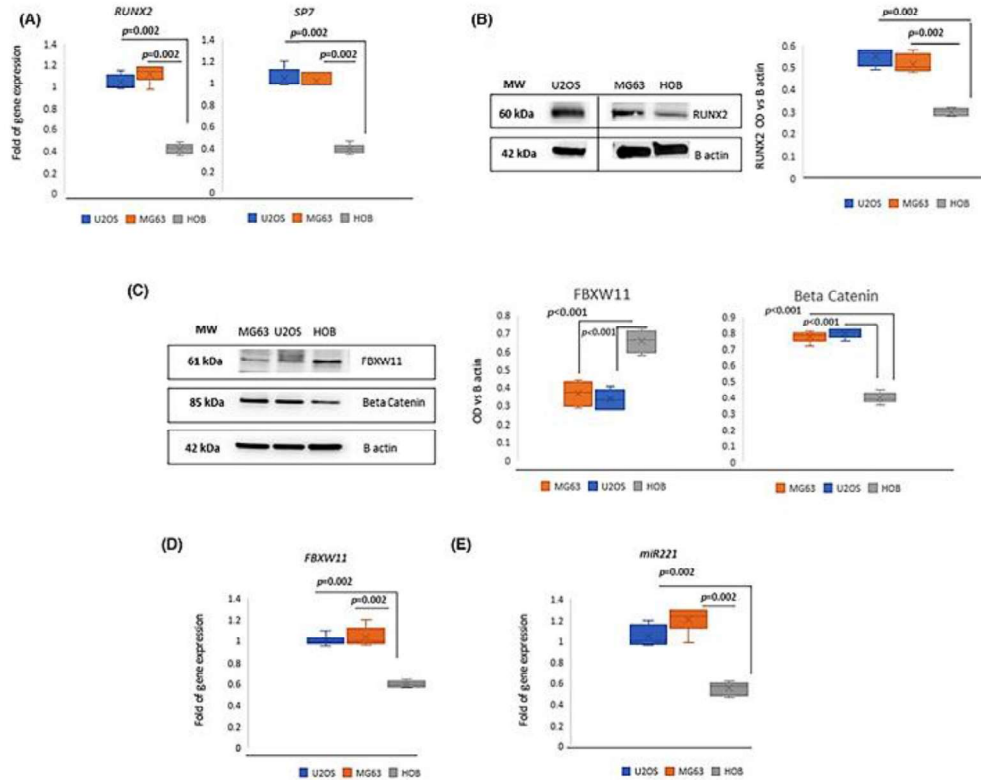


Figure 13 Expression of the RUNX2 and SP7 genes in normal osteoblasts (HOB) and osteosarcoma cells (MG63 and U2OS) (A). RUNX2 protein levels in HOB, MG63 osteosarcoma cells, and U2OS cells; the spliced WB picture (B) is shown by the dividing line. The amounts of beta-catenin and FBXW11 protein in MG63 and U2OS osteosarcoma cells as well as in HOB (C). The expression levels of miR-221 (E) and FBXW11 (D) in HOB, MG63, and U2OS osteosarcoma cells. p-Values were computed using either the one-way ANOVA (C) or the Mann-Whitney test (A, B, D-E). Six separate experiments have assessed gene expressions. The graphs display the information gathered from six densitometric analyses, and the WB photos are indicative of three separate tests.

4.2 Focus on examining mutations in RUNX2 gene in patients diagnosed with CCD

Basal expression of RUNX2 is essential for the proper proliferation and differentiation of osteoblasts. To comprehend the behavior of RUNX2 in individuals with Cleidocranial Dysplasia (CCD), we examined its expression in circulating progenitors from one of the two patients. Cultured cells from both individuals were subjected to analysis for RUNX2 gene expression and their osteogenic potential. Furthermore, through string analyses, we assessed the potential interactions of RUNX2 with proteins that regulate osteogenic maturation.

4.2.1 RUNX2 mutations

In patient 1 's fibroblast DNA, we found the presence of c.897T>G substitution leading to a premature stop-codon: p.(Tyr299*) at the RUNX2 protein's c-terminus

(Figure 14A). Similarly, a C nucleotide deletion in RUNX2 exon 7 (c.1019del) caused a reading frameshift and an early stop codon, p.(Ser340*), according to direct Sanger sequencing of patient 2's DNA (Figure 14B).

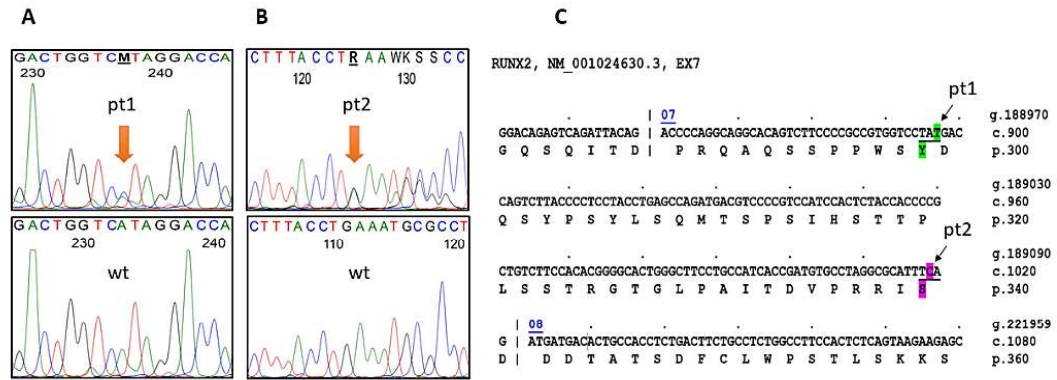


Figure 14 The gDNA sequences of the two newly identified RUNX2 mutations in Cleidocranial Dysplasia (CCD) patients 1 (A) and 2 (B) were reverse-transcribed to align with the respective wild-type sequences. Forward gDNA sequencing confirmed the mutations, highlighted in green and purple for a c.897T > G transition (Pt1) and a c.1019del of a C nucleotide (Pt2), respectively (C).

The Cluster Differentiation profile in patient 2 showed that we were able to identify cMSCs. Specifically, it was shown that the Mesenchymal Markers CD105 and CD73 exhibited over 60% expression, but the remaining Cluster Differentiation markers were either undetectable or exhibited modest expression (Figure 15A). Next, we examined the regulation of RUNX2 and SPARC expression during in vitro osteogenesis, contrasting the results with those from a control MSC line. Following seven days of osteogenic differentiation, Pt2's cMSCs showed nearly 40-fold higher RUNX2 gene expression levels than the control group ($p < 0.0001$). In contrast, following 7 days of differentiation, Pt2's cMSCs showed lower SPARC levels than the control group (Figure 15B).

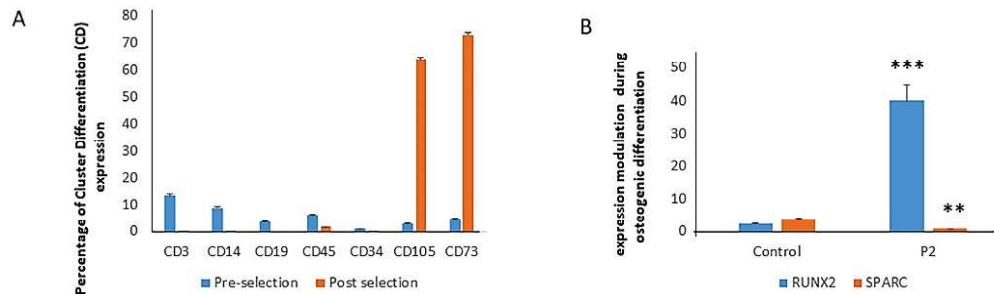


Figure 15 Hematopoietic markers exhibited minimal expression, while mesenchymal markers CD105 and CD73 were expressed at a rate exceeding 60% (A). In circulating mesenchymal stem cells (cMSCs), the gene expression of RUNX2 increased after osteogenic differentiation, but SPARC expression in Pt2 cMSCs was reduced compared to the control (B). The presented data represents the mean \pm standard deviation (SD) from two separate studies (for the assessment of the percentage of Cluster Differentiation expression) or three (for the evaluation of RUNX2 and SPARC expression), conducted in triplicate for each participant's samples. *** $p < 0.0001$; ** $p < 0.005$

4.2.2 Osteogenically-Stimulated CCD Fibroblasts Express Increased Levels of Runx2 Protein

Runx2 protein was found to be expressed at higher levels in osteogenically stimulated (os) cells from Pt1 and Pt2 in comparison to control (Figure 16A). On the other hand, Pt2 os-fibroblasts had increased RUNX2 gene expression in comparison to control, but not Pt1 os-fibroblasts (Figure 16B). SPARC gene expression was reduced in CCD os-fibroblasts compared to control, despite the observed levels of RUNX2 gene expression (Figure 16B). When alizarin red staining (ARS) was used to assess calcium deposition, we found that the os-fibroblasts of CCD patients showed less stained area than the control group (Figure 16C).

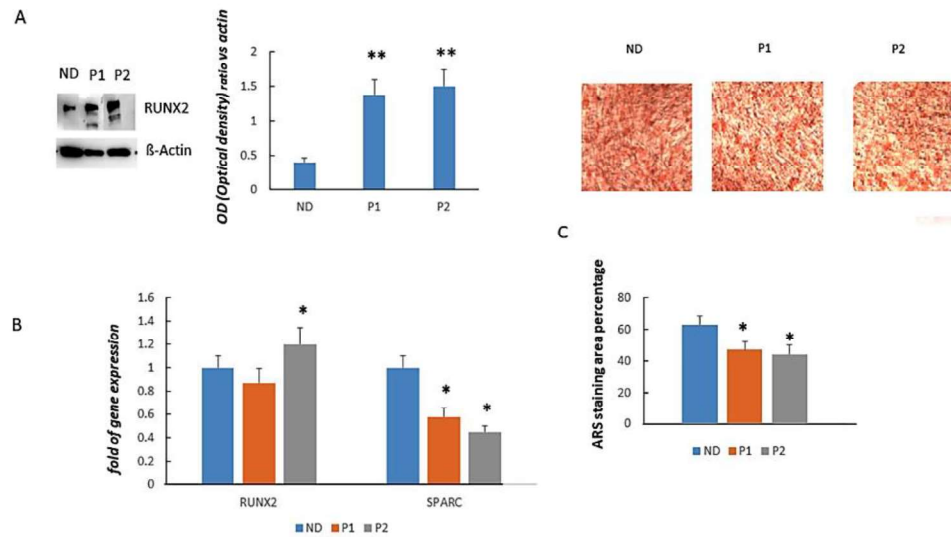


Figure 16 Western Blot results depict the levels of Runx2 protein in control (ND, normal donor), Pt1 (P1), and Pt2 (P2) osteogenically-stimulated fibroblasts (A). Densitometric analyses reveal higher RUNX2 protein levels in fibroblasts of Cleidocranial Dysplasia (CCD) patients compared to the control (A). Conversely, the gene expression of RUNX2 appears similar in osteogenically-stimulated fibroblasts of CCD patients and controls. The expression of SPARC gene is lower in osteogenically-stimulated fibroblasts of CCD patients compared to the control (B). Calcium deposition, assessed through alizarin red staining (ARS), is reduced in osteogenically-stimulated fibroblasts of CCD patients compared to the control (magnification: 10x) (C). All analyses were conducted on samples from each participant in three independent analyses, performed in triplicate. Data are presented as mean \pm standard deviation (SD). * $p < 0.05$; ** $p < 0.005$.

4.2.3 The Expression of P53 and PTEN Are Lowered in osteogenically-stimulated fibroblasts derived from individuals with CCD

To comprehend the consequences of RUNX2 dysregulation in the cells of CCD patients, we looked into the expression levels of P53, which is known to be crucial for osteogenesis.

Initially, we subjected the regulated proteins, SPARC and PTEN, as well as the gene products of RUNX2 and p53, to analysis on the STRING portal (<https://string-db.org/>) for an unbiased exploration of potential relationships among these proteins. The depiction of their functional interactions is illustrated in Figure 17.

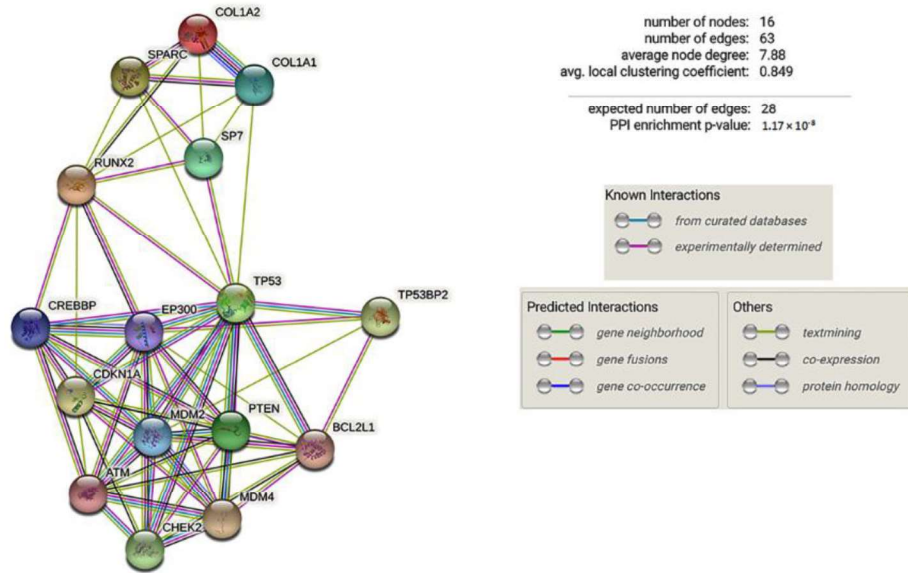


Figure 17 The STRING portal identifies connections between functional proteins. PPI enrichment p-value: 1.17×10^{-8} .

The biological processes identified through STRING analysis include replicative senescence (GO:0090399), stress-induced premature senescence (GO:0090400), adult lifespan determination (GO:0008340), and negative regulation of cell cycle arrest (GO:0071157). To examine p53 and PTEN expression, we examined MSCs from both a control cell line and cells from CCD patients. The MSC cell line's expression of PTEN and p53 increased throughout osteogenic differentiation, as seen in Figure 18A.

Specifically, we found that after 7 and 14 days of osteogenic differentiation, relative to 3 days, there was an increase in the expression of p53 and PTEN. On the other hand, CCD os-fibroblasts expressed less p53 than ND os-fibroblasts did. As a result, compared to normal os-fibroblasts, CCD os-fibroblasts had reduced expression of PTEN, a gene controlled by p53 (Figure 18B). In addition, CCD os-fibroblasts had reduced levels of PTEN and p53 protein when compared to control os-fibroblasts (Figure 18C).

In summary, these observations suggest that the heterozygous RUNX2 mutations identified in both cleidocranial dysplasia (CCD) patients may impede osteogenic

maturation. This hindrance is likely mediated through a reduction in p53 levels and the downregulation of RUNX2 downstream genes, such as SPARC (Scheme 3).

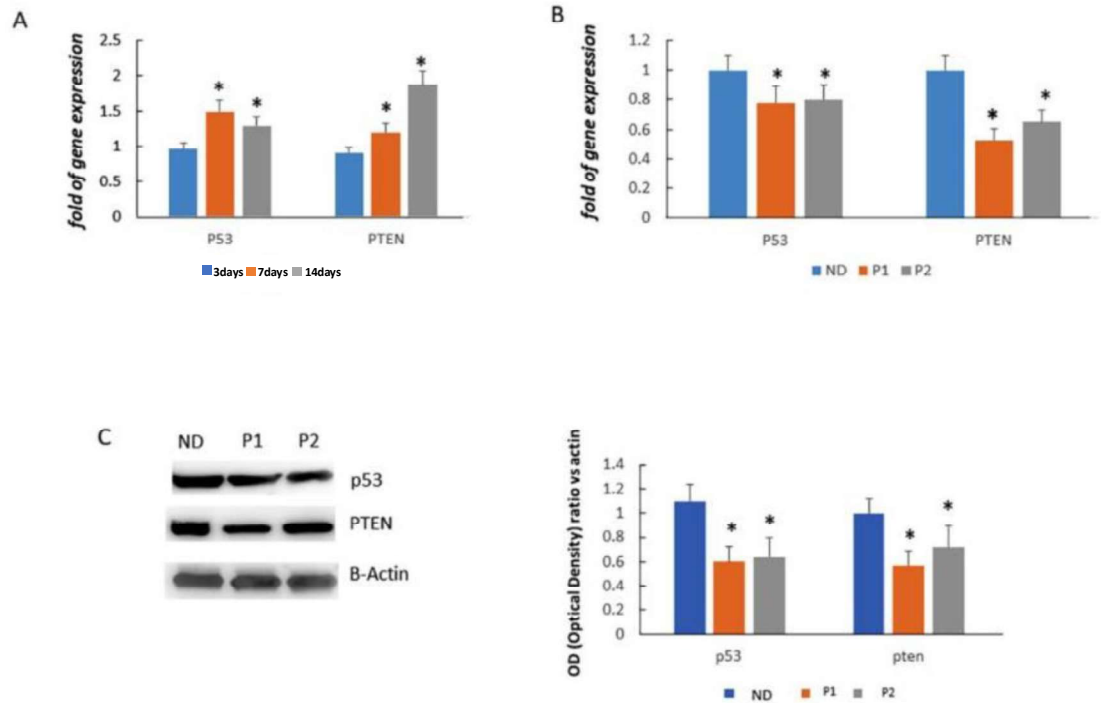
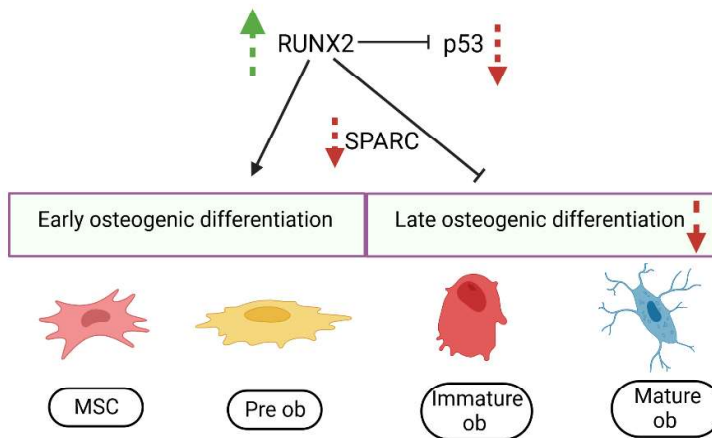


Figure 18 The expression of PTEN and p53 increased during osteogenic differentiation in a control mesenchymal stem cell (MSC) line (A). In the comparison between Cleidocranial Dysplasia (CCD) osteogenically-stimulated fibroblasts and control osteogenically-stimulated fibroblasts (ND = normal donor), gene expression levels of p53 and PTEN were reduced (B). Consequently, CCD osteogenically-stimulated fibroblasts exhibited lower levels of PTEN and p53 proteins compared to ND osteogenically-stimulated fibroblasts (C). Each analysis was conducted in triplicate, in three separate independent analyses, utilizing either MSC lines or participant samples. The data is presented as mean \pm standard deviation (SD). * $p < 0.05$



Scheme 3 A schematic representation of the changed processes resulting from mutations in the RUNX2 gene at exon 7. Arrows pointing up (higher) and down (lower) indicate how CCD patients' regulation is changing. (Created by Biorender.com)

4.3 iPSC-derived mesenchymal stem cells obtained from a patient with RUNX2-mutation

We aimed to investigate the effect of RUNX2 mutation on the expression levels of several genes involved in osteogenesis as well as on the autophagic process by analyzing Circulating Progenitors Cells (CPCs) and Induced Pluripotent Stem Cells-derived Mesenchymal Stem Cells (iPSCs-MSCs) obtained by using a non-integrating and non-transmissible Sendai viral vector system from the blood of RUNX2-mutation patient characterized by a heterozygous variant NM_001024630.3: c.505C>T in exon 4 of the gene RUNX2. This variation determines the amino acid change NP_001019801.3: p.(Arg169Trp) at the protein level, which effect is unknown.

4.3.1 Gene arrays for expression analysis in Control and RUNX2 mutation-patient

We first compared gene expression array in the control and patient' circulating progenitors. This employed technique was necessary to examine the simultaneous differential expression of several mRNA species (messenger RNA) involved in osteogenesis in the two distinct samples. The analysis entailed tagged complementary DNA (cDNA) synthesis and hybridization to identical gene arrays, that comprehend 4 endogenous controls and 92 osteogenesis-linked genes (Figure 19).

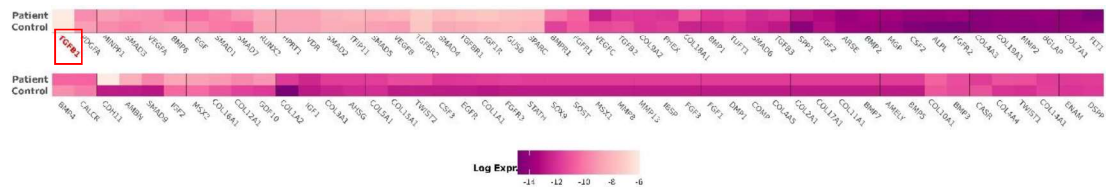


Figure 19 Comparison between control and RUNX2-mutation patient in circulating progenitors' cells to examine the simultaneous differential expression of several mRNA species involved in osteogenesis commitment.

4.3.2 Characterization of iPSCs-derived MSCs and evaluation of iPSCs-derived MSCs through cytofluorimetric analysis

In the following picture (Figure20), there are represented the iPSCs-derived MSCs for this study both for the control and the patient showing a fibroblast-like morphology typical of MSCs and plastic adherence in culture conditions.

A cytofluorimetric analysis was performed on both control and patient iPSC-derived mesenchymal stem cell lines to evaluate whether this cell type population resembles MSC-line. For this purpose, a selection of surface molecules characteristic of MSCs-like population was taken into consideration.

The results show how the iPSC-derived MSCs taken into consideration are indeed expressing surface markers that are typical of this cell type population (Figure 20). In fact, for both populations, we showed a high expression of CD73, CD105, AND CD90 which are the positive surface markers for MSC cell line¹²⁴.

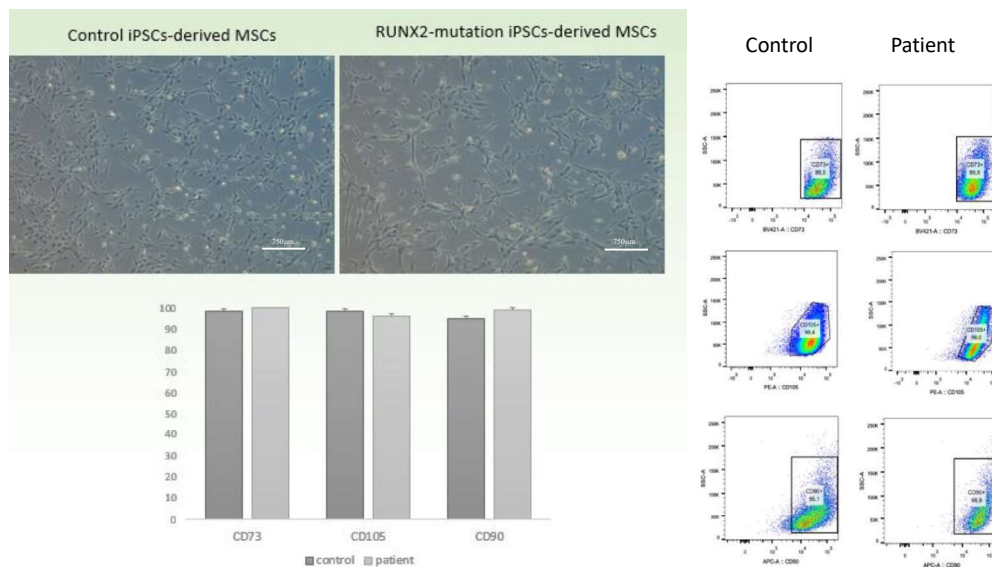


Figure 20 Morphology comparison between control and RUNX2-mutation patients of iPSC-derived MSCs and cytofluorimetric analysis of positive MSC surface markers¹²⁴. Both control and RUNX2-mutation patient seem to be MSCs cells as shown in the graph.

4.3.3 Modulation of TGF β 1, TGF β R1 and miR9 in circulating progenitors' cells and iPSCs-derived MSCs

The miR-9 gene expression was investigated considering the fundamental role miRNAs have in the regulation of osteogenic differentiation. In particular, miR-9 was analyzed in previous studies showing a role in the development of many different tumors, but also acting as a positive regulator in the modulation of RUNX2 expression¹²⁵.

Moreover, TGF- β 1 has been found to regulate the expression and activity of RUNX2. TGF- β 1 signaling pathway can activate or enhance the expression of Runx2 in osteoblasts, contributing to osteoblast differentiation and bone formation. Runx2, in turn, can regulate the expression of TGF- β 1, forming a feedback loop.

TGF- β 1 and RUNX2 are key players in bone biology, with TGF- β 1 influencing osteoblast and osteoclast activity, and RUNX2 acting as a pivotal transcription factor for osteoblast differentiation and bone formation. The interaction between TGF- β 1 and RUNX2 highlights the complex regulatory network involved in bone development and maintenance^{126,127}. In addition, the intricate interplay between miR-9, RUNX2, and TGF- β 1 is crucial for unraveling the molecular mechanisms underlying bone development, and dysregulation in these pathways could have implications in conditions such as osteoporosis or other bone-related disorders.

Results from Real-Time PCR analysis exhibited a coherent significant reduction in miR-9 activity in a patient, compared to control, both in circulating progenitors and iPSC-derived MSCs, thus deducing that if miR-9 expression is impaired, then RUNX2 is also decreased (Figure 21). In contrast, TGF- β 1 and his receptor TGF- β R1 gene, a negative regulator of RUNX2¹²⁷, were observed to be increased in both RUNX2-mutation cell populations. These results exploited the impaired effect of this mutation on osteogenesis (Figure 21).

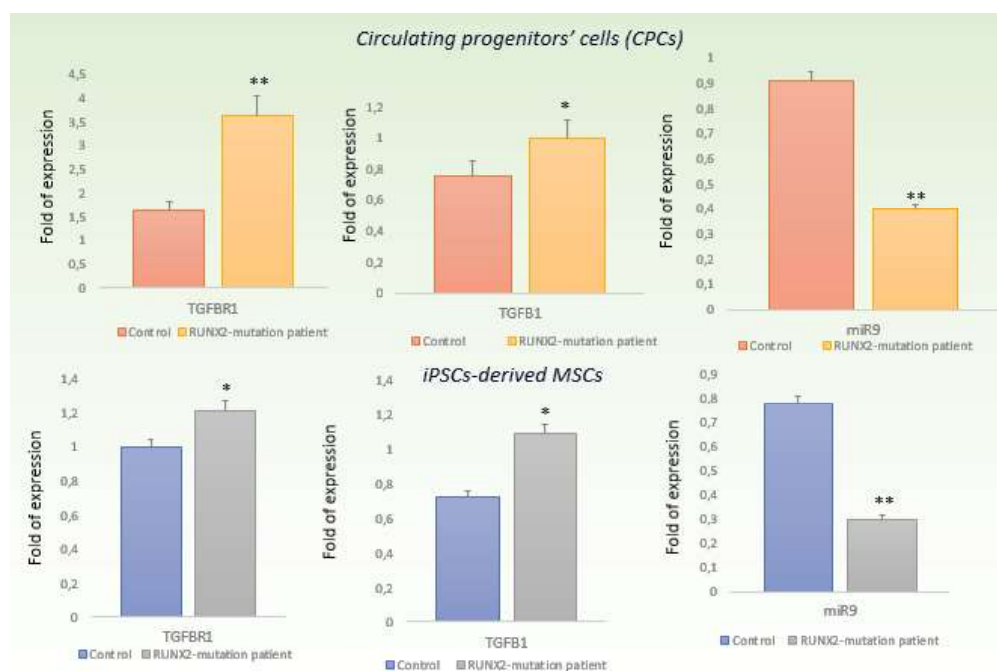


Figure 21 TGF- β 1 and his receptor TGF- β R1 gene, a negative regulator of RUNX2 was observed to be increased in both RUNX2-mutation cell populations. The RUNX2-positive modulator miR-9 was examined, showing a significantly lower expression level in both RUNX2-mutation cell populations compared to the control. These results exploited the impaired effect of this mutation on osteogenesis. * $p < 0.05$; ** $p < 0.005$.

4.3.4 Autophagy in circulating progenitors' cells and iPSCs-derived MSCs.

Autophagy is an evolutionary conserved catabolic process necessary to maintain cellular homeostasis mediating the breakdown of damaged or extraneous materials and providing energy for cell maintenance¹²⁸. It is also known to promote osteoblastic differentiation, contributing to skeletal homeostasis¹²⁹. Considering RUNX2 mutation, a decreased osteoblastic differentiation is expected also thanks to the action of autophagy, which if impaired will induce bone loss and the onset of skeletal disorders. Results for gene expression showed a decrease in all ATGs activity in patient, compared to control, both in circulating progenitors and iPSC derived MSCs, thus suggesting that this pathway is involved in RUNX2 osteoblastic differentiation and the lower levels in patients are coherent with RUNX2 mutation presence. Furthermore, the protein accumulation of p62 and LC3B in iPSCs-MSCs confirms the role of the mutation in RUNX2-mutation patient (Figure 22).

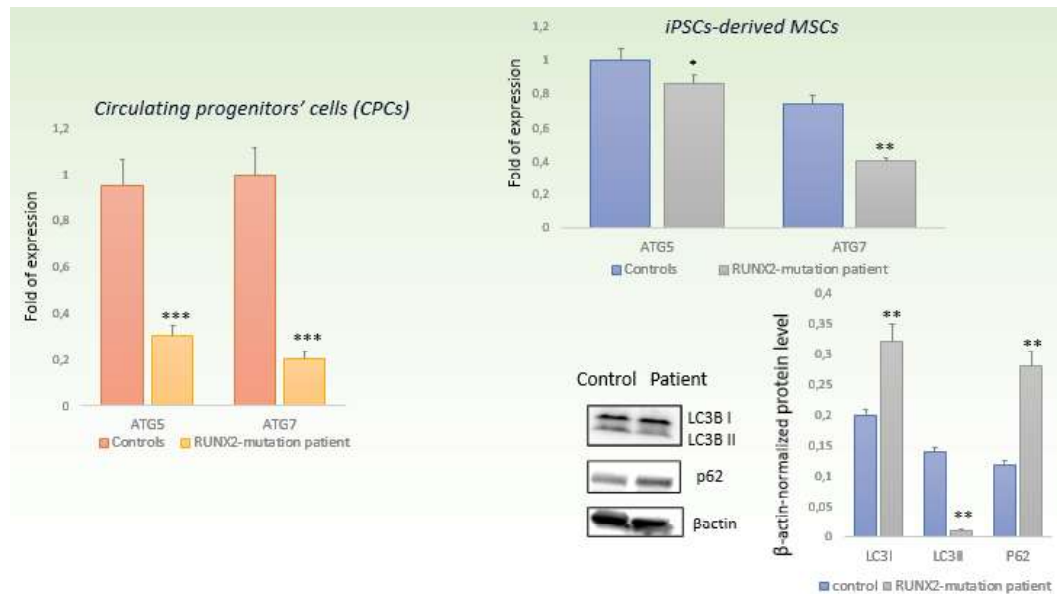


Figure 22 Expression of autophagy-related genes (ATG) was analyzed in circulating progenitors' cells and iPSCs-derived MSCs. Gene expression of ATGs was lower (0.9 vs 0.3 for ATG5; 1 vs 0.2 for ATG7 in CPCs and 1 vs 0.9 for ATG5; 0.7 vs 0.4 for ATG7 in iPSCs-derived MSCs) in both RUNX2-mutation cell populations. In addition, we have also observed p62/SQSTM1 and LC3B accumulation in iPSCs-MSCs where p62 is overexpressed in RUNX2-mutation patient. *p < 0.05; **p < 0.005; ***p < 0.001.

4.3.5 Transfection in MSCs cell line with MiR9 mimic and MiR9 silencer

To confirm the role of autophagy in Runx2 and mir9 modulation we silenced mir9 expression in lineage MSCs and increased mir9 expression via the transfection method. By analysis of gene expression via real-time PCR and by levels of protein production we can confirm that silencing mir9 expression leads to a decrease in

RUNX2 expression and an increase in proteins linked to autophagy. On the contrary, mir9 production restores the expression levels of RUNX2 and reduces the production of proteins linked to the autophagic process (Figure 23).

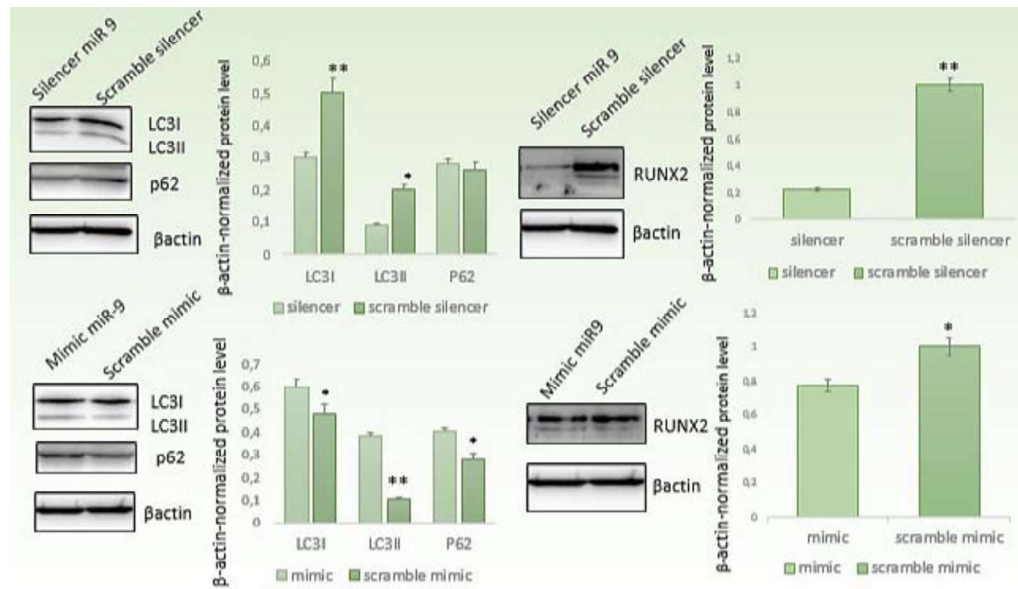
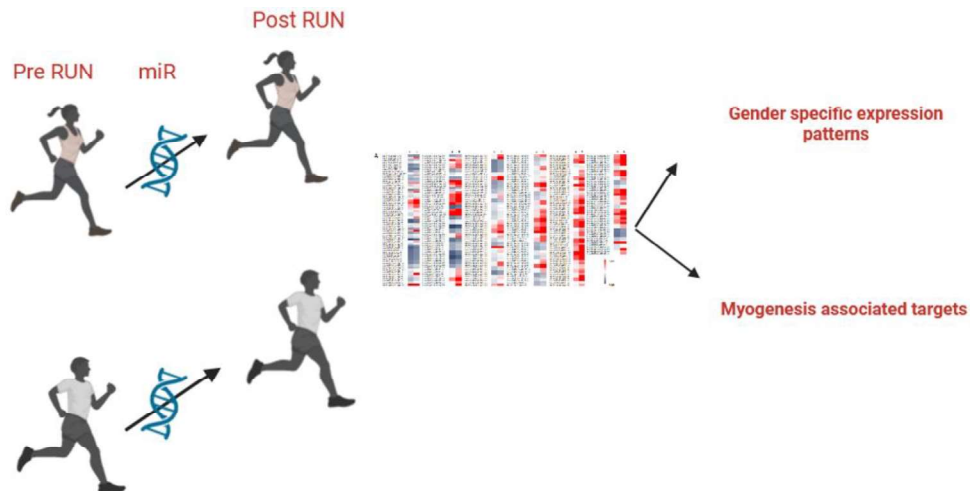


Figure 23 Silencing of miR9 in MSCs cell line negatively modulated RUNX2 protein production and increased LC3B production. Otherwise, stimulation of miR9 decreased the production of LC3B and restored RUNX2 production. *p < 0.05; **p < 0.005.

4.4 Impact of physical activity in MSCs

The modulation of miRNA expression plays a crucial role during physical exercise, and changes in miRNA levels can be considered valuable biomarkers for assessing physical performance, stress, and muscle recovery.

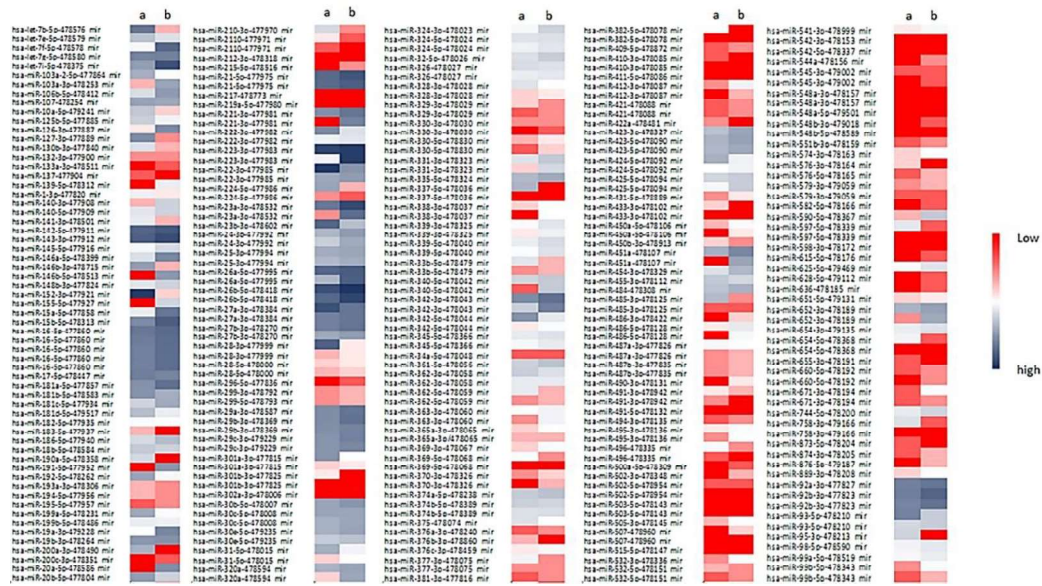
4.4.1 Gender-Associated microRNAs Profiles in Peripheral Blood



Scheme 4 Graphical abstract of participants.

4.4.2 Regardless of Gender, Half Marathon Distinctly Alters the Expression of Other PBMCs miRNAs

PBMCs from both male and female subjects were examined for miRNA patterns post-physical activity. Comparing the expression profiles, we found that some miRNAs, which did not seem to be gender-associated, were similarly modulated in male and female PBMCs. After the half marathon, we specifically saw a decrease in the expression of miR30b-3p and an increase in the expression of miR152-3p, miR143-3p, and miR27a-3p. (Figure 25). Yet, we also noticed that in contrast to males, female post-half marathon (pHM)-PBMCs had higher expression levels of miR 22-3p, miR100-5p, and miR216-5p. The array results were validated by Real-Time PCR gene expression investigation for certain miRNAs (Figure 25).



A

Fold of expression in post female

miR 22-3p, miR 152-3p, miR 100-5p, miR 143-3p, miR 216-5p, miR 27a-3p, miR 30b-3p, miR 200b-3p

B

Fold of expression in post male

miR 22-3p, miR 152-3p, miR 100-5p, miR 143-3p, miR 216-5p, miR 27a-3p, miR 30b-3p, miR 200b-3p

Figure 25 Following the half marathon, there was an observed increase in the expression of miR152-3p, miR143-3p, miR27a-3p, and a decrease in the expression of miR30b-3p and miR200b-3p in both female and male peripheral blood mononuclear cells (PBMCs). Additionally, a heightened expression of miR22-3p, miR100-5p, and miR216-5p was specifically noted in female PBMCs. *p < 0.05; **p < 0.005; ***p < 0.001

4.4.3 Modulation of Circulating miRNAs After Half Marathon

We measured the corresponding expression levels in circles for a few of the miRNAs mentioned above by obtaining sera both before and after the performance. Complementing the data in PBMCs, we saw decreased expression of miR30b-5p and miR200b-3p and increased expression of circulating miRNAs 143-3p and 27a-3p following HM (Figure 26).

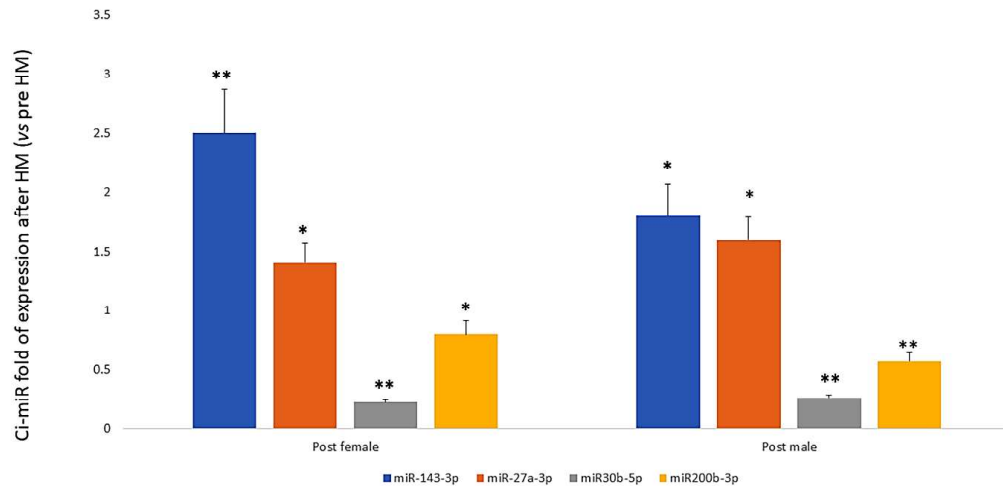


Figure 26 Elevated levels of circulating miRNAs, specifically miR143-3p and miR27a-3p, were observed, while the expression of miR30b-5p and miR200b-3p was diminished in the sera of both female and male participants following the half marathon. * $p < 0.05$; ** $p < 0.005$.

4.4.4 Half Marathon Performance Enhances MYOD Expression in Myoblasts

Since circulating miRNAs relevant to post-HM myogenesis appeared to be regulated, we investigated how runners' sera affected cultured cells during myogenic differentiation. The first indicator of myogenic commitment, MYOD, and the gene encoding muscle myosin heavy chain 2 (MHY2) were the indicators under observation. The myoblast cells were stained with hematoxylin after being cultured for either 3 or 7 days in sera obtained from female (F) or male (M) participants before (PRE) and after (POST) running a half marathon (Fig. 27A).

MHY2 expression in both genders did not alter when myoblast cells were cultivated for three days in the presence of sera obtained before and during the half marathon (pHM, Half Marathon) (Fig. 27B). Nevertheless, we found that pHM sera-conditioned cells had higher MYOD gene expression (Fig. 27C). After seven

days of cultivation in the presence of pHM sera, the expression of the MHY2 gene rose (Fig. 27D) while the expression of the MYOD gene decreased (Fig. 27E).

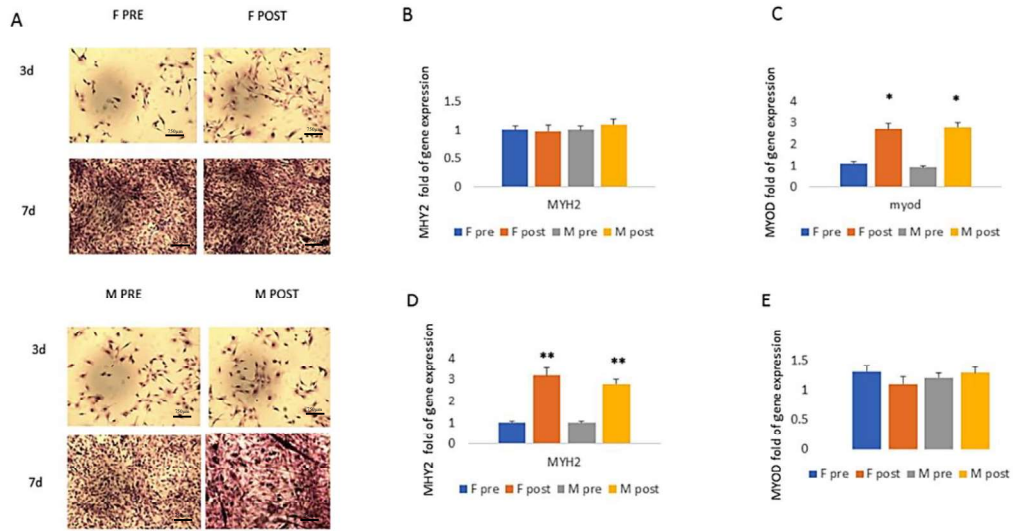


Figure 27 The myoblast cells were stained with hematoxylin after being cultured for either 3 or 7 days in sera collected before (PRE) and after (POST) a half marathon, specifically in females (F) or males (M) (A). In both genders, the expression of MYH2 did not show any significant changes after 3 days of cultivation (B). However, the gene expression of MYOD increased in cells conditioned with sera collected after the half marathon (pHM) (C). After 7 days of cell culture, in both females and males, the gene expression of MYH2 showed an increase (D), while the expression of MYOD remained unaffected (E) when cells were cultured in the presence of pHM sera. *p < 0.05; **p < 0.005.

After three days of incubation, both male and female pHM sera-conditioned cells showed increased MYOD protein levels (Fig. 28B) and a greater number of MYOD-positive cells (Fig. 28A). However, after 7 days, we also noticed elevated MYOD protein levels in male and female pHM sera conditioned-cells (Fig. 28C). Additionally, following 14 days of growth, no variations in MYOD gene expression or protein levels were seen in pHM sera conditioned-cells of either gender (Fig. 28D).

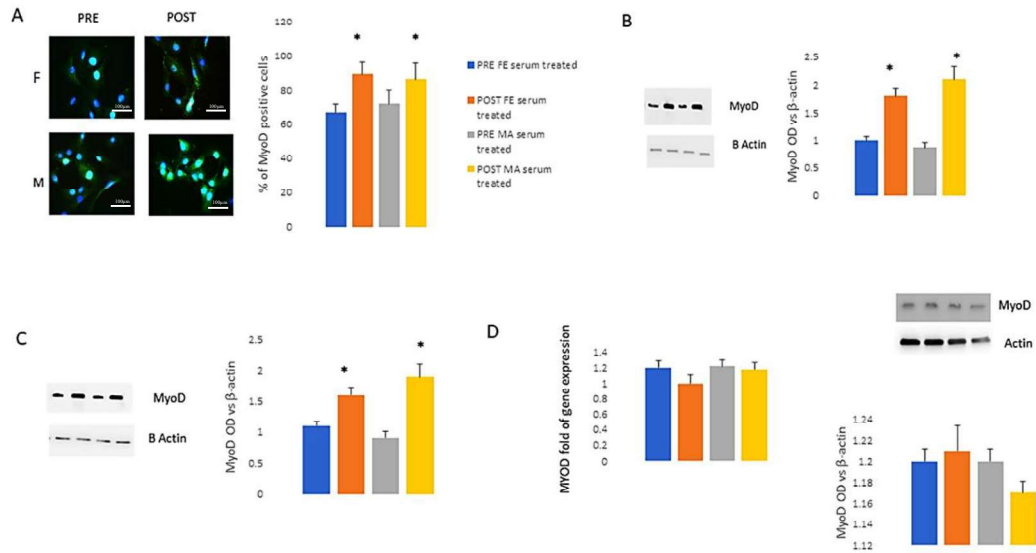


Figure 28 An Increased number of MYOD-positive cells (A) as well as MYOD protein levels (B) in both female and male pHM sera-conditioned cells was observed after 3 days of culture. MYOD protein levels were higher in cells cultured for 7 days in the presence of female or male pHM sera (C). After 14 days of culture, no difference related to MYOD expression was observed in female or male pHM sera-conditioned cells (D). * $p < 0.05$.

4.5 NorthCape4000 (NC4000) race

The most popular ultra-endurance unsupported cycling expedition is called NorthCape4000 (NC4000).

The Fourth Edition commenced on July 24, 2021. It was an unsupported, non-drifting race that took place over 4,400 km with an elevation gain of 40,000 m. Participants started in Rovereto (ITA) and traveled via four required checkpoints (Lake Balaton, Krakow, Riga, and Rovaniemi) to reach North Kapp (NRW). The organizers gave themselves 22 days to finish.

	BPP	BN	P
Age (years)	47.5 ± 13.5		
Height (cm)	178.8 ± 5.1	-	
Weight (kg)	79.25 ± 8.98	77.68 ± 8.16	0.042*
BMI (kg/m ²)	24.79 ± 2.50	24.31 ± 2.54	0.040*
Training sessions	3.13 ± 0.84	3.50 ± 1.20	0.80
Time per week (hours)	11.25 ± 3.54	11.25 ± 2.44	0.999
Distance per week (km)	241.25 ± 148.75	259.38 ± 113.34	0.448
Sleeping hours	7.13 ± 1.00	6.81 ± 1.13	0.279

BMI body mass index; BPP before preparation period; BN before NC4000 performance (post training period); AN after NC4000 performance
* $p < 0.05$

Table 17 Features of the cyclists and preparation for NC4000.

Table 17 reports the anthropometric features of cyclists. Six of the eight participants finished the NC4000 in 22 days, with an average finishing time of 21.24 ± 8.41 days and an average daily distance of 229.85 ± 68.76 km. The starting weight of the bike and baggage was 20.44 ± 4.30 kg. A multi-day ultra-cycling race was

something that none of the cyclists had ever done before. None of them adhered to a particular diet or professional training, and there were no appreciable variations in the individuals' eating patterns. None of them had dietary intolerances or allergies, nor were they vegetarians.

4.5.1 Impact of training and NC4000 on the commitment of mesenchymal stem cells

We assessed the expression of the transcription factors RUNX2 and PPARG2, associated with osteogenesis and adipogenesis, respectively, in circulating Mesenchymal Stem Cells (MSCs) to investigate the influence of training and NC4000 on MSC commitment.

RUNX2 and PPARG2, two osteogenic and adipogenic transcription factors, were increased in response to a week before NC4000 (BN) and after NC4000 (AN), as seen in Figure 29. In circulating MSCs, both ultra-cycling and training increased the expression of sestrin 1 (SESN1).

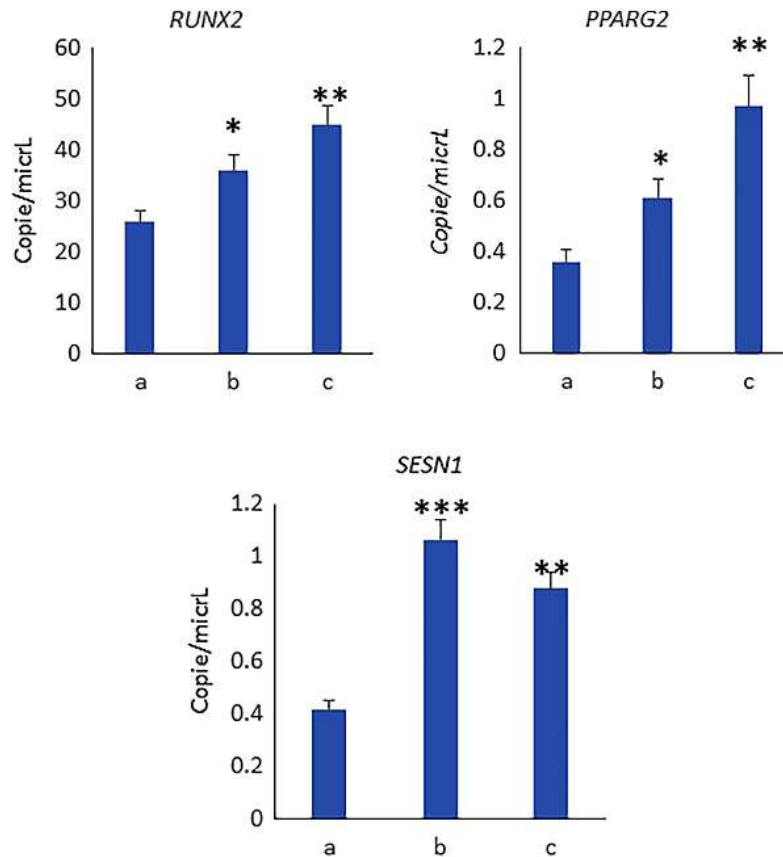


Figure 29 In comparison to BPP (a), RUNX2 and PPARG2 showed increased levels in BN (b) and AN (c). SESN1 expression was increased in circulating MSCs by BN (b) and AN (c): a (BPP, before the preparation

period); b (BN, one week before NC4000); c (AN, ten days following NC4000). ** $p < 0.005$; *** $p < 0.001$; * $p < 0.05$.

4.5.2 In SK muscle cells, training raises the amounts of sestrins and sirtuin.

We examined the SESN1 and SESN2 levels in SK muscle cells cultivated in the presence of sera obtained from before the preparation period (BPP), a week before NC4000 (BN), and after NC4000 (AN) since sestrins control the homeostasis of muscle stem cells¹³⁰. Following training, both sestrins increased as seen in Figure 28, and ultra-cycling helped to recover their protein levels. Consequently, following training with NC4000, MyoD levels rose (Figure 30). We examined the protein levels of sirtuin 1 (SIRT1) in SK muscle cells cultivated in the presence of sera obtained before, during, and after ultra-cycling, taking into account that SIRT1 is involved in the control of cellular metabolism in the presence of MyoD. SIRT1 levels rose in cells cultivated with sera obtained from BN and AN, as Figure 30B shows.

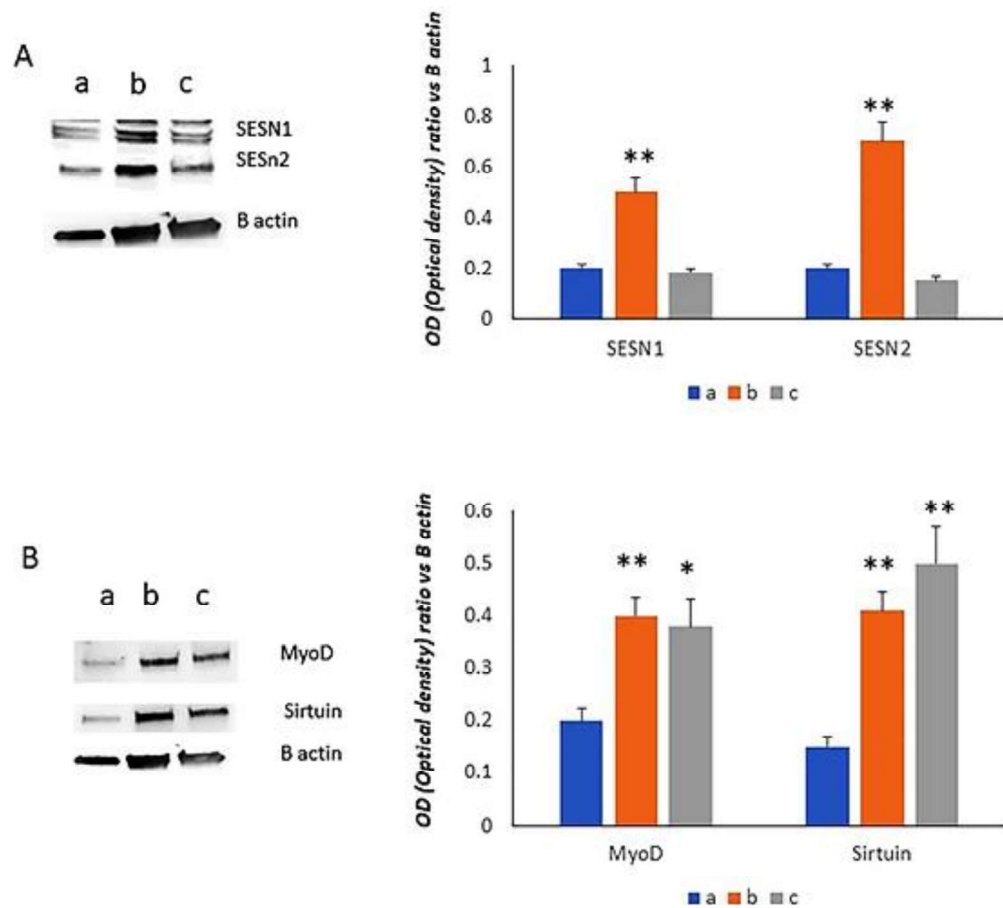


Figure 30 Following training, sestrin levels increased (b, BN), but NC4000 performance (c, AN) allowed protein levels to return. Following training, MyoD levels increased (b, BN) and NC4000 performance (c, AN). Cells grown in the presence of sera obtained from subjects during training (b, BN) and NC4000 performance

(c, AN) showed an increase in SIRT1 levels. A (BPP, before the prep period); Bn (BN, one week before NC4000); and AN (c, ten days after NC4000). ** $p < 0.005$; * $p < 0.05$.

4.5.3 Training and ultra-cycling mitigate the aging process of adipogenesis and enhance brown adipogenesis.

To assess the impact of training and ultra-cycling on adipogenesis, we cultured Mesenchymal Stem Cells (MSCs) during adipogenesis using sera collected before the preparation period (BPP), one week before NC4000 (BN), and ten days after NC4000 (AN). We observed elevated levels of sirtuin in differentiating adipogenic cells following both training and NC4000 (Figure 31). Furthermore, there were increased levels of p53 and decreased levels of p21, a p53 target gene associated with senescence (Figure 31). The reduced expression of p21 suggests a diminished transcriptional activity of p53. Interestingly, previous studies have indicated that p21 deficiency leads to the suppression of adipocyte differentiation¹³¹.

To elucidate the mechanism behind the increased sirtuin levels, we examined the expression of its targeted microRNA, miR146b, as depicted in Figure 31B. MiR146b was downregulated in MSCs exposed to sera collected from subjects after training and NC4000 performance. Given that sirtuin is known to play a crucial role in the induction of brown adipose tissue (BAT)-associated genes¹³², we assessed the levels of uncoupling protein (UCP1) in differentiating cells. As illustrated in Figure 32, UCP1 levels increased following both training and ultra-cycling.

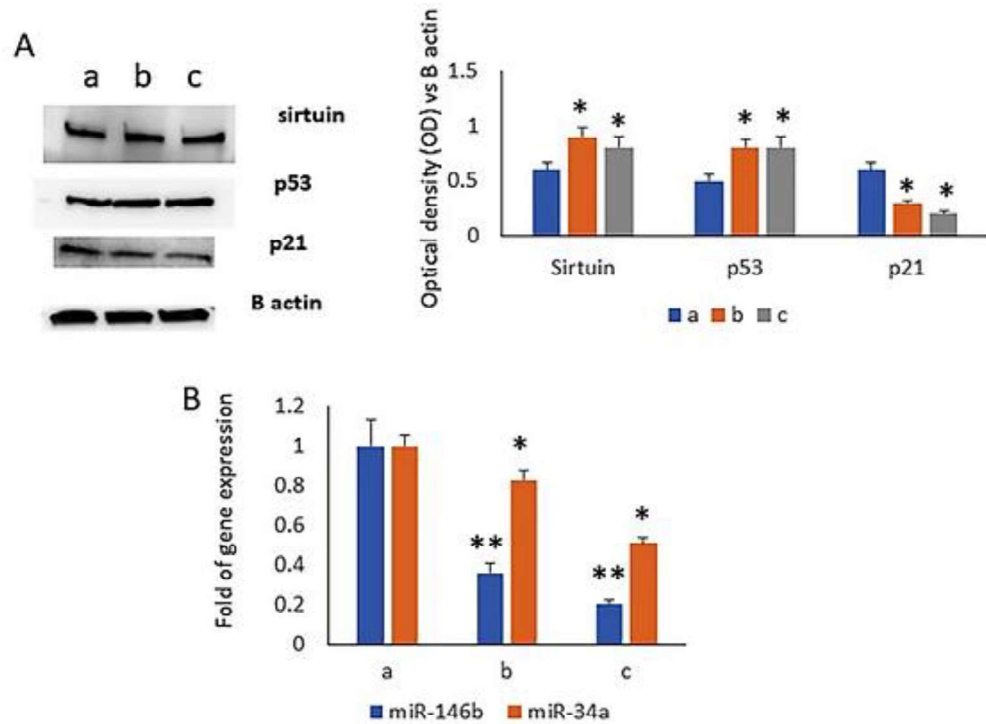


Figure 31 Elevated levels of Sirtuins and p53, along with reduced levels of p21 and miR-146b expression, were noted in Mesenchymal Stem Cells (MSCs) exposed to sera collected from subjects after training (b, BN) and NC4000 performance (c, AN). The time points for serum collection were designated as a (BPP, before the preparation period), b (BN, the week before NC4000), and c (AN, 10 days after NC4000). Statistical significance is denoted as * $p < 0.05$; ** $p < 0.005$.

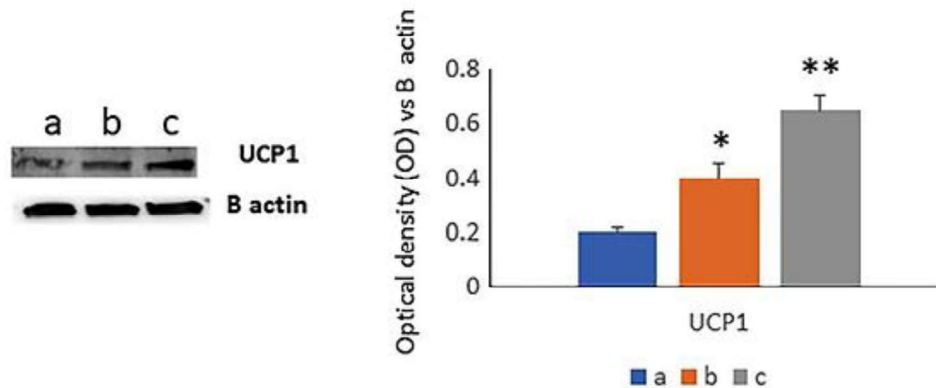


Figure 32 The levels of UCP1, associated with brown adipose tissue (BAT) differentiation, increased both after training and ultra-cycling. The designated time points for analysis were a (BPP, before the preparation period), b (BN, the week before NC4000), and c (AN, 10 days after NC4000). Statistical significance is indicated as * $p < 0.05$; ** $p < 0.005$.

4.6 3D mid-brain organoid models

Degenerative conditions of the skeleton and the brain are significant issues with significant socioeconomic effects. We investigated the effects of nutraceuticals in 3D mid-brain organoid models which have an impact on skeletal metabolism.

Using 3D mid-brain organoids as models offers several significant advantages in biomedical research and neuroscience because replicate the complexity of human brain structure and function better than 2D models, allowing for more accurate study of neurological processes, diseases, and treatments¹³³. In particular, 3D mid-brain organoids enable modeling of complex brain disorder like Parkinson's. In addition we are able to study human brain development in a controlled environment, gaining better understanding of developmental mechanisms and congenital brain defects and reduces reliance on animal models, addressing ethical concerns related to animal testing^{134 135}.

Moreover, we would try to understand the effect of some molecules chronically treating 3D mid-brain organoids derived from two different cell lines, for up to 40 days. The T413 cell line is one of the cell lines used for our studies and is characterized by LRRK2 mutation G2019S which is the most common genetic cause of Parkinson's disease (PD). T413 cells line derived induced pluripotent stem cells from PD patients harboring LRRK2 G2019S and then specifically corrected the mutant LRRK2 allele as reported by Reinhardt et al.¹³⁶. The second cell line under study is defined as BIL and is characterized by the generation of a footprint-free LRRK2-G2019S isogenic hiPS cell line edited with the CRISPR/Cas9 and piggyBac technologies¹³⁷.

4.6.1 Comparison between wild-type/gene correct mid-brain organoids vs mutated mid-brain organoids

JH-II-127 is a potent and selective inhibitor of both wild-type and G2019S mutant LRRK2. At concentrations of 0.1–0.3 μM , it significantly inhibits the phosphorylation of Ser910 and Ser935 in both wild-type and G2019S mutant LRRK2 in a variety of cell types¹³⁸.

The other molecule of interest was lipoic acid as previous studies have shown positive effects in combination with vitamin D3. As for vitamin D3, we already know its benefits for bone metabolism^{139–141}. The synergy of vitamin D3 and lipoic acid compounds has shown beneficial effects on the vitality of astrocytes since the substances can cross the brain barrier. Additionally, combined LA and vitD3 attenuated H₂O₂-induced apoptosis through the mitochondria-mediated pathway. Moreover, the combination was effective in mitigating the adverse effects induced by iron, thereby preventing its accumulation¹⁴².

Here, we investigated the modulation of LRP5 and CTNNB1 genes in mid-brain organoids affected by LRRK2- G2019S mutation with wild-type/gene correct organoids, using the two different molecules discussed before. We observed an increase of LRP5 and CTNNB1, which are involved in the Wnt/ β catenin pathway in the T413 cell line compared with the BIL cell line. Additionally, we also investigated the gene modulation of PARK2 and NR2F1, which are known to be dysregulated in patients affected by Parkinson's disease. Also, in this case, we saw an increase in both genes in the T413 cell line (Figure 33).

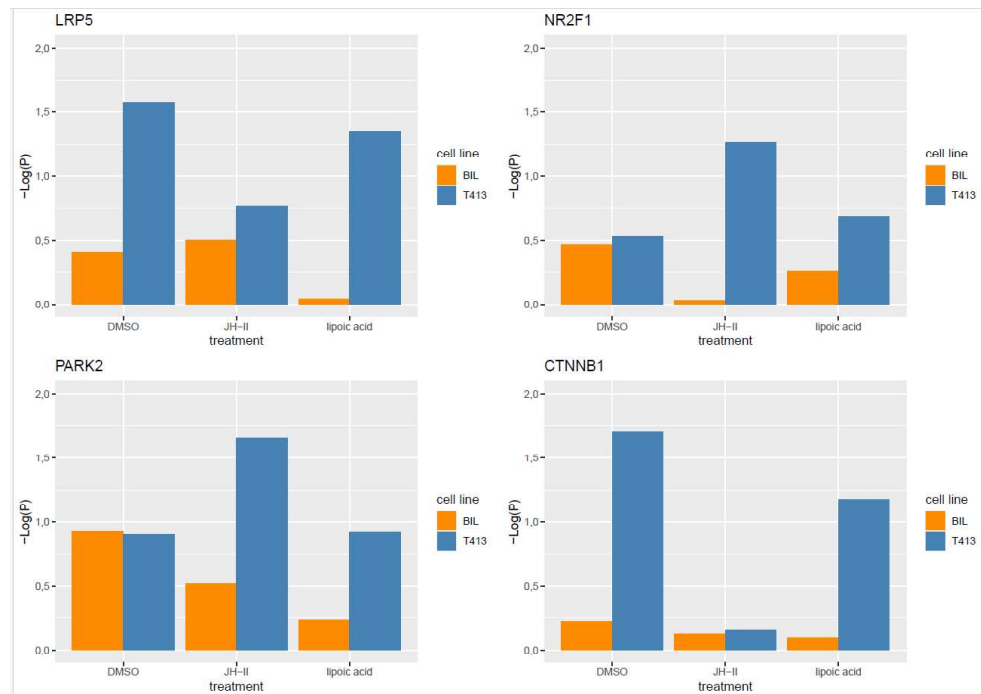


Figure 33 Comparison between BIL organoids vs T413 organoids at 40 days of differentiation. We analyzed the modulation of the expressions of CTNNB1, NR2F1, LRP5 and PARK2 and graphically represented the significance levels of gene expression performed with t-test for the different genes with the treatments (Figure 33).

4.6.2 Comparison between BIL wild-type mid-brain organoids vs T413 mutated organoids

We were also interested in understanding the expression of our 4 genes of interest in the two different mid-brain organoids, always comparing the mutated condition to the control. Specifically, the analysis performed involved comparing the wild-type organoid line BIL with the mutated T413 organoid line. As shown in Figure 34 below, the treatments increase the expression levels of the genes of interest. Lipoic acid seems to have a greater effect than the JH-II-127 inhibitor.

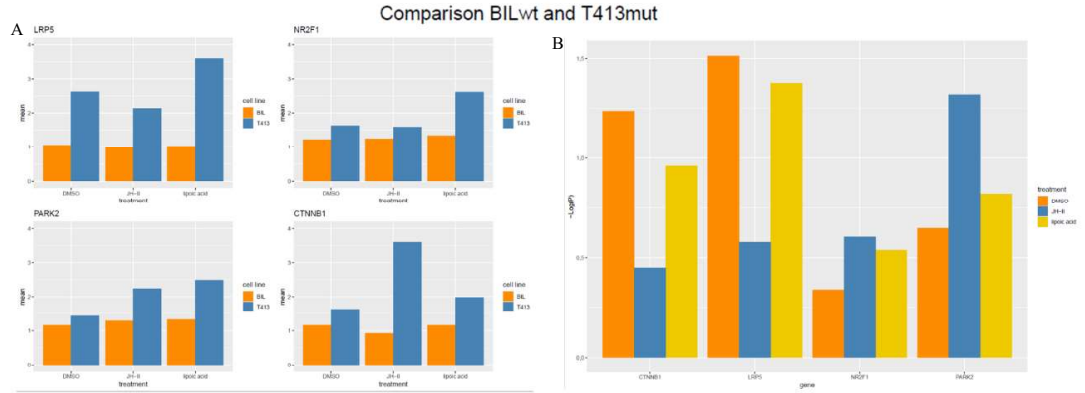


Figure 34 Comparison between BIL wild-type organoids vs T413 mutated organoids at 40 days of differentiation. We analyzed the modulation of the expression CTNNB1, NR2F1, LRP5, and PARK2 and graphically represented the mean values of gene expression (Figure 34a) and the significance levels of gene expression obtained with t-test, for the different genes with the treatments (Figure 34b).

4.6.3 Immunofluorescence analysis of organoids at 40 days of differentiation

We also conducted an analysis using a confocal microscope to examine the expression of three neuronal markers that exhibit down-regulation in Parkinson's disease (PD) patients. Among these markers is Glial Fibrillary Acidic Protein (GFAP), an intermediate filament-III protein exclusively found in astrocytes within the central nervous system (CNS), non-myelinating Schwann cells in the peripheral nervous system (PNS), and enteric glial cells. The expression of GFAP mRNA is subject to modulation by various factors, including nuclear-receptor hormones, growth factors, and lipopolysaccharides¹⁴³. Tyrosine Hydroxylase (TH) serves as a marker for neurons and endocrine cells containing dopamine, norepinephrine, and epinephrine (catecholamine). It is expressed transiently during development in neurons and neuroendocrine cells, which in adulthood either cease to express TH or express it at very low levels¹⁴⁴. Microtubule-associated protein 2 (MAP2) plays a crucial role in the growth, differentiation, and plasticity of neurons. It has key functions in neuronal responses to growth factors, neurotransmitters, synaptic activity, and neurotoxins¹⁴⁵. This analysis was conducted in the organoids derived from both the Gene-Correct (GC) and mutated T413 cell lines.

These markers were examined in the context of Gene-Correct (GC) and mutated (MUT) T413 cell line organoids using a confocal microscope to gain insights into their expression patterns and potential implications in Parkinson's disease pathology (Figure 35). We can observe that the 3D mid-brain organoids treated with the molecule JH-II, compared to those untreated (DMSO), appear to restore the

expression of neuronal markers. In particular, we notice a restoration of MAP2 and TH, as well as in the organoids treated with lipoic acid.

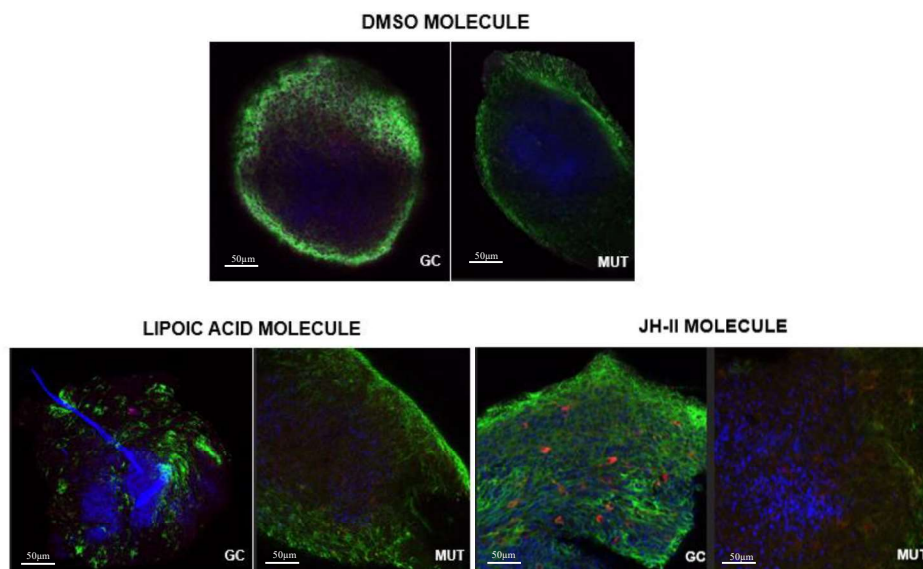


Figure 35 Confocal images of mid-brain organoids at 40 days of differentiation derived from the mutated and non-mutated T413 cell lines, treated with DMSO, lipoic acid and JH-II respectively. In blue we can see the nuclei, in green the MAP2 marker, in red the TH marker and in purple the GFAP marker.

5 DISCUSSION

The function of FBXW11 in the cell cycle, differentiation, and tumorigenesis has been previously demonstrated⁵⁰. However, there is a gap in research regarding the role of FBXW11 in osteogenesis. In this study, we examined the upregulation of FBXW11 expression during the middle phase of osteogenesis. Notably, there was a decrease in β -catenin expression during the middle and late phases of differentiation. Previous reports indicate that β -catenin is a target of FBXW11¹⁴⁶, and our findings suggest that FBXW11 regulates RUNX2 through the modulation of β -catenin. These conclusions are supported by data obtained from silencing FBXW11 in osteogenic cells, revealing elevated levels of both RUNX2 and β -catenin. However, in FBXW11 silenced cells, we observed a reduction in the expression of osteogenic maturation-associated genes, including BGLAP, SPP1, and ALPL, during the late phase of osteogenic differentiation. These results indicate a crucial role for FBXW11 in osteogenic maturation. Given the reported necessity for downregulating RUNX2 expression in the late phase of osteogenesis, the decreased levels of FBXW11, allowing continuous expression of RUNX2, may

impact osteogenic maturation. Additionally, we explored the impact of FBXW11 in the enforced expression of RUNX2, independent of β -catenin activation. In this regard, we inhibited the expression of miR-204, a microRNA targeting RUNX2. Our results revealed an increase in FBXW11 expression after 7 days, but not after 3 or 14 days, of osteogenic differentiation. This observation suggests a role for FBXW11 during the middle phase of differentiation, rather than in the early or late phases of osteogenesis. Consistent with this, Wang et al.⁴⁹ demonstrated higher expression of FBXW11 in mature progenitors. Moreover, as observed in various malignancies, the ubiquitin-proteasome system plays a significant role in osteosarcoma as well¹⁴⁷. Osteosarcoma arises due to impaired osteogenic differentiation resulting from genetic or epigenetic alterations¹⁴⁸. The alteration of FBXW11 expression in osteosarcoma in contrast to regular osteoblasts has been insufficiently probed. To bridge this informational void, we scrutinized FBXW11 expression in two osteosarcoma cell lines (MG63 and U2OS) and primary human osteoblasts (HOB). Our results demonstrated reduced levels of FBXW11 protein in MG63 and U2OS osteosarcoma cells compared to normal osteoblasts. Furthermore, β -catenin levels were higher in osteosarcoma cells (MG63 and U2OS) than in normal osteoblasts. However, gene expression analyses revealed an overexpression of FBXW11 in osteosarcoma cells compared to HOB.

To elucidate the contrasting findings between RNA and protein levels, we investigated the expression of miR-221, known to target FBXW11. Correspondingly, miR-221 showed higher expression in osteosarcoma cells compared to HOB, suggesting that epigenetic alterations play a crucial role in osteosarcoma by influencing FBXW11 expression. Our data reveal a significant modulation of FBXW11 during differentiation, with elevated levels of FBXW11 leading to a reduction in target β -catenin levels under normal conditions. However, under pathological conditions such as cleidocranial dysplasia (CCD), the relationship between FBXW11 and RUNX2 or β -catenin deviates from normal conditions, indicating a lack of β -catenin degradation by FBXW11. In this disease model, FBXW11 levels might be increased to counteract the dysregulated levels of β -catenin. Conversely, in osteosarcoma cells, the decrease in FBXW11 protein levels increases β -catenin.

Our interest has also focused on investigating the effect of mutations in the RUNX2 where most of them have been associated with cleidocranial dysplasia (CCD), a congenital disorder affecting bone growth^{149 150}. We previously identified novel C-terminus RUNX2 mutations in CCD patients, observing RUNX2 overexpression in osteogenic differentiated cMSCs from these patients compared to control cells. In our study, we identified nonsense mutations in the c-terminus of RUNX2 in two unrelated patients with cleidocranial dysplasia (CCD). Additionally, a missense mutation in exon 7, c.1259C→T[p.T420I], was detected in a CCD Chinese family¹⁵¹. This threonine residue is conserved in vertebrate runt proteins, suggesting a pathogenic role¹⁵². The PST domain, which extends from exon 5 to exon 8, contains essential sequences for post-translational modifications and plays a significant role in transactivation or transcription repression functions¹⁵². Consequently, mutations in the PST domain may potentially impair the transactivation or transcription repression functions of RUNX2. Specifically, we identified two novel loss-of-function (LOF) mutations: c.897T>G->p.(Tyr299*) and c.1019del->p.(Ser340*). In the first case, the mutation led to the substitution of Tyrosine 299 with a premature STOP codon, while in the second case, a C deletion caused a frameshift, resulting in a premature STOP codon. Both mutations resulted in the heterozygous loss of the PST domain.

The PST domain is crucial as it contains sequences vital for post-translational regulation by extracellular signal-regulated kinase 1 and 2 (Erk1/2), protein kinase A (PKA), and Akt kinases¹⁵³. Additionally, the NMTS (Nuclear Matrix Targeting Signal) located within the PST domain regulates the association of RUNX2 with subnuclear locations in the nuclear matrix, playing a significant role in RUNX2 activity¹⁵³. Studies have shown that mice lacking NMTS and the remaining C-terminus are incapable of bone production, preventing osteoblastic maturation and emphasizing the importance of the NMTS region for RUNX2 function in vivo¹⁵⁴. The reported mutations also affect other crucial sequences within the PST domain, such as AD3 (a transactivation domain) and RD (repression domain)¹⁵⁵. By culturing MSCs in the presence or absence of an osteogenic medium, our study revealed an opposing modulation between FBXW11 and RUNX2. Specifically, FBXW11 expression demonstrated higher levels in Mesenchymal Stem Cells (MSCs) compared to cells committed to osteogenesis. Conversely, gene expression analyses performed on circulating MSCs derived from individuals with

cleidocranial dysplasia (CCD), cultured with or without osteogenic medium, revealed an increase in both FBXW11 and RUNX2 levels during osteogenic commitment. Furthermore, FBXW11 levels were found to be elevated in osteogenically stimulated CCD fibroblasts in comparison to control cells. This suggests that the overexpression of FBXW11 aims to adjust the levels of mutated RUNX2 transcription factors. However, the excessive expression of FBXW11, leading to alterations in the ubiquitin-proteasome system, could potentially contribute to impaired osteogenesis in CCD patients. Indeed, ubiquitin protease signaling is a crucial regulatory pathway in the differentiation process of bone marrow-derived MSCs, such as osteogenesis¹⁵⁶. Surprisingly, in osteogenically stimulated CCD fibroblasts, elevated levels of β -catenin were also observed. As FBXW11 binds to its target proteins at phosphorylated sites to induce degradation, the increased β -catenin, along with heightened FBXW11 levels, suggests reduced phosphorylated β -catenin levels in CCD samples, highlighting the dysregulation of the cellular signal associated with RUNX2 mutations. Moreover, our previous report indicated reduced osteogenic maturation in fibroblasts from CCD patients compared to controls.

Moreover, despite the observed upregulation of the RUNX2 gene in Pt.2 cMSCs and increased RUNX2 protein levels in the os-fibroblasts of both CCD patients, we identified a reduction in RUNX2 transcriptional activity in their cultured cells. Other authors have reported that mutations affecting the carboxy terminus of RUNX2 can impair its transcriptional activity¹⁵⁷. In line with this, we noted a decrease in the expression of SPARC, a target gene of RUNX2, in cells from CCD patients.

SPARC is an osteonectin-rich, secreted acidic protein abundant in cysteine, and is one of the most prevalent non-collagenous proteins in mineralized tissues¹⁵⁸. Studies have shown that SPARC-null mice exhibit intervertebral disc degeneration and are nonresponsive to bone-anabolic parathyroid treatment, suggesting a role in mineralization¹⁵⁹. The reduced mineralization observed in os-cells of CCD patients, as indicated by decreased SPARC gene expression and Alizarin red staining, may contribute to skeletal features such as clavicle hypoplasia, delayed bone maturation, absence of carpal bone ossification, and skeletal dysmorphisms. Despite the increased levels of RUNX2 protein, which seems contradictory to the established

RUNX2 haploinsufficiency in CCD patients, our data indicate that mutations in exon 7 of RUNX2 may result in protein overproduction. It is important to note that haploinsufficiency can manifest in various complex scenarios, depending on the nature of the mutations. Our study's limitation includes the absence of a female pediatric control; however, previous research has shown that gender differences in RUNX2 expression become significant only from age 20, and age-related changes in bone mineral density start becoming evident from age 15 in the young population¹⁶⁰. In healthy prepubertal individuals, variations in RUNX2 expression based on gender are not anticipated. The inclusion of a 10-year-old child in our study is deemed suitable for comparative analysis with the two pediatric CCD patients. Therefore, the observed increase in RUNX2 protein levels in the os-fibroblasts of both CCD patients may result from compensation mechanisms for the diminished expression of downstream osteogenic genes, such as SPARC, or the accumulation of dysfunctional RUNX2. It is noteworthy that the excessive expression of RUNX2 has been shown to compromise bone quality, as previously demonstrated in acromegaly patients^{160,161}. The dual role of p53 in osteogenesis has been established, affecting both osteogenic commitment and terminal osteogenic differentiation¹⁶². Recent findings by Zhou et al. emphasized the importance of Wnt/ β -catenin-mediated p53 suppression for the osteogenic differentiation of mesenchymal progenitor cells¹⁶³. To investigate the effects of RUNX2 mutations on p53 expression, we explored putative protein interactions using the STRING portal. Our bioinformatics analysis revealed a robust interaction between RUNX2 and p53, influencing various biological processes such as replicative senescence, stress-induced premature senescence, determination of adult lifespan, and negative regulation of cell cycle arrest, among others. Furthermore, it has been established that PTEN is a downstream gene of p53¹⁶⁴. In our *in vitro* experiments involving a Mesenchymal Stem Cell (MSC) cell line, we detected heightened expression of p53 and PTEN genes during osteogenic differentiation. Conversely, CCD cells displayed lower expression levels of both p53 and PTEN mRNAs and proteins compared to the control. These observations corresponded with decreased calcification in CCD cells, as evidenced by Alizarin red staining, indicating that the dysregulation of RUNX2 hinders osteogenic maturation by diminishing p53 levels. Another goal of this study was to investigate the effect of RUNX2 mutation in relation to the autophagic process. We analyzed Circulating Progenitors Cells

(CPCs) and Induced Pluripotent Stem Cells-derived Mesenchymal Stem Cells (iPSCs-MSCs) from RUNX2-mutation patient characterized by a heterozygous variant NM_001024630.3: c.505C>T in exon 4 of the gene RUNX2 that determines the amino acid change NP_001019801.3: p.(Arg169Trp) at the protein level, which effect is unknown. We initially confirmed that iPSC-MSCs expressed typical markers of mesenchymal stem cell⁷. Following an initial screening of genes related to bone metabolism through TaqMan Human Osteogenesis Array, we directed our attention towards examining the interaction between TGF- β and its receptor. The expression levels of TGF- β 1 and its receptor were observed to be elevated in both RUNX2-mutation cell populations. In non-pathological scenarios, TGF- β initiates the upregulation of miR-9, a microRNA that subsequently acts to the expression of RUNX2. This regulatory mechanism suggests that TGF- β influences the cellular milieu by inducing the production of miR-9, which, in turn, exerts a positive effect on the expression of the RUNX2 gene^{165 166}. However, in RUNX2-mutation patient, examination of the RUNX2-positive modulator miR-9 revealed significantly diminished expression levels in both RUNX2-mutation cell populations compared to the control. These findings underscore the compromised impact of this mutation on osteogenesis. A mutation in the RUNX2 gene leads to a decrease in the expression of genes linked to autophagy, and this mutation results in an accumulation of these genes at the protein level. This phenomenon can be elucidated by the pivotal role of RUNX2 as the master gene in bone metabolism¹⁵⁴, facilitating continual bone regeneration and formation. A mutation in the RUNX2 sequence leads to an obstruction at the osteogenic commitment level, impeding the breakdown of mutated cells and resulting in an accumulation of autophagic genes incapable of fulfilling their function^{167,168}. Our findings were supported by additional evidence from our investigation in the MSC cell line. When miR-9 was silenced, there was a detrimental impact on the production of the RUNX2 protein, accompanied by an increase in LC3B production. Conversely, when miR-9 was stimulated, there was a reduction in LC3B production, and the production of RUNX2 was restored.

Moreover, in bone cellular metabolism, a fundamental role in regulation occurs at the epigenetic level. In particular is known that microRNAs (miRNAs) are short molecules, approximately 22 nucleotides in length, and are critical regulators in a broad range of cellular and physiological processes⁸⁶. These processes include

proliferation, differentiation, repair mechanisms, signaling, and apoptosis¹⁶⁹. MiRNAs exert their influence by modulating the expression of target genes. They achieve this by binding to the 3' untranslated region (3'UTR) of the target gene transcripts, leading to either their degradation or the inhibition of the translational process^{170,171}. In addition, it was reported that the levels of circulating miRNAs can be linked to exercise intensity and activity, particularly about maximum oxygen uptake⁸⁸ and we have recently shown that engaging in physical activity induces osteogenic differentiation by regulating the expression of multiple miRNAs¹⁷². We analyzed the impact of high-intensity exercise on the modulation of progenitor cell abundance and differentiation immediately after the activity. It would be interesting to investigate these cells after a more extended interval from physical performance. It has been proposed that physical exercise leads to an augmentation in the quantity of Bone-Marrow-Derived Mesenchymal Stem Cells, concurrently enhancing their osteogenic potential while reducing their commitment to adipogenesis¹⁷³. Previous studies examining miRNA responses to exercise have predominantly focused on male athletes. However, it is well-established that females exhibit gender-specific responses in cardiovascular, musculoskeletal, and metabolic¹⁷⁴ patterns following physical exercise. Sex-specific miRNA patterns are believed to arise in response to gonadal steroids, such as dihydrotestosterone and progesterone. Notably, since gonadal steroids are affected during exercise, sex-specific miRNA expression levels have been considered in response to dihydrotestosterone and progesterone stimulation¹⁷⁵. Therefore, our study aimed to examine the gender-specific role in miRNA modulation following a half-marathon. We initially assessed potential differences in miRNA expression between men and women. Interestingly, we observed similar miRNA expressions, with few exceptions. Specifically, Mir223-3p and Mir-26b levels were 17 and 14 times higher, respectively, in women compared to men. Based on our findings, we hypothesized that the miRNA expression profiles observed in PBMCs before the competition might be reliable. In particular, the expression of certain gender-related miRNAs aligns with female physiology. The elevated levels of Mir223-3p in female PBMCs correlate with their known role in the endometrium, as suggested by Dong et al.¹⁷⁶. MiR-26b is abundantly expressed in adipose tissue¹⁷⁷. During adipogenic differentiation, the expression of miR-26b is upregulated¹⁷⁸. Additionally, it has been suggested that the expression of MiR-26b is directly related to the composition of milk fatty acids¹⁷⁸. MiR-26b

expression is also involved in the regulation of mammary epithelial cells along with lipid-related transcription factors in goats¹⁷⁷. Hence, our data suggest that differences in gender-associated miRNA modulation might be linked to female physiology and, consequently, different hormonal statuses. Upon analyzing miRNA modulation in PBMCs post-half-marathon (HM), heightened expression of miR152-3p, miR143-3p, miR27a-3p, and diminished expression of miR30b were evident in both female and male participants. Notably, the augmented expression of specific miRNAs, including miR22-3p and miR100-5p, was exclusively observed in female PBMCs. It is worth noting that decreased levels of miR-22-3p have been documented in individuals with premature ovarian failure¹⁷⁶. Estrogen receptor 1 (ESR1) and phosphatase and tensin homolog (PTEN) have been identified as potential candidate genes associated with ovarian failure¹³⁶. Furthermore, bioinformatic analyses have predicted that MiR-22-3p acts as a negative regulator of ESR1 and PTEN. Likewise, elevated expression of miR100-5p has been noted in granulosa cells from women exhibiting a normal ovarian reserve in contrast to those with diminished ovarian reserve¹⁷⁹. Therefore, our data suggests a protective role of physical activity in preventing ovarian dysfunctions. The expression of miR-143 and its target gene is disrupted in primary myoblasts, affecting muscle regeneration¹⁸⁰. MiR-152 has been noted for its role in suppressing cell proliferation and promoting myoblast differentiation in the C2C12 cell line¹⁸¹. In porcine myotubes, the increased expression of miR-152 has been associated with the facilitation of slow-twitch myofiber formation and myogenesis¹⁸². Similarly, the demonstrated impact of miR-27a includes the promotion of myoblast proliferation by targeting the inhibitor of skeletal myogenesis, Myostatin. Recent studies have highlighted the regulatory influence of miR-23a and miR-27a, both clustered together, on proteins involved in the atrophy process. Notably, the overexpression of miR-23a/27a in muscle has been shown to counteract diabetes-induced muscle cachexia¹⁸³. Given the validation of PBMCs as surrogate models for skeletal muscle tissue¹⁸⁴, we posit that the observed modulation of miRNAs in PBMCs may similarly manifest in cells participating in myogenesis.

To strengthen this hypothesis, we assessed the expression of circulating miRNAs and explored the potential modulation of these miRNAs following exercise. Our findings indicate that circulating miRNAs mirror the alterations observed in PBMCs. Notably, we observed a significant downregulation of circulating miRNA

200b-3p following the half marathon. It is worth noting that miR-200b has been demonstrated to target the GATA transcription factor, which plays a role in cardiac myocyte proliferation and differentiation¹⁸⁵. To reinforce the findings related to altered myogenesis-associated circulating miRNAs post half-marathon, we conducted cell cultures using sera obtained from runners before and after the race. Our findings, particularly regarding the expression of MYOD (a transcription factor crucial for myogenic commitment)¹⁶, validated heightened myogenic differentiation in cells treated with sera collected after the physical activity. Consequently, despite the gender-specific differential expression of certain miRNAs observed in PBMCs under normal physiological conditions, it can be concluded that physical activity induces the modulation of miRNAs associated with muscle differentiation in both women and men.

Furthermore, in our study, we aimed to investigate how another stimulus different from HM may influence cellular metabolism.

Ultra-endurance cycling represents a highly demanding performance, commonly characterized as a race exceeding 100 miles. This form of cycling is associated with a variety of physiological consequences. Despite the growing interest in ultra-endurance sports in recent years, only a limited number of studies have explored the impact of this physical exertion on the modulation of biochemical parameters and the commitment of progenitor cells. This is a significant aspect as the homeostasis of progenitor cells plays a crucial role in the pathogenesis of degenerative diseases, and factors influencing and maintaining this homeostasis are potential targets for disease prevention. Another distinctive feature of our study is that it was conducted on amateur competitive cyclists who underwent lower training volumes compared to professional cyclists¹⁸⁶. Consequently, our study sheds light on the potential correlation between changes in body composition, adipogenesis, and myogenesis.

In this study, we conducted the first-ever evaluation of potential driver genes and transcriptional factors involved in the observed mechanism. Physical training, as reported previously promotes the differentiation of Mesenchymal Stem Cells (MSCs)¹⁷². Specifically, we noted an increased expression of RUNX2 in circulating progenitor (CP) MSCs post-training, suggesting an osteogenic commitment, a response maintained after normalization. Additionally, elevated levels of PPARG2 were observed post-training and post-NC4000, suggesting a potential increase in adipogenic commitment. However, the heightened expression

of PPARG2 aligns with its role in regulating insulin sensitivity and glucose utilization for energy homeostasis maintenance¹⁸⁷. Correspondingly, we observed the expression of the SESN1 gene in CP-MSCs, encoding a small stress-inducible protein known to enhance insulin sensitivity¹³⁰. Notably, we investigated, for the first time, the expression of sestrin in circulating progenitor cells, highlighting the effective role of physical exercise in degenerative diseases due to the protective nature of sestrin¹⁸⁸.

To further explore the role of sestrins in modulating muscle metabolism following exercise, SESN1, and SESN2 protein levels were examined in skeletal muscle cells treated with sera collected before and after training, as well as after NC4000. Interestingly, increased levels of SESN1 and SESN2 were observed in skeletal muscle cells treated with sera collected post-training, while both SESN1 and SESN2 levels returned to baseline in cells treated with serum post-NC4000 performance. Considering the protective activity of sestrins against musculoskeletal diseases¹⁸⁸, it can be inferred that training is beneficial in countering conditions such as sarcopenia, muscle atrophy, osteopenia, and arthritic pathologies.

Hence, we explored the effects of training and ultra-cycling on skeletal muscle cells. The induction of SESN1 during myotube differentiation has been documented¹³⁰. Consistent with this, we observed heightened levels of sestrins and MYOD in SK muscle cells treated with sera collected post-training. Increased MYOD levels persisted even after NC4000, despite a tendency to decrease. Sirtuin1, a histone/protein deacetylase linked to caloric restriction-mediated longevity¹¹⁸, demonstrated elevated levels in SK muscle cells post-training. In the presence of MyoD, SIRT1 positively self-regulates the expression of peroxisome proliferator-activated receptor- γ co-activator-1 α (PGC-1 α), a master regulator of genes governing metabolism¹⁸⁹. Exercise-induced PGC-1 α expression in skeletal muscle likely responds to decreased ATP levels¹⁹⁰. The heightened levels of MYOD and Sirtuin 1 in SK muscle cells after training imply the influence of physical exercise in promoting muscle-specific gene expression and metabolism. Additionally, Sirtuin 1 levels increased in MSCs during adipogenic differentiation after both training and ultra-cycling. The increased levels of Sirtuin 1 led to a reduction in the transcriptional activity of p53. Despite an increase in p53 levels after training and NC4000, we noted a decrease in the levels of p21, a downstream target gene of p53. SIRT1 activation during adipogenesis is known to promote the transcription of

brown adipose tissue-specific genes¹⁹¹. Additionally, SIRT1 is involved in downregulating white adipose tissue (WAT) gene expression¹⁹². Thus, we observed increased levels of uncoupling protein 1 (UCP1), unique to brown adipose tissue (BAT) cells, in MSCs during adipogenesis post-training. Remarkably, the surge in UCP1 exhibited a more pronounced elevation in the presence of sera obtained post-NC4000. These findings emphasize the correlation between BAT and the significant decrease in truncal and visceral adipose tissue (VAT) as markers of negative energy balance following NC4000. Considering that BAT activation, coupled with the modification of body composition, has been suggested to mitigate diseases linked to obesity, delving further into the impact of rigorous physical exercise on cardiovascular and degenerative diseases proves particularly captivating. To pinpoint epigenetic elements involved in the elevation of sirtuin1, we investigated the expression of miRs that target sirtuin1. Consequently, we observed diminished levels of miR146b and miR34a in cells subjected to sera collected post-BN and post-NC4000. Intriguingly, miR-146b has been identified as a regulator of human visceral adipogenesis, and its altered expression is connected to human obesity¹⁹³, emphasizing the importance of modulating this metabolic pathway to prevent cardiovascular and degenerative diseases.

Hence, our research represents the inaugural examination of functional biochemical parameters in conjunction with alterations in progenitor cells. We explore, akin to the scenario with sestrins, the influence of physical activity on molecules implicated in the development of degenerative ailments. The outcomes of our investigation, carried out on individuals in good health, may enhance comprehension regarding the effects of physical prowess, particularly in the realm of ultra-endurance endeavors, on the dedication of progenitor cells and the potential mitigation of degenerative diseases.

However, physical activity is not the sole means that can impact cellular metabolism. Indeed, the use of nutraceuticals also plays a crucial role in stimulating mesenchymal stem cells toward a specific differentiation^{194,195}. Nutraceuticals are food substances or products that provide health benefits beyond basic nutrition. Many of them contain bioactive compounds that can interact with cells and affect various metabolic processes. Many nutraceuticals are known for their antioxidant action^{196,197}. Antioxidants help neutralize free radicals, reducing oxidative stress in cells. This can have a positive impact on cellular metabolism and the prevention of

cellular damage. In addition, the vitamins and minerals present in nutraceuticals are essential for many metabolic reactions within cells. For example, vitamin D is involved in the regulation of calcium metabolism¹⁴⁰. It is important to note that the effects of nutraceuticals on cellular metabolism may vary depending on the dose, duration of intake, and individual characteristics. For instance, it is reported that the use of alpha-lipoic acid in combination with vitamin D3 positively influences dopaminergic neurons¹⁴². According to the findings, in our study, we found that molecules' impacts on the expression of the genes associated with the Wnt / β -catenin pathway upstream and downstream appear to have a beneficial impact on the rise in the expression of the target genes. An increase in LRP5 gene expression encourages an increase in β -catenin expression, which is likewise influenced by PARK2 gene expression. In fact, through the expression of particular osteomarkers, PARK2 overexpression may trigger the expression of β -catenin and the process of autophagy¹¹⁰.

Furthermore, PARK2 which is frequently mutated and has lower expression in people with Parkinson's, is responsible for these findings and our preliminary data reported a greater expression in 3D models that have been treated with molecules. Similar to NR2F1, which is also referred to as nuclear receptor 2 families 1 and is a member of the Human Hormone Nuclear Receptor (hHNR) family¹¹¹, NR2F1 transcript is significantly downregulated in dopaminergic neurons and midbrain organoids produced from Parkinson's disease (PD) patients carrying the LRRK2-G2019S mutation compared to healthy controls¹¹². Considering an improvement in the conditions of Parkinson's patients, the treatment with the molecules we examined would increase the expression of gene link to the crosstalk brain-bone.

6 CONCLUSIONS

Our study investigated varied aspects of mesenchymal stem cells and their differentiation. Offers novel perspectives on the impact of RUNX2 mutations in cleidocranial dysplasia (CCD) patients. It suggests that a comprehensive analysis of the gene network associated with RUNX2 could enhance our understanding of the intricate molecular and phenotypic changes observed in individuals with these mutations. In addition, our study represents the first exploration of FBXW11 expression in both normal and impaired osteogenic lineages. Furthermore, it

reaffirms the involvement of ubiquitin-proteasome system (UPS)-associated proteins in cell differentiation and alterations. The study proposed FBXW11 as a potential negative prognostic factor in osteosarcoma, emphasizing its role as a marker for disease progression. Further studies are required to deepen the understanding of the molecular mechanisms involved, confirming the involvement of ubiquitin-proteasome system-associated proteins in cell differentiation and related alterations. Our data suggest that physical activity induces the modulation of myogenesis-associated miRNAs in both females and males, despite the gender-associated differential expression of specific miRNAs. These findings hold potential value for identifying targets in microRNA-based therapies for diseases affecting the myogenic stem cell population. The training program produces beneficial effects on body composition and biochemical lipid parameters, accompanied by a shift in brown adipogenesis and significant modifications in cellular processes related to SESN1 and SESN2 expression. Notably, these effects are observed even when oxygen uptake and ventilatory thresholds remain unchanged in trained amateur cyclists. In the case of ultra-cycling, although it does not impact body weight or aerobic capacity, it induces an acute and prolonged energy imbalance leading to a reduction in fat mass. Moreover, ultra-cycling brings about changes in Mesenchymal Stem Cells (MSCs) commitment, with a notable increase in brown adipogenesis and UCP1, along with the maintenance of MYOD levels in skeletal muscle cells. Given the growing participation in ultra-endurance events, future research should focus on non-elite ultra-cyclers, emphasizing preparation and training for ultra-endurance performance. Additionally, there is a need for research investigating the long-term effects of ultra-cycling and the persistence of post-acute metabolic modifications.

In addition, the data available to investigate the crosstalk between brain-bone is still raw and needs more in-depth study. Furthermore, after critically investigating the results, the prospects are those of testing the molecules used for mid-brain organoids in mesenchymal cells in osteogenic differentiation.

7 REFERENCES

1. Heidari, B. *et al.* Comparison of Proliferative and Multilineage Differentiation Potential of Sheep Mesenchymal Stem Cells Derived from Bone Marrow, Liver, and Adipose Tissue. *Avicenna J Med Biotechnol* **5**, 104–117 (2013).
2. Friedenstein, A. J., Petrakova, K. V., Kurolesova, A. I. & Frolova, G. P. Heterotopic of bone marrow. Analysis of precursor cells for osteogenic and hematopoietic tissues. *Transplantation* **6**, 230–247 (1968).
3. Friedenstein, A. J., Piatetzky-Shapiro, I. I. & Petrakova, K. V. Osteogenesis in transplants of bone marrow cells. *J Embryol Exp Morphol* **16**, 381–390 (1966).
4. Gai Via, A., Frizziero, A. & Oliva, F. Biological properties of mesenchymal Stem Cells from different sources. *Muscles Ligaments Tendons J* **2**, 154–162 (2012).
5. Nauta, A. J. & Fibbe, W. E. Immunomodulatory properties of mesenchymal stromal cells. *Blood* **110**, 3499–3506 (2007).
6. Ullah, I., Subbarao, R. B. & Rho, G. J. Human mesenchymal stem cells - current trends and future prospective. *Biosci Rep* **35**, e00191 (2015).
7. Ghaneialvar, H., Soltani, L., Rahmani, H. R., Lotfi, A. S. & Soleimani, M. Characterization and Classification of Mesenchymal Stem Cells in Several Species Using Surface Markers for Cell Therapy Purposes. *Indian J Clin Biochem* **33**, 46–52 (2018).
8. Almalki, S. G. & Agrawal, D. K. Key Transcription Factors in the Differentiation of Mesenchymal Stem Cells. *Differentiation* **92**, 41–51 (2016).
9. Han, Y. *et al.* The secretion profile of mesenchymal stem cells and potential applications in treating human diseases. *Sig Transduct Target Ther* **7**, 1–19 (2022).

10. Liu, Q. *et al.* Advances in the application of bone morphogenetic proteins and their derived peptides in bone defect repair. *Composites Part B: Engineering* **262**, 110805 (2023).
11. Du, X., Cai, L., Xie, J. & Zhou, X. The role of TGF-beta3 in cartilage development and osteoarthritis. *Bone Res* **11**, 1–16 (2023).
12. Niu, T. & Rosen, C. J. The insulin-like growth factor-I gene and osteoporosis: A critical appraisal. *Gene* **361**, 38–56 (2005).
13. Gattazzo, F., Urciuolo, A. & Bonaldo, P. Extracellular matrix: a dynamic microenvironment for stem cell niche. *Biochim Biophys Acta* **1840**, 2506–2519 (2014).
14. Mevel, R., Draper, J. E., Lie-a-Ling, M., Kouskoff, V. & Lacaud, G. RUNX transcription factors: orchestrators of development. *Development* **146**, dev148296 (2019).
15. Lefebvre, V. & Dvir-Ginzberg, M. SOX9 and the many facets of its regulation in the chondrocyte lineage. *Connect Tissue Res* **58**, 2–14 (2017).
16. Kim, J. A. *et al.* MYOD mediates skeletal myogenic differentiation of human amniotic fluid stem cells and regeneration of muscle injury. *Stem Cell Research & Therapy* **4**, 147 (2013).
17. GE, C. *et al.* Reciprocal Control of Osteogenic and Adipogenic Differentiation by ERK/MAP Kinase Phosphorylation of Runx2 and PPAR γ Transcription Factors. *J Cell Physiol* **231**, 587–596 (2016).
18. Valenti, M. T., Dalle Carbonare, L. & Mottes, M. Osteogenic Differentiation in Healthy and Pathological Conditions. *Int J Mol Sci* **18**, 41 (2016).
19. Day, T. F., Guo, X., Garrett-Beal, L. & Yang, Y. Wnt/beta-catenin signaling in mesenchymal progenitors controls osteoblast and chondrocyte differentiation during vertebrate skeletogenesis. *Dev Cell* **8**, 739–750 (2005).

20. Duan, P. & Bonewald, L. The Role of the Wnt/ β -catenin Signaling Pathway in Formation and Maintenance of Bone and Teeth. *Int J Biochem Cell Biol* **77**, 23–29 (2016).
21. Vimalraj, S., Arumugam, B., Miranda, P. J. & Selvamurugan, N. Runx2: Structure, function, and phosphorylation in osteoblast differentiation. *Int J Biol Macromol* **78**, 202–208 (2015).
22. Kim, W.-J., Shin, H.-L., Kim, B.-S., Kim, H.-J. & Ryoo, H.-M. RUNX2-modifying enzymes: therapeutic targets for bone diseases. *Exp Mol Med* **52**, 1178–1184 (2020).
23. Zhang, Q. *et al.* RUNX2 co-operates with EGR1 to regulate osteogenic differentiation through Htra1 enhancers. *J Cell Physiol* **235**, 8601–8612 (2020).
24. Qin, X. *et al.* RUNT-RELATED TRANSCRIPTION FACTOR-2 (RUNX2) is required for bone matrix protein gene expression in committed osteoblasts in mice. *J of Bone & Mineral Res* **36**, 2081–2095 (2021).
25. Komori, T. Whole Aspect of Runx2 Functions in Skeletal Development. *Int J Mol Sci* **23**, 5776 (2022).
26. Komori, T. Molecular Mechanism of Runx2-Dependent Bone Development. *Mol Cells* **43**, 168–175 (2020).
27. Komori, T. Whole Aspect of Runx2 Functions in Skeletal Development. *Int J Mol Sci* **23**, 5776 (2022).
28. Kawane, T. *et al.* Runx2 is required for the proliferation of osteoblast progenitors and induces proliferation by regulating Fgfr2 and Fgfr3. *Sci Rep* **8**, 13551 (2018).
29. Wnt/ β -catenin signalling: function, biological mechanisms, and therapeutic opportunities | Signal Transduction and Targeted Therapy. <https://www.nature.com/articles/s41392-021-00762-6>.

30. Chen, H. *et al.* Runx2 Regulates Endochondral Ossification through Control of Chondrocyte Proliferation and Differentiation. *J Bone Miner Res* **29**, 2653–2665 (2014).
31. Fujita, T. *et al.* Runx2 induces osteoblast and chondrocyte differentiation and enhances their migration by coupling with PI3K-Akt signaling. *The Journal of Cell Biology* **166**, 85 (2004).
32. Vlashi, R., Zhang, X., Wu, M. & Chen, G. Wnt signaling: Essential roles in osteoblast differentiation, bone metabolism and therapeutic implications for bone and skeletal disorders. *Genes & Diseases* **10**, 1291–1317 (2023).
33. Komori, T. Regulation of Proliferation, Differentiation and Functions of Osteoblasts by Runx2. *Int J Mol Sci* **20**, 1694 (2019).
34. Gaur, T. Canonical WNT Signaling Promotes Osteogenesis by Directly Stimulating Runx2 Gene Expression*. *Gene Expression* **280**, (2005).
35. Komori, T. Regulation of bone development and extracellular matrix protein genes by RUNX2. *Cell and tissue research* **339**, 189–95 (2009).
36. Blair, H. C. *et al.* Osteoblast Differentiation and Bone Matrix Formation In Vivo and In Vitro. *Tissue Eng Part B Rev* **23**, 268–280 (2017).
37. Qin, X. *et al.* Cbfb regulates bone development by stabilizing Runx family proteins. *J Bone Miner Res* **30**, 706–714 (2015).
38. Deiana, M. *et al.* New Insights into the Runt Domain of RUNX2 in Melanoma Cell Proliferation and Migration. *Cells* **7**, 220 (2018).
39. Riminucci, M. *et al.* Coexpression of bone sialoprotein (BSP) and the pivotal transcriptional regulator of osteogenesis, Cbfa1/Runx2, in malignant melanoma. *Calcif Tissue Int* **73**, 281–289 (2003).

40. Boregowda, R. K. *et al.* RUNX2 is overexpressed in melanoma cells and mediates their migration and invasion. *Cancer Lett* **348**, 61–70 (2014).
41. Perduca, M. *et al.* Runx2 downregulation, migration and proliferation inhibition in melanoma cells treated with BEL β -trefoil. *Oncology Reports* **37**, 2209–2214 (2017).
42. Cecconi, D. *et al.* Runx2 stimulates neoangiogenesis through the Runt domain in melanoma. *Sci Rep* **9**, 8052 (2019).
43. The ubiquitin system: from cell signalling to disease biology and new therapeutic opportunities | Cell Death & Differentiation. <https://www.nature.com/articles/s41418-020-00703-w>.
44. Fornari, F. *et al.* p53/mdm2 feedback loop sustains miR-221 expression and dictates the response to anticancer treatments in hepatocellular carcinoma. *Mol Cancer Res* **12**, 203–216 (2014).
45. Kitagawa, K. & Kitagawa, M. The SCF ubiquitin ligases involved in hematopoietic lineage. *Curr Drug Targets* **13**, 1641–1648 (2012).
46. Wang, L. *et al.* Fbxw11 promotes the proliferation of lymphocytic leukemia cells through the concomitant activation of NF- κ B and β -catenin/TCF signaling pathways. *Cell Death Dis* **9**, 427 (2018).
47. Bi, Y., Cui, D., Xiong, X. & Zhao, Y. The characteristics and roles of β -TrCP1/2 in carcinogenesis. *FEBS J* **288**, 3351–3374 (2021).
48. Cui, D. *et al.* The cross talk of two family members of β -TrCP in the regulation of cell autophagy and growth. *Cell Death Differ* **27**, 1119–1133 (2020).
49. Wang, L. *et al.* Fbxw11 Variants Control the Quiescence of HSCs. *Blood* **128**, 5052 (2016).
50. Wang, L. *et al.* Fbxw11 impairs the repopulation capacity of hematopoietic stem/progenitor cells. *Stem Cell Res Ther* **13**, 245 (2022).

51. Fbxw11 promotes the proliferation of lymphocytic leukemia cells through the concomitant activation of NF- κ B and β -catenin/TCF signaling pathways - PubMed. <https://pubmed.ncbi.nlm.nih.gov/29555946/>.
52. MicroRNA-221 promotes cisplatin resistance in osteosarcoma cells by targeting PPP2R2A - PubMed. <https://pubmed.ncbi.nlm.nih.gov/31221814/>.
53. Dalle Carbonare, L. *et al.* Modulation of miR-204 Expression during Chondrogenesis. *Int J Mol Sci* **23**, 2130 (2022).
54. Moseti, D., Regassa, A. & Kim, W.-K. Molecular Regulation of Adipogenesis and Potential Anti-Adipogenic Bioactive Molecules. *International Journal of Molecular Sciences* **17**, 124 (2016).
55. González-Casanova, J. E., Pertuz-Cruz, S. L., Caicedo-Ortega, N. H. & Rojas-Gomez, D. M. Adipogenesis Regulation and Endocrine Disruptors: Emerging Insights in Obesity. *Biomed Res Int* **2020**, 7453786 (2020).
56. Farmer, S. R. Transcriptional control of adipocyte formation. *Cell Metab* **4**, 263–273 (2006).
57. Biomedicines | Free Full-Text | The Role of Adipokines in Health and Disease. <https://www.mdpi.com/2227-9059/11/5/1290>.
58. Syverud, B. C., VanDusen, K. W. & Larkin, L. M. Growth Factors for Skeletal Muscle Tissue Engineering. *Cells Tissues Organs* **202**, 169–179 (2016).
59. Thanaskody, K. *et al.* MSCs vs. iPSCs: Potential in therapeutic applications. *Front. Cell Dev. Biol.* **10**, 1005926 (2022).
60. Jin, Y.-Z. & Lee, J. H. Mesenchymal Stem Cell Therapy for Bone Regeneration. *Clin Orthop Surg* **10**, 271 (2018).
61. Jovic, D. *et al.* A Brief Overview of Global Trends in MSC-Based Cell Therapy. *Stem Cell Rev and Rep* **18**, 1525–1545 (2022).

62. Zhang, J. *et al.* Induced Pluripotent Stem Cell-Derived Mesenchymal Stem Cells Hold Lower Heterogeneity and Great Promise in Biological Research and Clinical Applications. *Front. Cell Dev. Biol.* **9**, 716907 (2021).
63. Bilgiç, E., Boyacıoğlu, Ö., Gizer, M., Korkusuz, P. & Korkusuz, F. Chapter 6 - Architecture of bone tissue and its adaptation to pathological conditions. in *Comparative Kinesiology of the Human Body* (eds. Angin, S. & Şimşek, I. E.) 71–90 (Academic Press, 2020). doi:10.1016/B978-0-12-812162-7.00006-0.
64. Florencio-Silva, R., Sasso, G. R. D. S., Sasso-Cerri, E., Simões, M. J. & Cerri, P. S. Biology of Bone Tissue: Structure, Function, and Factors That Influence Bone Cells. *BioMed Research International* **2015**, 1–17 (2015).
65. Currall, V. *et al.* Cleidocranial dysplasia. *Current Orthopaedics* **21**, 159–162 (2007).
66. Xue, R., Zhang, G., Chen, X. & Ye, X. Cleidocranial Dysplasia Causing Respiratory Distress in Neonates: A Case Report and Literature Review. *Frontiers in Genetics* **12**, (2021).
67. Dalle Carbonare, L. *et al.* Two Novel C-Terminus RUNX2 Mutations in Two Cleidocranial Dysplasia (CCD) Patients Impairing p53 Expression. *Int J Mol Sci* **22**, 10336 (2021).
68. Toptancı, İ. R., Çolak, H. & Köseoğlu, S. Cleidocranial dysplasia: Etiology, clinicoradiological presentation and management. *J CLIN EXP INVEST* **3**, 133–136 (2012).
69. Jamali, E., Khalesi, R., Bitarafan, F., Almadani, N. & Garshasbi, M. Identification of a Novel Splice Site Mutation in RUNX2 Gene in a Family with Rare Autosomal Dominant Cleidocranial Dysplasia. *Iran Biomed J* **25**, 297–302 (2021).
70. Otto, F. *et al.* Cbfa1, a candidate gene for cleidocranial dysplasia syndrome, is essential for osteoblast differentiation and bone development. *Cell* **89**, 765–771 (1997).

71. Karsenty, G. & Mera, P. Molecular bases of the crosstalk between bone and muscle. *Bone* **115**, 43–49 (2018).
72. Qiu, Y. *et al.* Exercise sustains the hallmarks of health. *J Sport Health Sci* **12**, 8–35 (2023).
73. Liu, Y. *et al.* The beneficial effects of physical exercise in the brain and related pathophysiological mechanisms in neurodegenerative diseases. *Laboratory Investigation* **99**, 943–957 (2019).
74. Brunet, A., Goodell, M. A. & Rando, T. A. Ageing and rejuvenation of tissue stem cells and their niches. *Nat Rev Mol Cell Biol* **24**, 45–62 (2023).
75. Luan, X. *et al.* Exercise as a prescription for patients with various diseases. *J Sport Health Sci* **8**, 422–441 (2019).
76. Myers, J. Exercise and Cardiovascular Health. *Circulation* **107**, e2–e5 (2003).
77. Booth, F. W., Roberts, C. K. & Laye, M. J. Lack of exercise is a major cause of chronic diseases. *Compr Physiol* **2**, 1143–1211 (2012).
78. Tieland, M., Trouwborst, I. & Clark, B. C. Skeletal muscle performance and ageing. *J Cachexia Sarcopenia Muscle* **9**, 3–19 (2018).
79. Schnyder, S. & Handschin, C. Skeletal muscle as an endocrine organ: PGC-1 α , myokines and exercise. *Bone* **80**, 115–125 (2015).
80. Crosstalk between Bone and Muscles during Physical Activity - PMC. <https://www.ncbi.nlm.nih.gov/pmc/articles/PMC10453939/>.
81. Lippi, G. *et al.* The baseline serum value of α -amylase is a significant predictor of distance running performance. *Clin Chem Lab Med* **53**, 469–476 (2015).
82. Williams, C. & Nute, M. L. Some physiological demands of a half-marathon race on recreational runners. *Br J Sports Med* **17**, 152–161 (1983).

83. Ji, L. L. Antioxidants and oxidative stress in exercise. *Proc Soc Exp Biol Med* **222**, 283–292 (1999).
84. Fitts, R. H. The cross-bridge cycle and skeletal muscle fatigue. *J Appl Physiol (1985)* **104**, 551–558 (2008).
85. Mendell, J. T. & Olson, E. N. MicroRNAs in stress signaling and human disease. *Cell* **148**, 1172–1187 (2012).
86. Krol, J., Loedige, I. & Filipowicz, W. The widespread regulation of microRNA biogenesis, function and decay. *Nat Rev Genet* **11**, 597–610 (2010).
87. Valenti, M. T., Dalle Carbonare, L., Dorelli, G. & Mottes, M. Effects of physical exercise on the prevention of stem cells senescence. *Stem Cell Rev Rep* **16**, 33–40 (2020).
88. Circulating MicroRNAs as Potential Biomarkers of Exercise Response - PubMed. <https://pubmed.ncbi.nlm.nih.gov/27782053/>.
89. van Rooij, E., Liu, N. & Olson, E. N. MicroRNAs flex their muscles. *Trends Genet* **24**, 159–166 (2008).
90. Rosenkilde, M. *et al.* Inability to match energy intake with energy expenditure at sustained near-maximal rates of energy expenditure in older men during a 14-d cycling expedition. *Am J Clin Nutr* **102**, 1398–1405 (2015).
91. Knechtle, B. Nutrition and Ultra-Endurance. in *Nutrition and Enhanced Sports Performance* 161–170 (Elsevier, 2013). doi:10.1016/B978-0-12-396454-0.00016-3.
92. Rüst, C. A., Rosemann, T., Lepers, R. & Knechtle, B. Gender difference in cycling speed and age of winning performers in ultra-cycling - the 508-mile ‘Furnace Creek’ from 1983 to 2012. *J Sports Sci* **33**, 198–210 (2015).
93. Scheer, V. Participation Trends of Ultra Endurance Events. *Sports Med Arthrosc Rev* **27**, 3–7 (2019).

94. Knechtle, B., Wirth, A., Knechtle, P., Rüst, C. A. & Rosemann, T. A comparison of ultra-endurance cyclists in a qualifying ultra-cycling race for Paris-Brest-Paris and Race Across America-Swiss cycling marathon. *Percept Mot Skills* **114**, 96–110 (2012).
95. Bircher, S., Enggist, A., Jehle, T. & Knechtle, B. Effects of an extreme endurance race on energy balance and body composition - a case study. *J Sports Sci Med* **5**, 154–162 (2006).
96. Kyle Levers, A. J. Effects of an Ultra-Endurance Event on Body Composition, Exercise Performance and Markers of Clinical Health: A Case Study. *Bioenergetics* **03**, (2014).
97. Rehrer, N. J., Hellemans, I. J., Rolleston, A. K., Rush, E. & Miller, B. F. Energy intake and expenditure during a 6-day cycling stage race. *Scand J Med Sci Sports* **20**, 609–618 (2010).
98. Knechtle, B., Knechtle, P. & Kohler, G. The effect of 1,000 km nonstop cycling on fat mass and skeletal muscle mass. *Res Sports Med* **19**, 170–185 (2011).
99. Soulet, D. & Rivest, S. Bone-marrow-derived microglia: myth or reality? *Current Opinion in Pharmacology* **8**, 508–518 (2008).
100. Passaro, A. P., Lebos, A. L., Yao, Y. & Stice, S. L. Immune Response in Neurological Pathology: Emerging Role of Central and Peripheral Immune Crosstalk. *Frontiers in Immunology* **12**, (2021).
101. Cartier, N., Lewis, C.-A., Zhang, R. & Rossi, F. M. V. The role of microglia in human disease: therapeutic tool or target? *Acta Neuropathol* **128**, 363–380 (2014).
102. Xiong, L., Pan, J.-X., Guo, H., Mei, L. & Xiong, W.-C. Parkinson's in the bone. *Cell Biosci* **11**, 190 (2021).
103. Allen, N. E. *et al.* Interventions for preventing falls in Parkinson's disease. *Cochrane Database Syst Rev* **6**, CD011574 (2022).

104. Freese, J. L., Pino, D. & Pleasure, S. J. Wnt signaling in development and disease. *Neurobiology of Disease* **38**, 148–153 (2010).
105. Berwick, D. C. & Harvey, K. The regulation and deregulation of Wnt signaling by PARK genes in health and disease. *Journal of Molecular Cell Biology* **6**, 3–12 (2014).
106. Inestrosa, N. C. & Arenas, E. Emerging roles of Wnts in the adult nervous system. *Nat Rev Neurosci* **11**, 77–86 (2010).
107. L'Episcopo, F. *et al.* Wnt/ β -Catenin Signaling Is Required to Rescue Midbrain Dopaminergic Progenitors and Promote Neurorepair in Ageing Mouse Model of Parkinson's Disease. *Stem Cells* **32**, 2147–2163 (2014).
108. Castelo-Branco, G. *et al.* Differential regulation of midbrain dopaminergic neuron development by Wnt-1, Wnt-3a, and Wnt-5a. *Proc Natl Acad Sci U S A* **100**, 12747–12752 (2003).
109. Kane, L. A. *et al.* PINK1 phosphorylates ubiquitin to activate Parkin E3 ubiquitin ligase activity. *Journal of Cell Biology* **205**, 143–153 (2014).
110. Zhang, W. *et al.* Upregulation of Parkin Accelerates Osteoblastic Differentiation of Bone Marrow-Derived Mesenchymal Stem Cells and Bone Regeneration by Enhancing Autophagy and β -Catenin Signaling. *Front. Cell Dev. Biol.* **8**, 576104 (2020).
111. Manikandan, M. *et al.* NR2F1 mediated down-regulation of osteoblast differentiation was rescued by bone morphogenetic protein-2 (BMP-2) in human MSC. *Differentiation* **104**, 36–41 (2018).
112. Walter, J. *et al.* The Parkinson's-disease-associated mutation LRRK2-G2019S alters dopaminergic differentiation dynamics via NR2F1. *Cell Reports* **37**, 109864 (2021).
113. Marion, N. W. & Mao, J. J. Mesenchymal Stem Cells and Tissue Engineering. *Methods Enzymol* **420**, 339–361 (2006).

114. Hernández, R. *et al.* Differentiation of Human Mesenchymal Stem Cells towards Neuronal Lineage: Clinical Trials in Nervous System Disorders. *Biomolecules & Therapeutics* **28**, 34 (2020).
115. Drela, K., Siedlecka, P., Sarnowska, A. & Domanska-Janik, K. Human mesenchymal stem cells in the treatment of neurological diseases. *Acta Neurobiol Exp (Wars)* **73**, 38–56 (2013).
116. Valenti, M., Dalle Carbonare, L. & Mottes, M. Osteogenic Differentiation in Healthy and Pathological Conditions. *IJMS* **18**, 41 (2016).
117. Choi, S.-E. & Kemper, J. K. Regulation of SIRT1 by microRNAs. *Mol Cells* **36**, 385–392 (2013).
118. Zhou, Y. *et al.* SIRT1 suppresses adipogenesis by activating Wnt/ β -catenin signaling in vivo and in vitro. *Oncotarget* **7**, 77707–77720 (2016).
119. Ascorbic acid induces either differentiation or apoptosis in MG-63 osteosarcoma lineage - PubMed. <https://pubmed.ncbi.nlm.nih.gov/24692690/>.
120. Dalle Carbonare, L. *et al.* Methylsulfonylmethane enhances MSC chondrogenic commitment and promotes pre-osteoblasts formation. *Stem Cell Res Ther* **12**, 326 (2021).
121. Dalle Carbonare, L. *et al.* Increased Gene Expression of RUNX2 and SOX9 in Mesenchymal Circulating Progenitors Is Associated with Autophagy during Physical Activity. *Oxid Med Cell Longev* **2019**, 8426259 (2019).
122. Alloisio, G. *et al.* Effects of Extracellular Osteoanabolic Agents on the Endogenous Response of Osteoblastic Cells. *Cells* **10**, 2383 (2021).
123. Zhang, Q., Yin, X. & Zhang, Y. MicroRNA-221 Promotes Cell Proliferation and Inhibits Apoptosis in Osteosarcoma Cells by Directly Targeting FBXW11 and Regulating Wnt Signaling. *Arch Med Res* **52**, 191–199 (2021).

124. Fonseca, L. N. *et al.* Cell surface markers for mesenchymal stem cells related to the skeletal system: A scoping review. *Heliyon* **9**, e13464 (2023).
125. Fröhlich, L. F. MicroRNAs at the Interface between Osteogenesis and Angiogenesis as Targets for Bone Regeneration. *Cells* **8**, 121 (2019).
126. Katkat, E. *et al.* Canonical Wnt and TGF- β /BMP signaling enhance melanocyte regeneration but suppress invasiveness, migration, and proliferation of melanoma cells. *Front Cell Dev Biol* **11**, 1297910 (2023).
127. Lee, K. S. *et al.* Runx2 is a common target of transforming growth factor beta1 and bone morphogenetic protein 2, and cooperation between Runx2 and Smad5 induces osteoblast-specific gene expression in the pluripotent mesenchymal precursor cell line C2C12. *Mol Cell Biol* **20**, 8783–8792 (2000).
128. Das, G., Shrivage, B. V. & Bachrecke, E. H. Regulation and Function of Autophagy during Cell Survival and Cell Death. *Cold Spring Harb Perspect Biol* **4**, a008813 (2012).
129. Zhu, C. *et al.* Autophagy in Bone Remodeling: A Regulator of Oxidative Stress. *Front Endocrinol (Lausanne)* **13**, 898634 (2022).
130. Kim, M. *et al.* Sestrins are evolutionarily conserved mediators of exercise benefits. *Nat Commun* **11**, 190 (2020).
131. Inoue, N. *et al.* Cyclin-dependent kinase inhibitor, p21WAF1/CIP1, is involved in adipocyte differentiation and hypertrophy, linking to obesity, and insulin resistance. *J Biol Chem* **283**, 21220–21229 (2008).
132. Ronti, T., Lupattelli, G. & Mannarino, E. The endocrine function of adipose tissue: an update. *Clinical Endocrinology* **64**, 355–365 (2006).

133. Kim, S. & Chang, M.-Y. Application of Human Brain Organoids—Opportunities and Challenges in Modeling Human Brain Development and Neurodevelopmental Diseases. *Int J Mol Sci* **24**, 12528 (2023).
134. Jo, J. *et al.* Midbrain-like Organoids from Human Pluripotent Stem Cells Contain Functional Dopaminergic and Neuromelanin-Producing Neurons. *Cell Stem Cell* **19**, 248–257 (2016).
135. Chlebanowska, P., Tejchman, A., Sulkowski, M., Skrzypek, K. & Majka, M. Use of 3D Organoids as a Model to Study Idiopathic Form of Parkinson’s Disease. *Int J Mol Sci* **21**, 694 (2020).
136. Reinhardt, P. *et al.* Genetic Correction of a LRRK2 Mutation in Human iPSCs Links Parkinsonian Neurodegeneration to ERK-Dependent Changes in Gene Expression. *Cell Stem Cell* **12**, 354–367 (2013).
137. Qing, X. *et al.* CRISPR/Cas9 and piggyBac-mediated footprint-free LRRK2-G2019S knock-in reveals neuronal complexity phenotypes and α -Synuclein modulation in dopaminergic neurons. *Stem Cell Res* **24**, 44–50 (2017).
138. Hatcher, J. M. *et al.* Discovery of a Pyrrolopyrimidine (JH-II-127), a Highly Potent, Selective, and Brain Penetrant LRRK2 Inhibitor. *ACS Med Chem Lett* **6**, 584–589 (2015).
139. Hansen, K. E. *et al.* Treatment of Vitamin D Insufficiency in Postmenopausal Women: A Randomized Clinical Trial. *JAMA Intern Med* **175**, 1612–1621 (2015).
140. Kahwati, L. C. *et al.* Vitamin D, Calcium, or Combined Supplementation for the Primary Prevention of Fractures in Community-Dwelling Adults: Evidence Report and Systematic Review for the US Preventive Services Task Force. *JAMA* **319**, 1600–1612 (2018).

141. Muresan, G. C., Hedesiu, M., Lucaciu, O., Boca, S. & Petrescu, N. Effect of Vitamin D on Bone Regeneration: A Review. *Medicina* **58**, 1337 (2022).
142. Molinari, C. *et al.* Role of Combined Lipoic Acid and Vitamin D3 on Astrocytes as a Way to Prevent Brain Ageing by Induced Oxidative Stress and Iron Accumulation. *Oxidative Medicine and Cellular Longevity* **2019**, 1–16 (2019).
143. Yang, Z. & Wang, K. K. W. Glial Fibrillary acidic protein: From intermediate filament assembly and gliosis to neurobiomarker. *Trends Neurosci* **38**, 364–374 (2015).
144. Weihe, E., Depboylu, C., Schütz, B., Schäfer, M. K.-H. & Eiden, L. E. Three Types of Tyrosine Hydroxylase-Positive CNS Neurons Distinguished by Dopa Decarboxylase and VMAT2 Co-Expression. *Cell Mol Neurobiol* **26**, 659–678 (2006).
145. DeGiosio, R. A. *et al.* More than a marker: potential pathogenic functions of MAP2. *Frontiers in Molecular Neuroscience* **15**, (2022).
146. Holt, R. J. *et al.* De Novo Missense Variants in FBXW11 Cause Diverse Developmental Phenotypes Including Brain, Eye, and Digit Anomalies. *The American Journal of Human Genetics* **105**, 640–657 (2019).
147. Sharma, A. *et al.* Pharmacological Modulation of Ubiquitin-Proteasome Pathways in Oncogenic Signaling. *Int J Mol Sci* **22**, 11971 (2021).
148. Luo, X. *et al.* Osteogenic BMPs promote tumor growth of human osteosarcomas that harbor differentiation defects. *Lab Invest* **88**, 1264–1277 (2008).
149. Cleidocranial dysplasia and novel RUNX2 variants: dental, craniofacial, and osseous manifestations - PubMed. <https://pubmed.ncbi.nlm.nih.gov/35674542/>.
150. CRISPR/Cas system: An emerging technology in stem cell research - PMC. <https://www.ncbi.nlm.nih.gov/pmc/articles/PMC6851009/>.
151. Wang, G. X., Sun, R. P. & Song, F. L. A novel RUNX2 mutation (T420I) in Chinese patients with cleidocranial dysplasia. *Genet Mol Res* **9**, 41–47 (2010).

152. Bae, S. C. *et al.* PEBP2 alpha B/mouse AML1 consists of multiple isoforms that possess differential transactivation potentials. *Mol Cell Biol* **14**, 3242–3252 (1994).
153. Kim, H.-J., Kim, W.-J. & Ryoo, H.-M. Post-Translational Regulations of Transcriptional Activity of RUNX2. *Mol Cells* **43**, 160–167 (2020).
154. Bruderer, M., Richards, R. G., Alini, M. & Stoddart, M. J. Role and regulation of RUNX2 in osteogenesis. *Eur Cell Mater* **28**, 269–286 (2014).
155. Jung, Y.-J., Bae, H.-S., Ryoo, H.-M. & Baek, S.-H. A novel RUNX2 mutation in exon 8, G462X, in a patient with Cleidocranial Dysplasia. *J Cell Biochem* **119**, 1152–1162 (2018).
156. E3 ubiquitin ligase-mediated regulation of bone formation and tumorigenesis | Cell Death & Disease. <https://www.nature.com/articles/cddis2012217>.
157. Thaweesapphithak, S. *et al.* Functional consequences of C-terminal mutations in RUNX2. *Sci Rep* **13**, 12202 (2023).
158. Rosset, E. M. & Bradshaw, A. D. SPARC/osteonectin in mineralized tissue. *Matrix Biol* **52–54**, 78–87 (2016).
159. Gruber, H. E. *et al.* Targeted deletion of the SPARC gene accelerates disc degeneration in the aging mouse. *J Histochem Cytochem* **53**, 1131–1138 (2005).
160. Valenti, M. T. *et al.* Runx2 overexpression compromises bone quality in acromegalic patients. *Endocr Relat Cancer* **25**, 269–277 (2018).
161. Dalle Carbonare, L. *et al.* Bone histomorphometry in acromegaly patients with fragility vertebral fractures. *Pituitary* **21**, 56–64 (2018).
162. Tataria, M., Quarto, N., Longaker, M. T. & Sylvester, K. G. Absence of the p53 tumor suppressor gene promotes osteogenesis in mesenchymal stem cells. *J Pediatr Surg* **41**, 624–632; discussion 624-632 (2006).

163. Zhou, X. *et al.* Wnt/ β -catenin-mediated p53 suppression is indispensable for osteogenesis of mesenchymal progenitor cells. *Cell Death Dis* **12**, 521 (2021).
164. Stambolic, V. *et al.* Regulation of PTEN transcription by p53. *Mol Cell* **8**, 317–325 (2001).
165. Mazziotta, C. *et al.* MicroRNAs Modulate Signaling Pathways in Osteogenic Differentiation of Mesenchymal Stem Cells. *Int J Mol Sci* **22**, 2362 (2021).
166. Luo, H., Gao, H., Liu, F. & Qiu, B. Regulation of Runx2 by microRNA-9 and microRNA-10 modulates the osteogenic differentiation of mesenchymal stem cells. *International Journal of Molecular Medicine* **39**, 1046–1052 (2017).
167. Qin, H. & Cai, J. Effect of Runx2 silencing on autophagy and RANKL expression in osteoblasts. *Archives of Oral Biology* **95**, 74–78 (2018).
168. Ren, C. *et al.* Effects of runt-related transcription factor 2 (RUNX2) on the autophagy of rapamycin-treated osteoblasts. *Bioengineered* **13**, 5262–5276.
169. Lu, T. X. & Rothenberg, M. E. MicroRNA. *J Allergy Clin Immunol* **141**, 1202–1207 (2018).
170. Krützfeldt, J. & Stoffel, M. MicroRNAs: A new class of regulatory genes affecting metabolism. *Cell Metabolism* **4**, 9–12 (2006).
171. Taipaleenmäki, H. Regulation of Bone Metabolism by microRNAs. *Curr Osteoporos Rep* **16**, 1–12 (2018).
172. Valenti, M. T. *et al.* Physical Exercise Modulates miR-21-5p, miR-129-5p, miR-378-5p, and miR-188-5p Expression in Progenitor Cells Promoting Osteogenesis. *Cells* **8**, 742 (2019).
173. Marędziak, M., Śmieszek, A., Chrzęstek, K., Basinska, K. & Marycz, K. Physical Activity Increases the Total Number of Bone-Marrow-Derived Mesenchymal Stem

- Cells, Enhances Their Osteogenic Potential, and Inhibits Their Adipogenic Properties. *Stem Cells Int* **2015**, 379093 (2015).
174. Magkos, F. *et al.* The bone response to non-weight-bearing exercise is sport-, site-, and sex-specific. *Clin J Sport Med* **17**, 123–128 (2007).
175. Hicks, S. D., Jacob, P., Middleton, F. A., Perez, O. & Gagnon, Z. Distance running alters peripheral microRNAs implicated in metabolism, fluid balance, and myosin regulation in a sex-specific manner. *Physiol Genomics* **50**, 658–667 (2018).
176. Dong, X. *et al.* MicroRNA-223-3p suppresses leukemia inhibitory factor expression and pinopodes formation during embryo implantation in mice. *Am J Transl Res* **8**, 1155–1163 (2016).
177. Xu, G. *et al.* MiR-26b modulates insulin sensitivity in adipocytes by interrupting the PTEN/PI3K/AKT pathway. *Int J Obes (Lond)* **39**, 1523–1530 (2015).
178. Association between the expression of miR-26 and goat milk fatty acids - Wang - 2018 - *Reproduction in Domestic Animals* - Wiley Online Library. <https://onlinelibrary.wiley.com/doi/10.1111/rda.13291>.
179. Woo, I. *et al.* Micro-RNAs involved in cellular proliferation have altered expression profiles in granulosa of young women with diminished ovarian reserve. *J Assist Reprod Genet* **35**, 1777–1786 (2018).
180. Age-related changes in miR-143-3p:Igfbp5 interactions affect muscle regeneration - PubMed. <https://pubmed.ncbi.nlm.nih.gov/26762731/>.
181. Gan, M. *et al.* miR-152 regulates the proliferation and differentiation of C2C12 myoblasts by targeting E2F3. *In Vitro Cell Dev Biol Anim* **54**, 304–310 (2018).
182. MicroRNA-152 Promotes Slow-Twitch Myofiber Formation via Targeting Uncoupling Protein-3 Gene - PMC. <https://www.ncbi.nlm.nih.gov/pmc/articles/PMC6769457/>.

183. MicroRNA-27a promotes myoblast proliferation by targeting myostatin - PubMed.
<https://pubmed.ncbi.nlm.nih.gov/22640741/>.
184. Rudkowska, I. *et al.* Validation of the use of peripheral blood mononuclear cells as surrogate model for skeletal muscle tissue in nutrigenomic studies. *OMICS* **15**, 1–7 (2011).
185. Yao, C.-X. *et al.* miR-200b targets GATA-4 during cell growth and differentiation. *RNA Biol* **10**, 465–480 (2013).
186. Jeukendrup, A. E., Craig, N. P. & Hawley, J. A. The bioenergetics of World Class Cycling. *J Sci Med Sport* **3**, 414–433 (2000).
187. Leonardini, A., Laviola, L., Perrini, S., Natalicchio, A. & Giorgino, F. Cross-Talk between PPARgamma and Insulin Signaling and Modulation of Insulin Sensitivity. *PPAR Res* **2009**, 818945 (2009).
188. Chen, Y. *et al.* The functions and roles of sestrins in regulating human diseases. *Cell Mol Biol Lett* **27**, 2 (2022).
189. Amat, R. *et al.* SIRT1 controls the transcription of the peroxisome proliferator-activated receptor-gamma Co-activator-1alpha (PGC-1alpha) gene in skeletal muscle through the PGC-1alpha autoregulatory loop and interaction with MyoD. *J Biol Chem* **284**, 21872–21880 (2009).
190. Russell, A. P., Hesselink, M. K. C., Lo, S. K. & Schrauwen, P. Regulation of metabolic transcriptional co-activators and transcription factors with acute exercise. *FASEB J* **19**, 986–988 (2005).
191. Lo, K. A. & Sun, L. Turning WAT into BAT: a review on regulators controlling the browning of white adipocytes. *Biosci Rep* **33**, e00065 (2013).

192. Adipose Tissue | Diabetes | American Diabetes Association.
<https://diabetesjournals.org/diabetes/article/55/6/1537/15609/Adipose-TissueFrom-Lipid-Storage-Compartment-to>.
193. Chen, L. *et al.* MiR-146b is a regulator of human visceral preadipocyte proliferation and differentiation and its expression is altered in human obesity. *Mol Cell Endocrinol* **393**, 65–74 (2014).
194. Dalle Carbonare, L. *et al.* Fisetin: An Integrated Approach to Identify a Strategy Promoting Osteogenesis. *Front Pharmacol* **13**, 890693 (2022).
195. Funakoshi-Tago, M., Nakamura, K., Tago, K., Mashino, T. & Kasahara, T. Anti-inflammatory activity of structurally related flavonoids, Apigenin, Luteolin and Fisetin. *International Immunopharmacology* **11**, 1150–1159 (2011).
196. Pandey, M., Verma, R. K. & Saraf, S. A. Nutraceuticals: new era of medicine and health. *Asian Journal of Pharmaceutical and Clinical Research* (2010).
197. Role of nutraceuticals in human health - PMC.
<https://www.ncbi.nlm.nih.gov/pmc/articles/PMC3550857/>.

RINGRAZIAMENTI

Desidero esprimere la mia sincera gratitudine al Prof. Dalle Carbonare per la fiducia che mi ha dimostrato fin dall'inizio e per l'opportunità che mi ha offerto nel svolgere questo progetto all'interno del suo Laboratorio.

Un profondo ringraziamento alla Dottoressa Valenti per essere stata la mia mentore, offrendomi supporto e incoraggiamento durante tutto il percorso di ricerca e di vita. Senza il suo prezioso contributo, questa tesi non sarebbe stata possibile.

Un ringraziamento speciale va a tutti i miei colleghi di laboratorio e collaboratori, le cui discussioni stimolanti, il sostegno reciproco e l'amicizia hanno reso l'esperienza di ricerca indimenticabile. Grazie anche a tutte le persone che hanno partecipato alla mia ricerca, fornendo informazioni, risorse e assistenza tecnica. Il loro contributo è stato fondamentale per il successo di questo lavoro.

Vorrei estendere il mio ringraziamento agli amici che ho incontrato durante questo percorso e che hanno reso le giornate di lavoro meno faticose e più divertenti: Anna, Mirko, Ornella, Andrea, Vittoria, Nino, Mariaelena e Shara. La vostra presenza è stata un grande sostegno in ogni momento.

Un grazie a Chiara, Valeria e Cristina per l'ascolto e gli abbracci quando più ne ho avuto bisogno.

Un profondo ringraziamento a Simona e Marilisa, amiche e confidenti incontrate lungo il percorso di dottorato. Le vostre parole, risate e abbracci sono stati fondamentali per rendere questo viaggio meraviglioso e affrontare le sfide più difficili, senza mai lasciarmi sola.

Ringrazio Alberto per essere stato un compagno di lavoro straordinario, la sua tranquillità e pazienza hanno contribuito a mantenere l'equilibrio anche nei momenti più intensi.

Grazie a Francesca, per essere stata in grado di farmi divertire anche nei momenti peggiori di questo periodo. Per le parole, l'aiuto e la vicinanza costante. Averti come compagna e amica di avventure e (sventure) è una grande fortuna e ne sono grata.

Ai miei nonni per il sostegno e l'amore che mi hanno sempre dimostrato nonostante la lontananza.

Ai miei animali, gatti e cani, che da sempre riempiono le mie giornate e sono parte essenziale della mia vita.

A Lorenzo, il mio fratellone con cui condivido la passione per la ricerca. Lo ringrazio per l'aiuto e l'ascolto che ogni giorno mi riserva e per esserci sempre, cercando di trovare il lato divertente e giusto in ogni situazione. Lo ringrazio anche per aver portato nella mia vita Guia, che oltre ad essere stata fondamentale nella stesura di questa tesi, ringrazio per i consigli che anche lei continua a darmi. Grazie davvero per esserci sempre!

A mio padre, ogni mio successo è principalmente per Te e la Mamma senza i quali tutto questo probabilmente non sarebbe mai stato possibile.

Infine, ma sottolineerei non per importanza, Andrea mio compagno di vita. Il tuo amore, incoraggiamento e sostegno incondizionato in ogni momento mi hanno permesso di arrivare fino a qui.

In conclusione, questa tesi è stata scritta durante il periodo più difficile della mia vita, e senza il sostegno e l'amore di tutti voi, non sarebbe stata possibile. Sono sicura che mia madre, in questo momento, è qui con noi, abbracciandoci forte.